

## ABSTRACT

Correlation of Selected Earthquakes with Seismogenic Faults, Central Oklahoma

Brandon M. Rasaka, M.S.

Committee Chairperson: Vincent S. Cronin, Ph.D.

Hypocenter locations for nearly 900 earthquakes of  $M \geq 2.0$  in central Oklahoma between the years 2014 and 2015 were used to attempt to locate seismogenic faults near the city of Guthrie. Focal mechanisms from 29 earthquakes of  $M \geq 3.5$  were analyzed using the Seismo-Lineament Analysis Method (SLAM). Focal mechanism solutions for these 29 events were projected as swaths on the ground surface represented by a digital elevation model (DEM). Within each swath the surface trace of a causative fault might be found if the nodal plane is coincident with the fault, the fault is emergent at the ground surface and is approximately planar. Analysis of the DEM within each swath revealed few geomorphic lineations that might be caused by fault movement associated with the earthquakes. It is inferred from these results and field work that the faults producing these earthquakes do not intersect the ground surface.

Correlation of Selected Earthquakes with Seismogenic Faults, Central Oklahoma

by

Brandon M. Rasaka, B.S.

A Thesis

Approved by the Department of Geosciences

---

Stacy C. Atchley, Ph.D., Chairperson

Submitted to the Graduate Faculty of  
Baylor University in Partial Fulfillment of the  
Requirements for the Degree  
of  
Master of Science

Approved by the Thesis Committee

---

Vincent S. Cronin, Ph.D., Chairperson

---

John A. Dunbar, Ph.D.

---

Bruce W. Byars, M.S.

Accepted by the Graduate School

May 2016

---

J. Larry Lyon, Ph.D., Dean

Copyright © 2016 by Brandon M. Rasaka

All rights related to this thesis are reserved, with the irrevocable exception that Vincent S. Cronin retains all rights to his intellectual property and to the research products/ideas that were shared with Brandon M. Rasaka in the course of this research.

## TABLE OF CONTENTS

LIST OF FIGURES .....	vi
LIST OF TABLES .....	viii
ACKNOWLEDGMENTS .....	ix
CHAPTER ONE.....	1
Introduction .....	1
CHAPTER TWO .....	8
Background .....	8
Geologic Setting.....	8
Previously Mapped Faults .....	8
Triggered Seismicity .....	10
CHAPTER THREE.....	13
Methods .....	13
Focal Mechanisms .....	13
Data Collection .....	14
The Seismo-Lineament Analysis Method.....	15
Defining Seismo-Lineament Boundaries .....	20
Event Groupings .....	21
Geomorphic Analysis.....	21
Field Investigations.....	23
Three-Dimensional Model.....	24
Drainage Network Trend Analysis.....	25

CHAPTER FOUR .....	27
Results .....	27
Seismo-lineaments .....	27
Event Groupings .....	33
Geomorphic Analysis.....	33
Field Investigations.....	46
Three-Dimensional Model.....	53
Drainage Network Trend Analysis.....	54
CHAPTER FIVE .....	55
Discussion & Conclusions .....	55
APPENDICES.....	57
APPENDIX A .....	58
ArcGIS Scripts and Workflow.....	58
Model 1: Creating Polylines of Seismo-Lineament Swaths .....	58
Model 2: Creating Polygons of Seismo-Lineament Swaths.....	60
Model 3: Drainage and Ridgeline Delineation part 1 .....	61
Model 4: Drainage and Ridgeline Delineation part 2 .....	63
Model 5: Linear Directional Mean .....	64
APPENDIX B .....	67
Seismo-Lineaments for all Events .....	67
References Cited.....	97

## LIST OF FIGURES

Figure	Page
1. Graph of the number of earthquakes each year in Oklahoma.....	1
2. Map of effects of shaking from two earthquakes .....	3
3. Location of the study area.....	4
4. Map of suspected fault based on early interpretations .....	5
5. Comparison of single-event location and double-difference epicenters.....	6
6. Location of the study area and events selected for SLAM .....	7
7. Cross section near the study area.....	9
8. Preliminary fault map .....	10
9. Map of faults in Oklahoma, colored based on rank of optimal orientation.....	11
10. Explanatory diagram of a pure strike-slip focal mechanism solution .....	14
11. Schematic diagram of entire workflow.....	20
12. Diagram of the geometry of a seismo-lineament swath .....	21
13. Sample location demonstrating ridgeline and drainage delineation .....	24
14. Three-dimensional model of hypocenters.....	26
15. Example of drainage selection for trend analysis .....	27
16. Characteristic seismo-lineament for the SW cluster .....	29
17. Characteristic seismo-lineament for the M cluster .....	30
18. Characteristic seismo-lineament for the NE cluster.....	31
19. Seismo-lineaments for the event SW-4.....	32
20. Seismo-lineaments for the event M-8 .....	33
21. Seismo-lineaments for the event NE-3 .....	34

22. Overlapping seismo-lineaments for event groups .....	36
23. Geomorphic lineaments throughout the study area.....	47
24. Map of locations of field stops and photos .....	49
25. Photo of Cottonwood Creek lineament .....	51
26. Photo of Liberty Lake lineament .....	51
27. Photo of the dam at Guthrie Lake.....	53
28. Photo of the ditch along Westminster Blvd .....	53
29. Photo of the cutbank in the stream bed along the College Avenue lineament.....	54
30. Photo of the dense foliage en route to reach the Henry Road lineament.....	54
31. Epicenters colorized by depth .....	55
32. Rose diagrams for drainage trend analysis .....	56
33. Inferred swaths from synthesis of event groups and 3D model.....	58
A1. Model 1 workflow .....	62
A2. Screenshots of a seismo-lineament contour shapefile .....	63
A3. Model 2 workflow .....	64
A4. Model 3 workflow .....	65
A5. Model 4 workflow .....	66
A6. Comparison of Stream to Feature tool versus Raster to Polyline tool.....	67
A7. Model 5 workflow .....	68
A8. Intermediate rasters and final vector shapefiles produced by Models 3–5.....	69
B1. Location of the study area.....	70
B2. All seismo-lineaments from the study .....	71

## LIST OF TABLES

Table	Page
1. Hypocenter data used for detailed analysis .....	16
2. Focal mechanism data used for SLAM.....	18
3. Comparison of single-event and double-difference catalogs.....	19
4. Potential geomorphic indicators of faulting.....	23
5. Geomorphic lineations.....	48
6. Locations of field investigations.....	49
7. Event groups that correlate with fault swaths.....	58



## ACKNOWLEDGMENTS

First and foremost I would like to thank my wonderful wife Natasha, without whom this thesis, nor even a great portion of my education, would not have been possible. It was because of her patience, support, and care of our family and household that I was able to spend the time and energy in this endeavor.

I also want to thank Dr. Vince Cronin for his wisdom, expertise and guidance throughout this work and for letting me work through problems on my own.

I want to thank Dr. Austin Holland, who at the time of this work was the head seismologist at the Oklahoma Geological Society, for access to data and suggestions of methods to use.

I want to thank Spencer Clayton and his wife for their assistance and hospitality while conducting my field work.

I would like to express appreciation to the AAPG Grants In Aid program for funding the field work and other expenses for this thesis.

And finally, I want to thank all those who have inspired passion for learning, especially for learning about Earth processes. The list is too long to mention them all here, but a few noteworthy individuals include my father, Eric Rasaka; his brother and my uncle Greg Rasaka; and the faculty of the Geology Department at Brigham Young University—Idaho: Robert Clayton, Julie Willis, Forest Gahn, Mark Lovell, Dan Moore, and Bill Little.

To my wife, Natasha  
“Not soon enough”

“... Two roads diverged in a wood, and I—  
I took the one less traveled by,  
And that has made all the difference.”

—Robert Frost, *The Road Not Taken*

# CHAPTER ONE

## Introduction

Oklahoma has not been known for earthquakes because it is located in a tectonically inactive region. But in 2014 the state surpassed California as the most seismically active state, based on the number of earthquakes of magnitude 3 or greater (USGS, 2015a). Oklahoma experienced an average of 2.3 earthquakes per year of  $M \geq 2$  from 1978 through 2008 (OGS, 2015). The average number of events of  $M \geq 3$  during the same period was 1.6 per year (OGS, 2015). In 2009, there were 20 events of  $M \geq 3$ , and that number has increased nearly each year (OGS, 2015; Figure 1). In 2014, there were 584 such earthquakes and in 2015, there 907 (OGS, 2015).

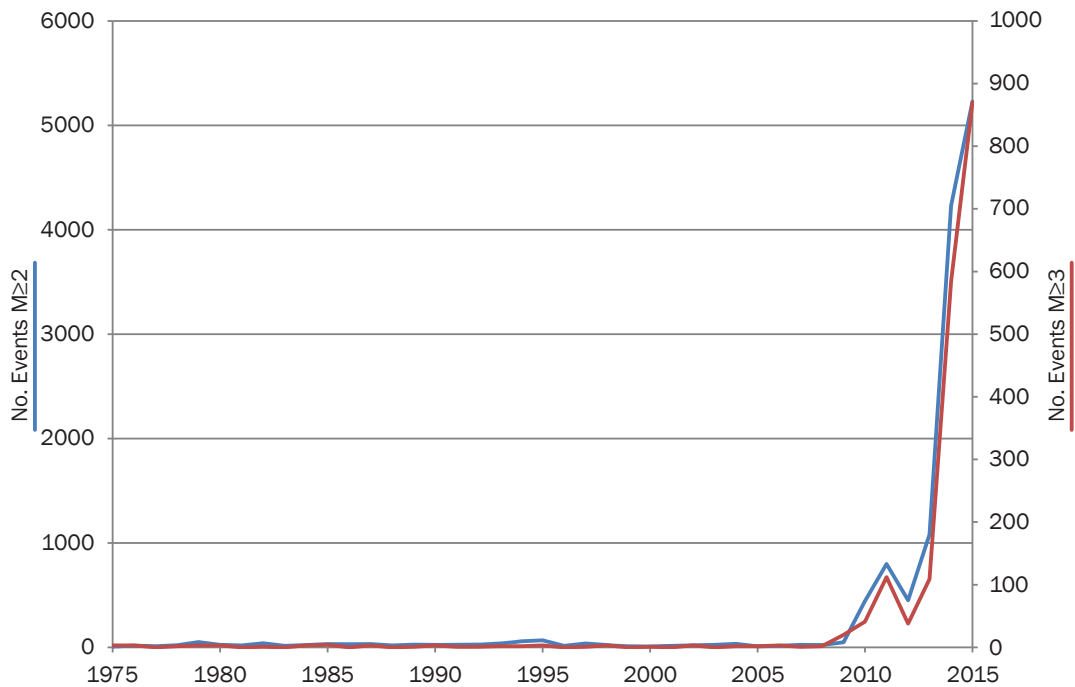


Figure 1. Graph of the number of earthquakes each year in Oklahoma, 1975–2014. (OGS, 2015)

The largest event in Oklahoma was M5.6 near Prague (~75 km east of Oklahoma City) on 5 November 2011 (USGS, 2011). It is believed to have occurred along the Wilzetta Fault (Keller and Holland, 2013), a strike-slip fault that extends ~90 km from central Pottawatomie County to western Creek County in a NNE trend (Gay, 2003a). At least two people were injured, 14 homes were destroyed, and many more were mildly damaged and portions of US Highway 62 buckled (USGS, 2011). The Oklahoma Department of Emergency Management reported that part of a turret collapsed from Benedictine Hall at St. Gregory's University in Shawnee, costing an estimated \$1.5 million in repairs (OEM, 2014). An area of ~65 km<sup>2</sup> experienced shaking of Intensity VIII on the Mercalli Intensity Scale (USGS, 2011). The U.S. Geological Survey reports that the shaking was felt as far away as Tennessee and Wisconsin (USGS, 2011). The next largest earthquake was M5.5 near El Reno, Oklahoma that occurred in 1952 (Stover and Coffman, 1993).

Part of the reason for so much damage and for why these earthquakes were felt so far away is due to seismic attenuation. Seismic waves in the tectonically-active western United States are absorbed by the Earth's crust much more readily than in the mid-continent, allowing the energy from an earthquake to travel much farther (Stein and Wysession, 2003, p. 197-198). This is illustrated in Figure 2, which shows the regions affected by the 1994 M6.7 Northridge, California earthquake and a M6 earthquake that struck near St. Louis, Missouri in 1895. Shaking was felt over a much broader area in the Midwest than in California (Filson et al., 2003).

The cause of the increase in seismicity in Oklahoma has been attributed to optimally-oriented sub-surface faults (relative to the regional stress field) and high-pressure/high-volume injection of waste water following hydraulic fracturing activities in oil and gas extraction (Keranen et al., 2013, 2014; Andrews and Holland, 2015; Holland, 2013a;

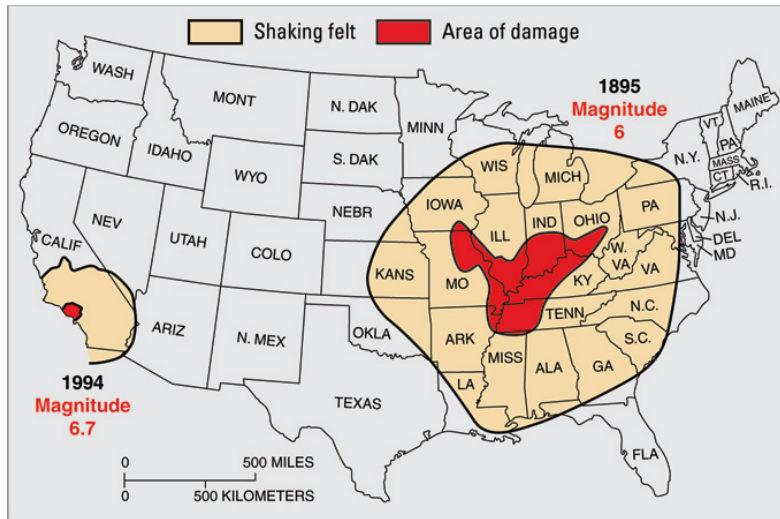


Figure 2. Map of effects of shaking from two earthquakes. The larger earthquake, in California, produced shaking that was felt over a much smaller area than the earthquake in Missouri. From Filson et al. (2003).

McNamara et al., 2015). Knowledge of the location and orientation of faults is critical to determining their likelihood of failure. In most cases these earthquakes have occurred where no known faults are located. Only 28% of events in 2014 are within 2 km of a mapped fault.

The purpose of this thesis is to correlate recent earthquake clusters with seismogenic faults and determine if they are emergent at the ground surface. The M5.6 Prague earthquake demonstrated that at least one fault in Oklahoma is capable of producing damaging earthquakes. It is vital that such faults be located to better understand the hazards.

Epicenters near the city of Guthrie (approximately 40 km north of downtown Oklahoma City) form three clusters in an approximately linear array (Figure 3). Hereafter, these clusters are labeled SW, M, and NE for southwest, middle, and northeast, respectively. Early in this study, the only data available for these earthquakes were single-event hypocenter locations. Their geometry gave the impression that each of the three clusters might be seismogenically related to the same fault with the clusters forming at intersections with smaller faults (Figure 4), an idea shared independently by Hartnady (2015). At the time the

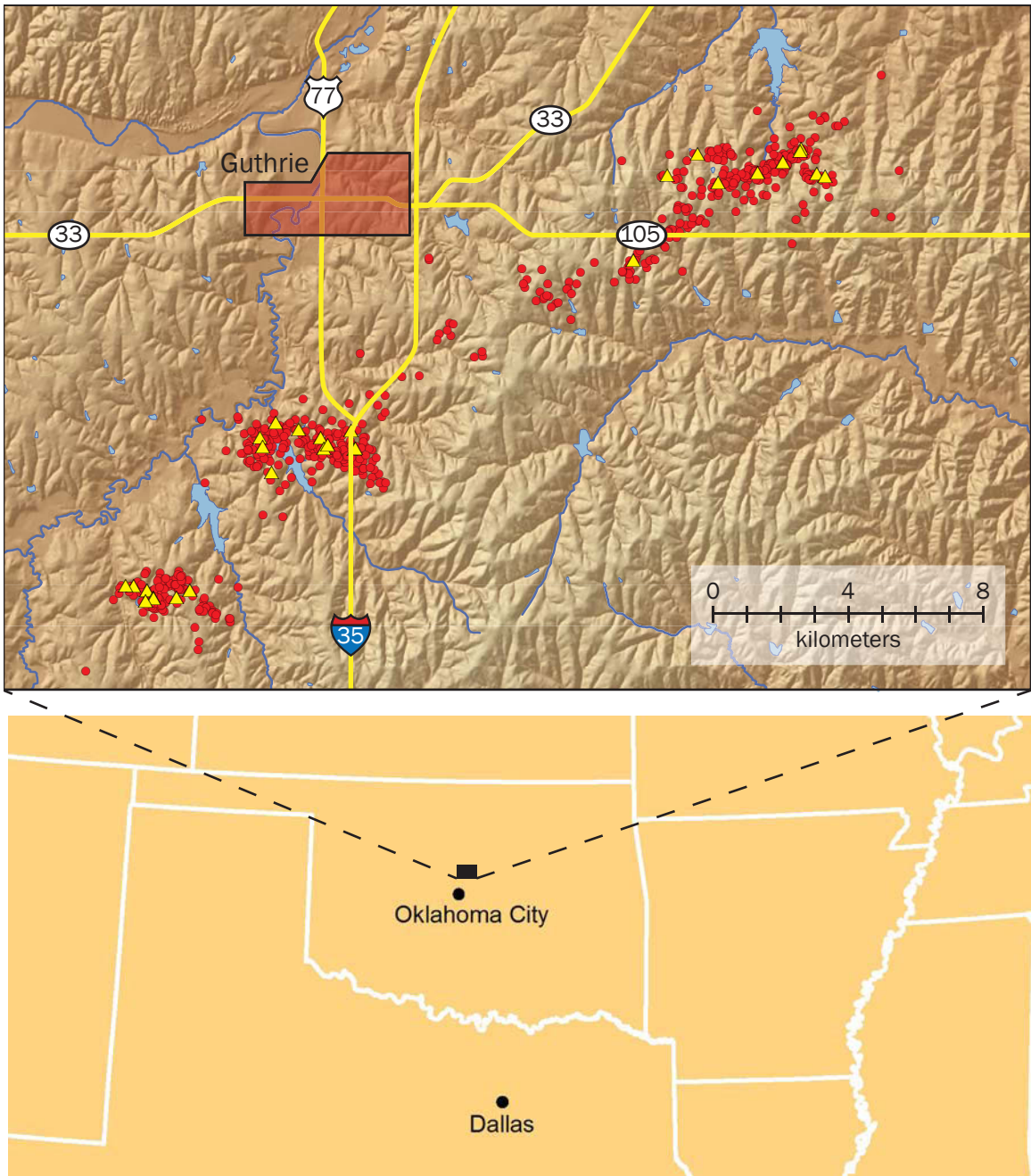


Figure 3. Location of the study area. The city of Guthrie is approximately 40 km north of Oklahoma City. Yellow triangles in the upper map mark the epicenters of events analyzed for correlation with faults. Red circles are epicenters of  $M \geq 2$  earthquakes. Hillshade is at 9x vertical exaggeration.

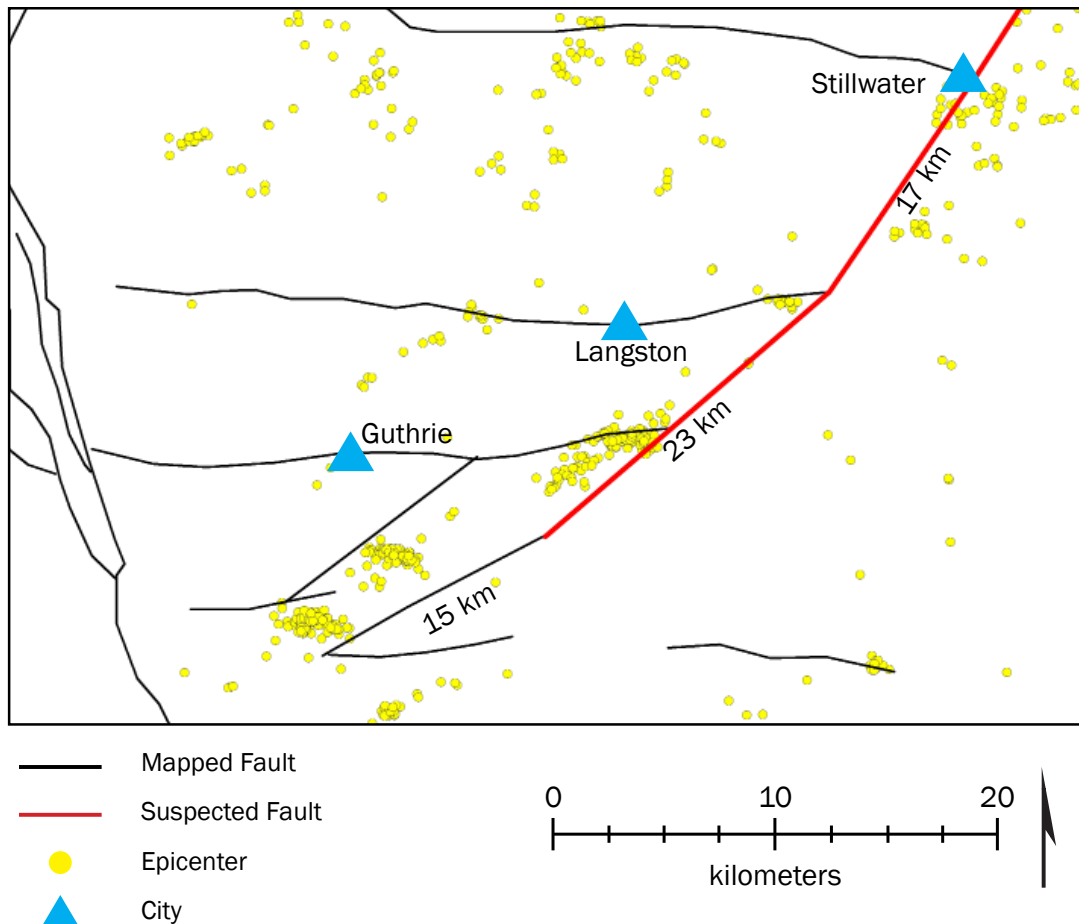


Figure 4. Map of suspected fault (red line) based on early interpretations of limited data. The length of each segment is shown, totaling 55 km. Black lines are faults from Gay (2003b).

only data I had of previously mapped faults in the study area were from a small fault map with very few details (Gay, 2003b). Had this proved to be true, the fault could have the potential of producing an earthquake of magnitude 6 or 7, based on regression relationships of fault length and earthquake magnitude developed by Wells and Coppersmith (1994).

In April 2015, the Oklahoma Geological Survey (OGS) published a preliminary fault map of Oklahoma, including the shapefile data for mapping in GIS software (Holland, 2015a). In June 2015, the OGS also made available relocated earthquake hypocenters (Darold et al., 2015; Figure 5). These new, more accurate data provided more reliable results.



The accuracy of single-event locations, like those available via the U.S. Geological Survey earthquake database, is limited by multiple factors including poor azimuthal distribution of seismometers, accuracy in arrival-time picks, inadequate crustal velocity models, and random recording errors (Cronin and Sverdrup, 2003). The accuracy of hypocenter locations can be improved using one of several relocation methods such as the double-difference method developed by Waldhauser and Ellsworth (2000), which utilizes observations from multiple events at a common station.

With the new fault and hypocenter data it became clear that the earthquakes in the three clusters were likely produced by different faults. I selected events of  $M \geq 3.5$  from these clusters for detailed analysis (Figure 6) using the Seismo-Lineament Analysis Method (SLAM) as described by Cronin et al. (2008) and Cronin (2014b).

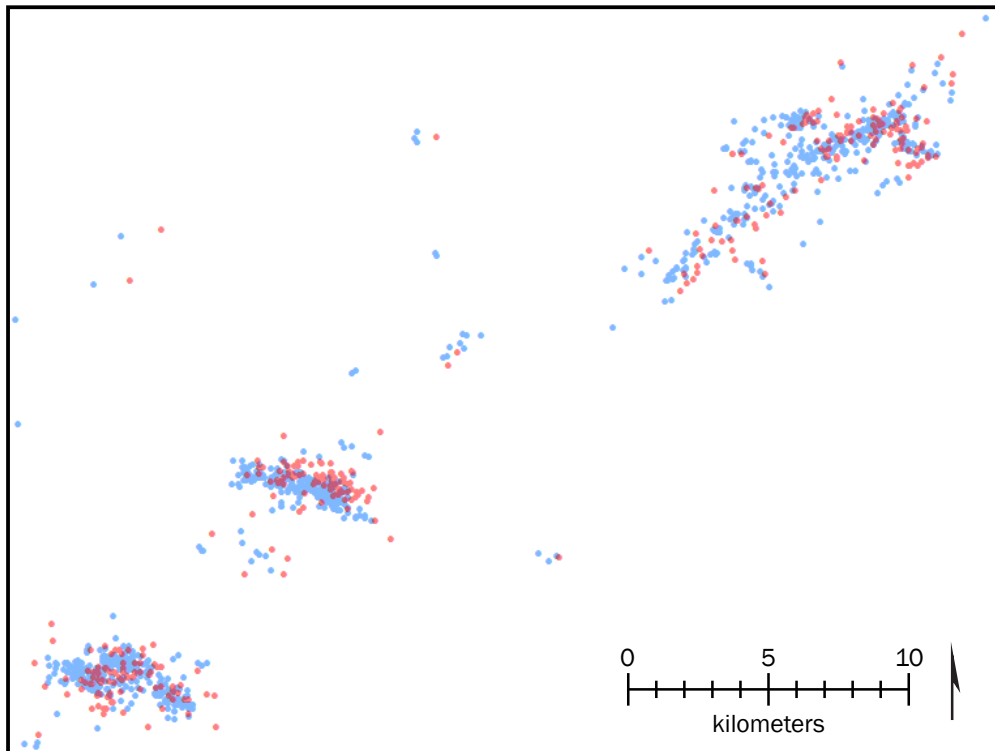


Figure 5. Comparison of single-event location (red dots; USGS, 2015a) and double-difference epicenters (blue dots; Darold et al., 2015) in the study area.

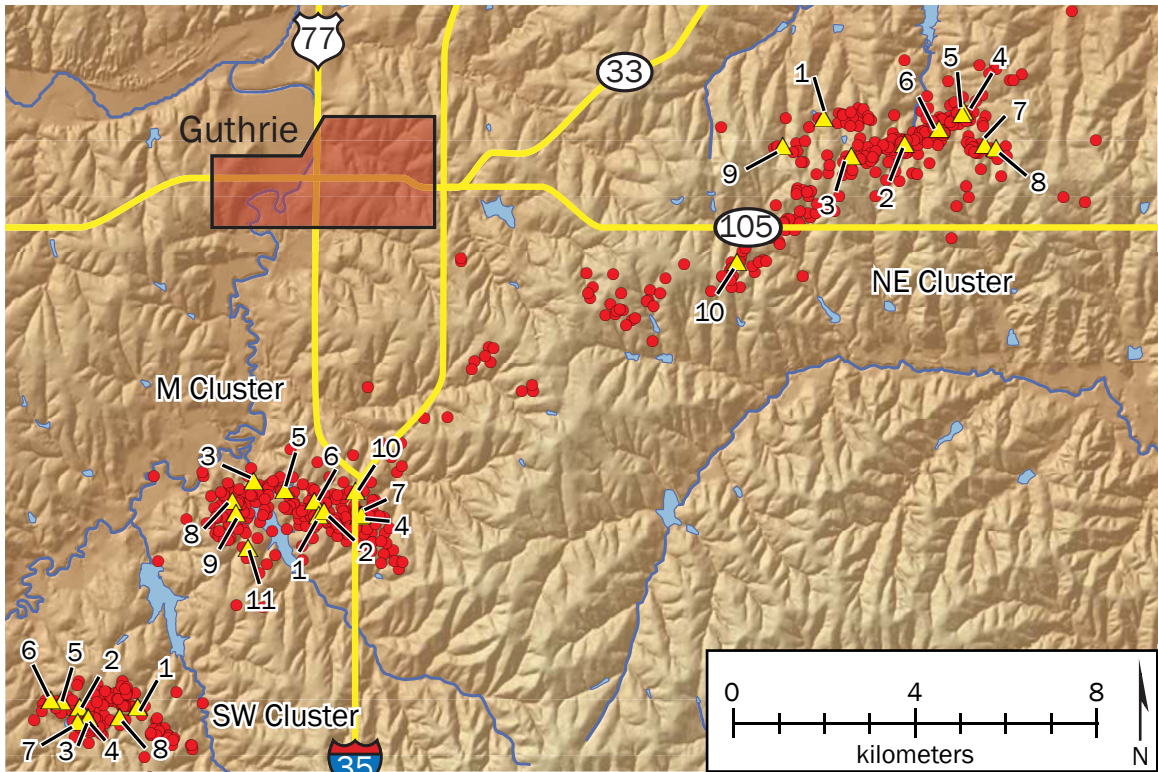


Figure 6. Location of the study area and events selected for SLAM, indicated by the yellow triangles and labeled with unmbers used as identifiers in Table 1. Red circles are all epicenters  $M \geq 2$ .

## CHAPTER TWO

### Background

#### *Geologic Setting*

Oklahoma sits on the stable interior of the Laurentian Craton and has been tectonically stable for approximately 300 million years (Johnson, 2008). Paleozoic marine strata overlie a complex basement throughout the region but comprise only a combined thickness of about 2 km in the study area (Figure 7). Due to its location in the mid-continent these strata are still mostly horizontal in the study area, dipping slightly to the southwest toward the Anadarko Basin. The rock has been relatively undisturbed for millions of years.

Contemporaneous with the Alleghenian and Ouachita orogenies, the Nemaha structure formed in an approximate NNE-SSW trending anticline through southeastern Nebraska, eastern Kansas and north central Oklahoma (Figure 7) and is a buried portion of the Ancestral Rocky Mountains (Gerhard, 2004). Its structural context has been interpreted as being both extensional (Serpa et al., 1989; Burchett et al., 1983), and compressional (Gay, 2003a, 2003b, Gerhard, 2004) with evidence for strike-slip movement as well (Berendsen and Blair, 1995).

Gerhard (2004) provides a literature review of the tectonic origin of the Nemaha structure with studies focused primarily on oil and gas development in Kansas, citing evidence from COCORP seismic studies, overlapping sedimentary bodies, erosional truncation, well logs, and theoretical models. He concludes that the Nemaha structure might be tectonically related to the much earlier Midcontinent Rift System. He argues that deformation and reactivation of rift faults continued from its origin approximately 1.1 Ga

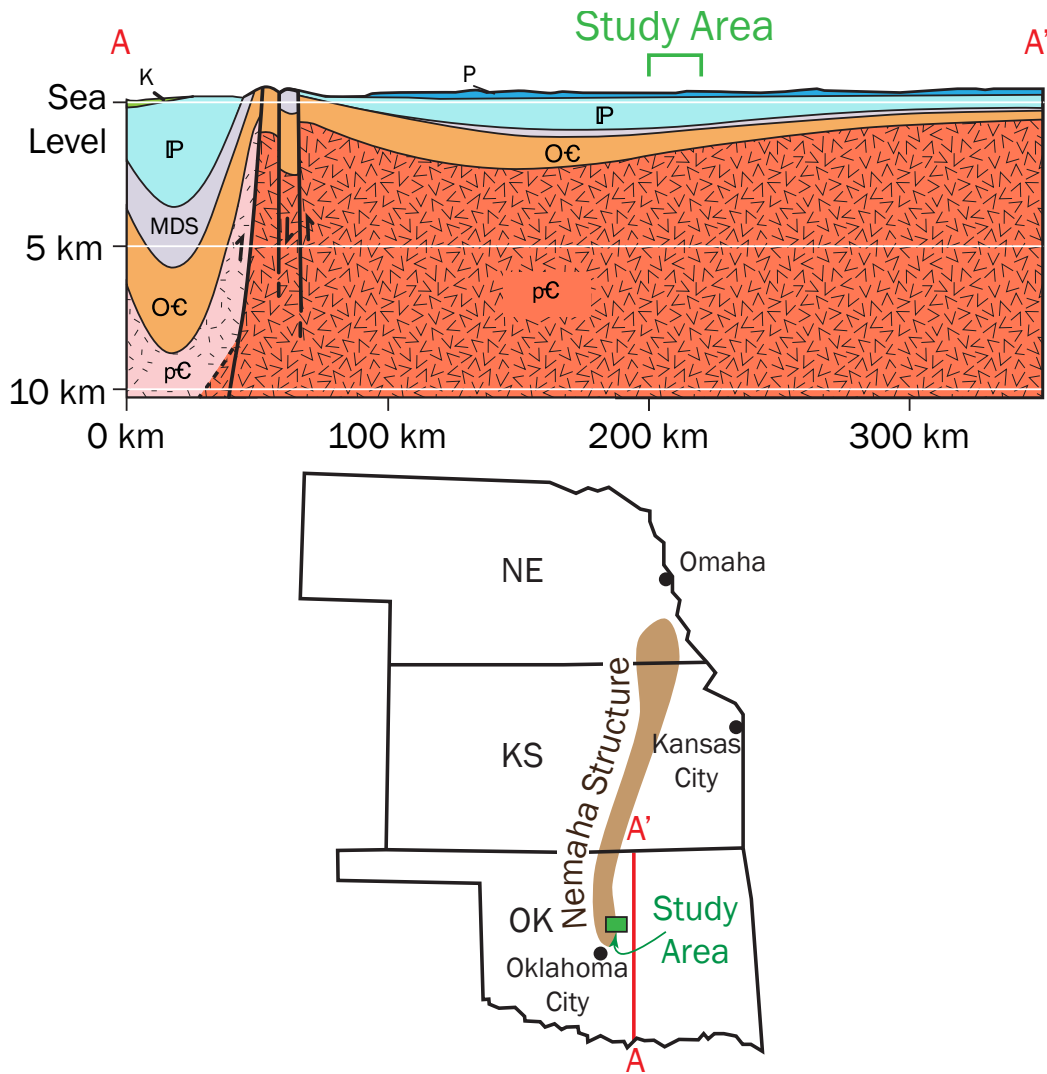


Figure 7. *Above* Cross section near the study area (Adapted from Johnson, 2008). *Below* Map showing location of cross section and the Nemaha Structure (Adapted from Steeples, 1982).

until the latest episode of deformation during the Ancestral Rocky Mountain orogenesis approximately 315 Ma.

Gay (1995, 1999, 2003a, 2003b) show that the Nemaha structure is reverse faulted, with west-dipping fault planes on the eastern margin and possibly east-dipping fault planes on the western margin, implying the Nemaha might be something like a ramp anticline.

### *Previously Mapped Faults*

The OGS published a preliminary fault map of the state (Holland, 2015a) which includes several faults in the Nemaha Fault Zone, along the eastern margin of the Nemaha structure (Figure 8). This database is a compilation of faults mapped from multiple sources, including the oil and gas industry and published literature. The OGS has noted that this database is preliminary, and for the purpose of disseminating the information in a timely manner. The map and database are still being updated as new data are made available.

Zoback et al. (2002) demonstrate that optimally-oriented faults throughout the continent are in a state of near-failure due to lithospheric stresses. Holland (2013b) uses probability density functions for 152 events in Oklahoma representing a period of 30 months to determine the range of statistically-optimal orientations in the region. An open-file report from the OGS (Darold and Holland, 2015) extends Holland's work to include

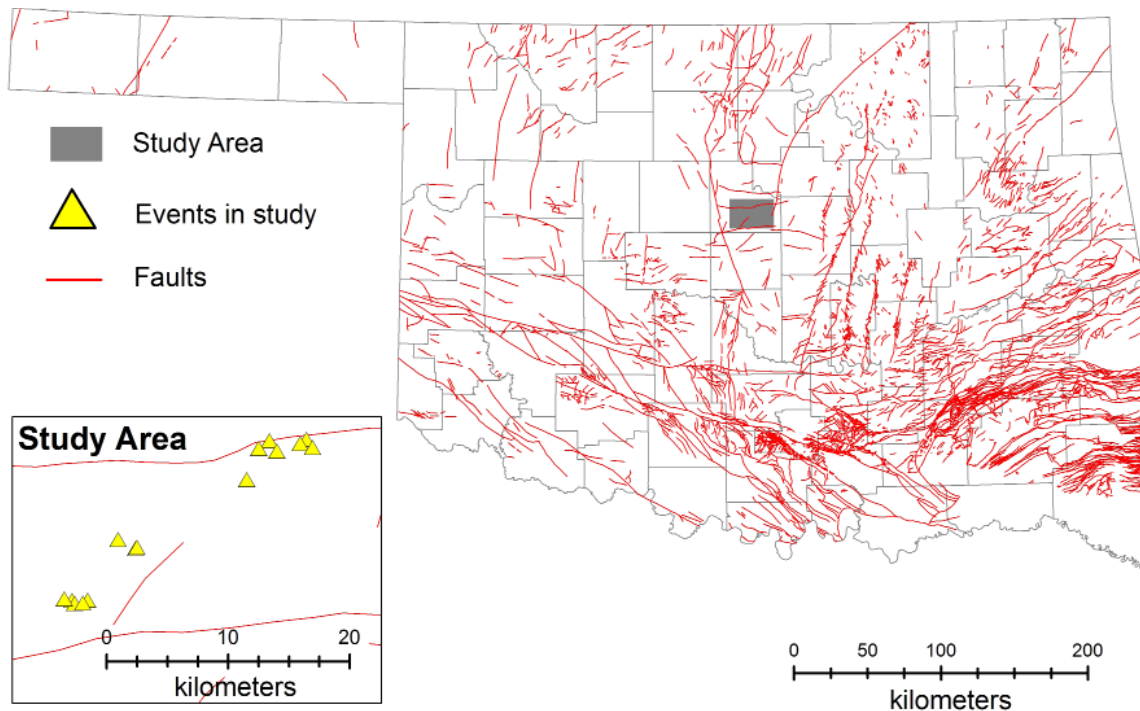


Figure 8. Preliminary Fault Map. From Holland (2015)

688 events from 2010 through 2015. Restricting the fault strike to the range of  $0^{\circ}$ - $180^{\circ}$ , he found the optimal range to be  $45^{\circ}$ - $60^{\circ}$ ,  $105^{\circ}$ - $120^{\circ}$  and  $135^{\circ}$ - $150^{\circ}$ . Faults whose strike is within the range of  $15^{\circ}$ - $45^{\circ}$ ,  $60^{\circ}$ - $75^{\circ}$ ,  $90^{\circ}$ - $105^{\circ}$  and  $120^{\circ}$ - $135^{\circ}$  have a moderate likelihood of generating an earthquake, and all other faults are considered sub-optimal (Figure 9).

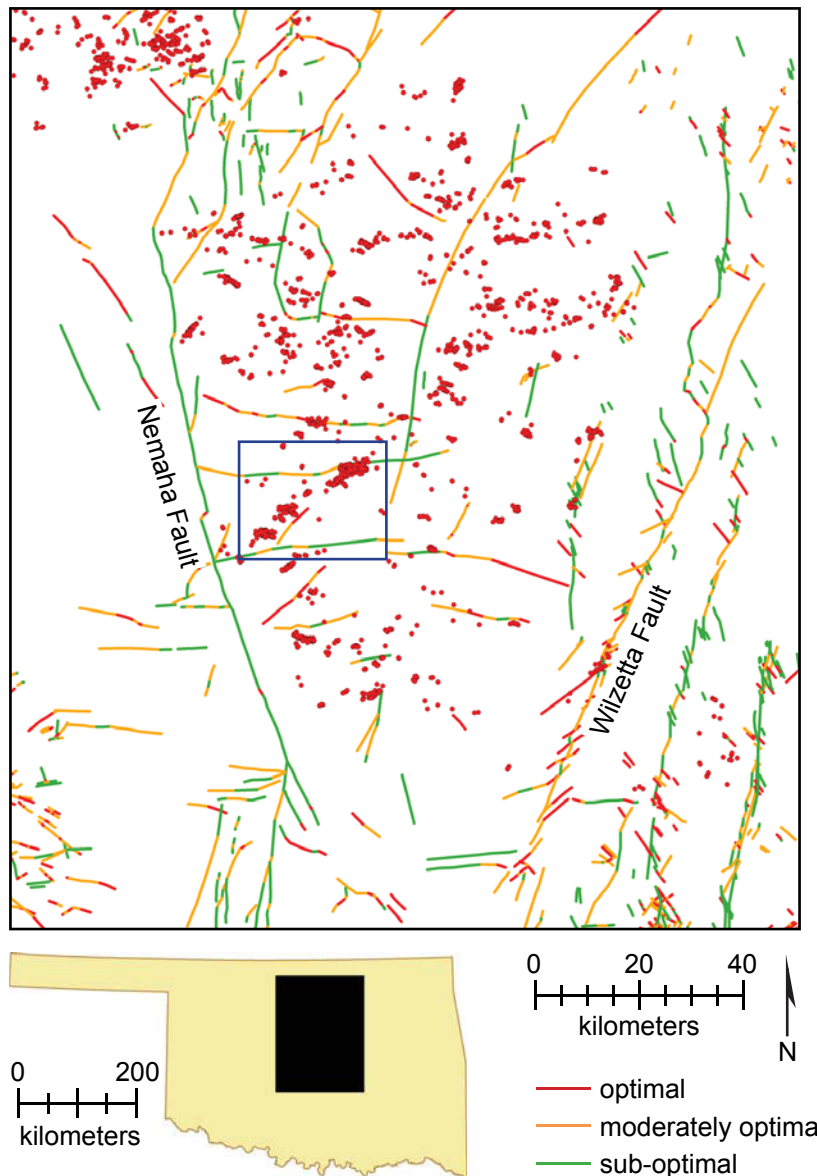


Figure 9. Map of faults in central Oklahoma, colored based on rank of optimal orientation (Darold and Holland, 2015). Blue rectangle is the study area for this thesis. Note the many epicenters (red dots) located far from any mapped fault, especially the optimally oriented faults.

### *Triggered Seismicity*

It is important to mention the role that wastewater injection has played in the increase in seismicity in Oklahoma although it is not a subject of study in this thesis. The OGS released a statement in April 2015 that “the rates and trends in seismicity are very unlikely to represent a naturally occurring process...The OGS considers it very likely that the majority of recent earthquakes...are triggered by the injection of produced water in disposal wells” (Andrews and Holland, 2015).

Hydraulic fracturing is not what causes these earthquakes, even though it is indirectly involved (Andrews and Holland, 2015). When a production well draws oil and gas out of the rock, water is also extracted. The water is usually briny and contaminated, and so is commonly called saltwater. It is injected back into the rock via saltwater disposal (SWD) wells at depths safe from drinking water aquifers. The 2011 M5.6 earthquake near Prague, Oklahoma and an earthquake swarm near Jones, Oklahoma have both been associated with SWD well injection (Keranen et al., 2013, 2014). It is possible that the events in the study area for this thesis are triggered by SWD injection; however, determining the trigger for seismicity will not be discussed in this thesis.

## CHAPTER THREE

### Methods

#### *Focal Mechanisms*

A focal mechanism is the geometry of the forces that produces a given seismic event (Stein and Wysession, 2003). The radiation pattern of P and S waves due to motion on a fault can be modeled as a pair of force couples, called a *double couple*. Using observations from multiple seismometers distributed around an earthquake epicenter, seismologists compute a *focal mechanism solution* for that earthquake, described mathematically as a *moment tensor*. The moment tensor has three orthogonal axial vectors (P, T, and N or B) whose direction and magnitude indicate the maximum instantaneous strain immediately surrounding the hypocenter during the initial pulse of energy. The P axis describes particle motion directed away from the hypocenter, the T axis describes motion toward it, and the N (or B) axis describes null particle motion perpendicular to P and T. Two orthogonal *nodal planes*, on which particle motion is also null, bisect the angle between the P and T axes, parallel to the N axis. One of the nodal planes is the fault plane solution; the other is designated the auxiliary plane. However, due to the double couple nature of earthquake focal mechanisms, the moment tensor is symmetrical, and therefore ambiguous as to which nodal plane is the fault plane solution and which one is the auxiliary plane. Thus, without additional information about the geology, it is impossible to determine the orientation of the actual fault.

Focal mechanism solutions are graphically represented by what is colloquially called a beachball diagram (Figure 10), although the term is misleading. The diagram is actually



a lower hemisphere projection, as though it was a bowl on a table rather than a beachball. In a focal mechanism diagram, the nodal planes are represented by lines dividing the black quadrants from the white, giving it a beachball appearance. These quadrants indicate the direction of the initial energy pulse as being toward the hypocenter (black) or away (white).

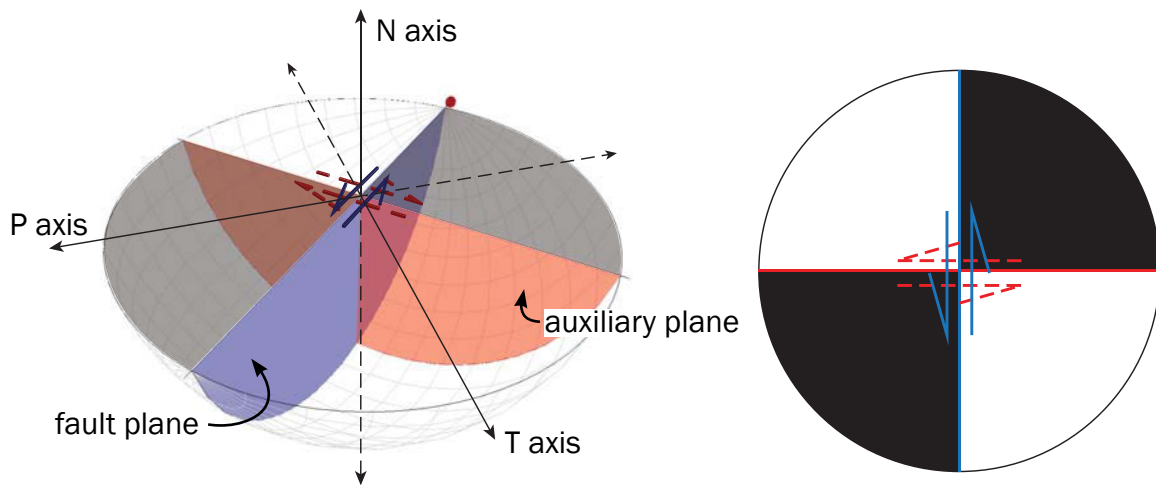


Figure 10. Explanatory diagram of a pure strike-slip focal mechanism solution. *Left* Lower hemisphere equal area projection is shown in 3D. The blue plane in this example is the fault plane. The red plane is the auxiliary plane. Relative motion indicated by the arrows *Right* The 2D focal mechanism diagram corresponding to the geometry on the left.

### *Data Collection*

Data for events in 2014 were obtained from an OGS catalog of relocated events (Darold et al., 2015) using the double-difference relocation method by Waldhauser and Ellsworth (2000) (Table 1). There are 22 events of  $M \geq 3.5$  from 2014 that were chosen for SLAM, most of which have strike-slip focal mechanisms. However, focal mechanism solutions (FMS) are not included in the double-difference catalog because they are computed individually (Darold et al., 2015), so I compared locations and origin times from both catalogs (Table 2) to cross correlate events and obtain the FMS for each event.

Hypocenter data for events in 2015 were obtained from a single-location event catalog provided by the Oklahoma Geological Survey (2015), because relocated events are not yet available. The FMS data for these events were obtained from the equivalent U.S. Geological Survey catalog because they were not available from the OGS. There are seven events of  $M \geq 3.5$  from 2014 that were chosen for SLAM in addition to the 22 obtained from the double-difference catalog.

Uncertainties in hypocenter location and in nodal plane orientation (strike and dip) are essential to the methods used in this study. The former were provided from all sources but the latter were not. When requested from the OGS, their response was that they had used multiple methods in generating focal mechanism solutions and the uncertainties are not consistent. Hence they chose not to report any associated uncertainty “for a variety of reasons” (Holland, personal communication, 2015a). I chose  $10^\circ$  as a reasonable but guessed uncertainty for all strikes and all dip angles.

#### *The Seismo-Lineament Analysis Method*

The Seismo-Lineament Analysis Method (SLAM) developed by Cronin et al. (2008) uses data from earthquake hypocenter locations and FMS, geomorphology, and geological fieldwork to spatially correlate an earthquake with the ground-surface trace of the fault that generated it. SLAM has been successfully used to locate several faults in various zones of active deformation such as the Santa Monica Mountains, California (Seidman, 2007; Millard, 2007; Cronin et al., 2008); Borah Peak, Idaho (Millard, 2007); Denali, Alaska (Millard, 2007); the Northern Arizona Seismic Belt (Lancaster, 2011); and the North Tahoe-Truckee area, California and Nevada (Lindsay, 2012; Reed, 2013). I used this method to attempt to correlate earthquakes in central Oklahoma with their genetic faults and determine if they rupture the ground surface, illustrated in a schematic diagram of the workflow (Figure 11).

Table 1. A. Hypocenter data used for detailed analysis. Uncertainties are 90% confidence intervals. Events marked with an asterisk (\*) occurred in 2015 and so these data were obtained from the single-events catalog, rather than the double-difference event catalog.

Thesis ID	OGS ID	Date	Time	Latitude	Longitude	Depth (km)	Mag-nitude	$e_x$ (km)	$e_y$ (km)	$e_z$ (km)
SW-1	467	2/17/2014	4:54:59	35.776603	-97.472339	5.276	3.7	0.1772	0.1334	0.2598
SW-2	1440	4/10/2014	7:33:57	35.776652	-97.486466	6.408	3.9	0.1810	0.1397	0.2126
SW-3	1503	4/13/2014	20:02:21	35.774736	-97.484416	6.214	3.5	0.1792	0.1387	0.2071
SW-4	1577	4/20/2014	19:07:13	35.774577	-97.484302	6.773	3.7	0.1803	0.1400	0.2080
SW-5	2123	5/22/2014	2:46:10	35.777865	-97.490788	6.609	3.5	0.2000	0.1735	0.2708
SW-6	2500	6/26/2014	5:26:44	35.778048	-97.49349	6.233	3.6	0.1812	0.1421	0.2135
SW-7	2501	6/26/2014	5:38:57	35.773816	-97.486947	5.794	3.5	0.1774	0.1458	0.2157
SW-8	3236	8/19/2014	12:41:35	35.774674	-97.476758	7.109	4.1	0.1826	0.1495	0.2345
M-1	3546	9/15/2014	20:08:03	35.814421	-97.428003	4.971	3.7	0.2917	0.2708	0.3092
M-2	3626	9/19/2014	17:23:17	35.815267	-97.426676	4.889	3.7	0.2906	0.2698	0.3213
M-3	5040	12/7/2014	22:13:08	35.821305	-97.44375	4.669	3.6	0.2918	0.2706	0.3101
M-4	5441	12/25/2014	20:32:49	35.814368	-97.41757	5.327	3.5	0.3035	0.2799	0.2870
M-5*	15757	1/4/2015	2:23:47	35.81959	-97.43621	6.604	3.6	1	0.6	1.7
M-6*	15858	1/7/2015	14:58:54	35.81728	-97.42906	6.933	3.8	0.8	0.5	1.5
M-7*	15900	1/9/2015	16:03:03	35.81433	-97.41796	6.964	3.5	0.8	0.4	1.4
M-8*	16481	2/16/2015	23:28:03	35.8175	-97.44904	5.274	3.5	0.7	0.4	0.9
M-9*	16755	3/9/2015	7:10:46	35.81503	-97.44809	4.525	3.9	0.8	0.5	1.1
M-10*	17428	4/8/2015	15:09:02	35.81925	-97.41908	2.487	4.3	0.9	0.6	2.2
M-11*	18086	5/18/2015	17:11:46	35.80821	-97.44524	5.398	3.8	1.6	1.1	3.1

Table 1.B. Hypocenter data used for detailed analysis. Uncertainties are 90% confidence intervals. Events marked with an asterisk (\*) occurred in 2015 and so these data were obtained from the single-events catalog, rather than the double-difference event catalog.

Thesis ID	OGS ID	Date	Time	Latitude	Longitude	Depth (km)	Mag-nitude	$e_x$ (km)	$e_y$ (km)	$e_z$ (km)
NE-1	329	2/9/2014	9:37:01	35.892692	-97.30424	2.827	3.8	0.3438	0.2463	0.5041
NE-2	938	3/11/2014	7:41:38	35.887512	-97.284595	5.231	3.5	0.2125	0.1274	0.3493
NE-3	1091	3/22/2014	6:44:16	35.885042	-97.297559	4.443	3.7	0.2239	0.202	0.3151
NE-4	1351	4/4/2014	9:50:26	35.89384	-97.270109	4.921	3.5	0.2129	0.1371	0.3445
NE-5	1377	4/6/2014	3:24:40	35.893323	-97.270475	5.132	3.7	0.2136	0.1348	0.3518
NE-6	1397	4/7/2014	8:52:01	35.890332	-97.276196	5.435	4.1	0.2140	0.1214	0.3410
NE-7	2517	6/26/2014	2:52:50	35.887134	-97.265031	4.742	3.6	0.2131	0.1411	0.3493
NE-8	2519	6/27/2014	2:16:01	35.886483	-97.262354	4.62	3.5	0.2134	0.1416	0.3526
NE-9	2523	6/27/2014	12:55:27	35.887097	-97.31425	4.941	3.7	0.2311	0.1461	0.3237
NE-10	2730	7/12/2014	3:05:58	35.86425	-97.325627	4.456	3.9	0.2358	0.1423	0.3474

Table 2. Focal mechanism data used for SLAM. The data were arranged so that the ~NE-SW trending nodal plane is labeled A and the nodal plane trending ~NW-SE is labeled B. Events marked with an asterisk (\*) occurred in 2015 and so these data were obtained from the single-events catalog, rather than the double-difference event catalog.

Thesis ID	Strike A	Dip A	Strike B	Dip B
SW-1	212	68	302	90
SW-2	23	88	113	90
SW-3	28	90	298	77
SW-4	202	51	302	78
SW-5	20	85	110	89
SW-6	13	68	280	82
SW-7	24	78	293	85
SW-8	204	68	294	90
M-1	30	72	297	81
M-2	41	65	303	74
M-3	57	85	327	85
M-4	50	79	316	72
M-5*	218	74	312	77
M-6*	216	84	309	63
M-7*	55	67	322	83
M-8*	216	82	120	55
M-9*	229	67	130	70
M-10*	33	80	301	81
M-11*	236	79	327	83
NE-1	201	67	101	68
NE-2	61	78	327	72
NE-3	203	36	76	66
NE-4	46	88	315	75
NE-5	51	90	321	77
NE-6	54	78	320	42
NE-7	212	69	117	78
NE-8	203	69	108	78
NE-9	191	88	101	78
NE-10	28	90	298	87

Table 3. Comparison of single-event and double-difference catalogs. The values in the table are the absolute values of the difference between the catalogs. There were three events in the single-event catalog that were possible matches for SW-2 from the double-difference catalog. The first record in this table is the one that was chosen. The last two records in this table were excluded from the study because they are too similar to each other and only one possible match exists in the single-event catalog.

Thesis ID	Origin Time (sec)	Latitude	Longitude	Depth (km)	Magnitude
SW-1	59	0.001	0.003	2.084	0
SW-2*	57	0.001	0.005	0.392	0
SW-3	21	0.004	0.001	0.074	0
SW-4	13	0.001	0.002	0.053	0
SW-5	10	0.000	0.023	0.371	0
SW-6	44	0.006	0.002	1.233	0
SW-7	57	0.005	0.002	0.234	0
SW-8	35	0.002	0.009	2.189	0
M-1	3	0.000	0.001	0.541	0
M-2	17	0.003	0.007	0.749	0
M-3	8	0.002	0.004	0.481	0.3
M-4	49	0.002	0.001	1.623	0.4
NE-1	1	0.000	0.013	2.173	0
NE-2	27	0.002	0.002	0.341	0
NE-3	58	0.003	0.001	1.503	0
NE-4	47	0.000	0.002	0.299	0
NE-5	54	0.001	0.004	0.052	0
NE-6	3	0.001	0.002	0.275	0
NE-7	3	0.001	0.002	0.248	0
NE-8	46	0.003	0.002	0.140	0
NE-9	2	0.001	0.004	0.059	0
NE-10	46	0.002	0.001	0.406	0
*SW-2	57	0.005	0.001	0.392	0
*SW-2	3	0.004	0.001	0.432	0.7
*SW-2	3	0.001	0.000	0.532	0.9
excluded	43	-0.005	0.003	0.409	0
excluded	41	-0.002	0.000	0.435	0

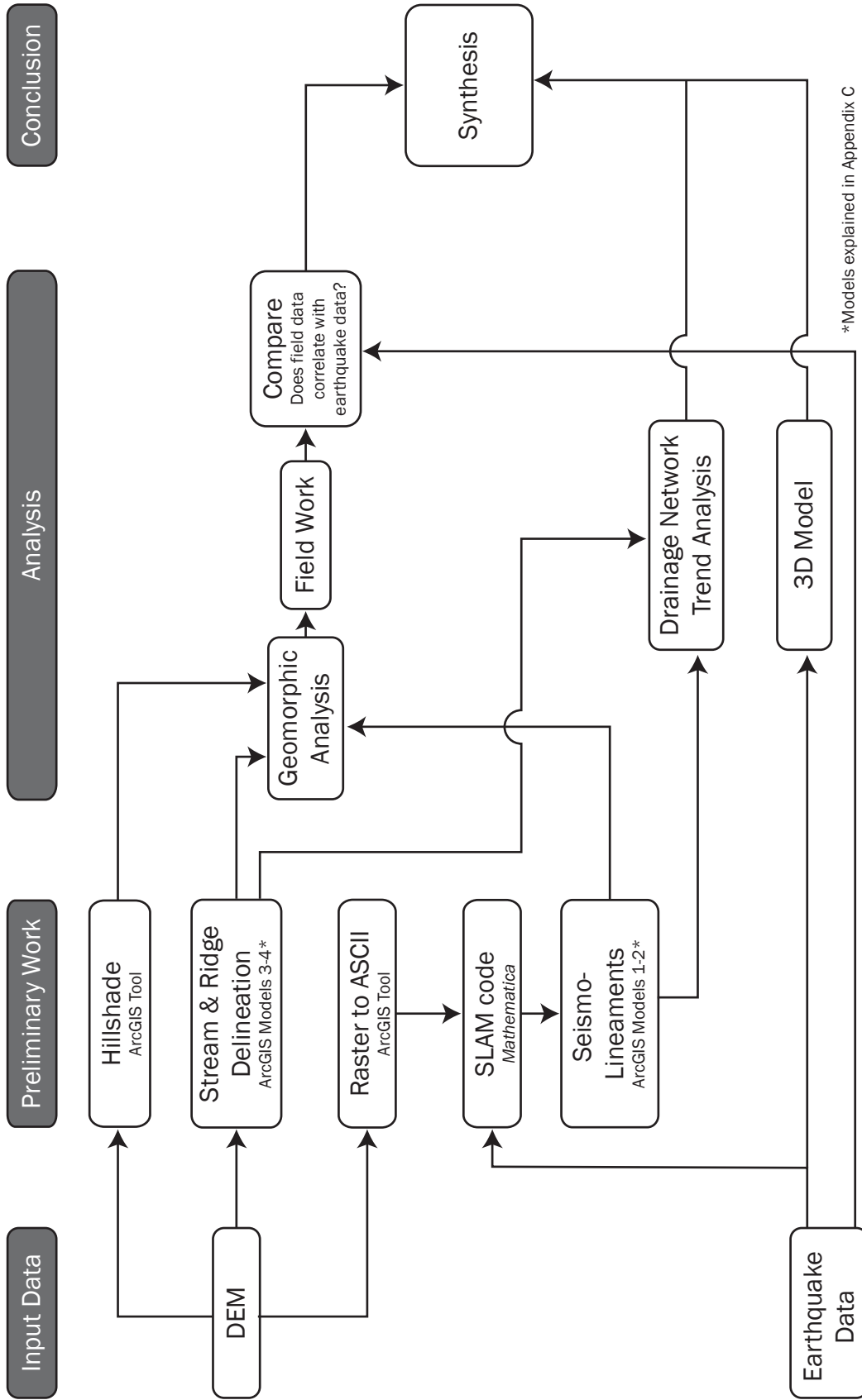


Figure 11. Schematic diagram of entire workflow.

### Defining Seismo-Lineament Boundaries

The ground surface is modeled by a hillshade image derived from a 1/3 arc-second (~10 meter resolution) digital elevation model (DEM) obtained from the U.S. Geological Survey (2015b). The uncertainties for a given hypocenter form a theoretical ellipsoid surrounding it. When all the uncertainties in hypocenter location and nodal plane orientation are null, the intersection of the nodal plane with the ground surface defines an irregular curve, controlled by the terrain. The SLAM code, written in *Mathematica* (Cronin, 2014a; Cronin and Rasaka, 2015), projects planes to the hillshade that are parallel to the nodal planes and tangent to the hypocenter uncertainty ellipsoid, to produce an aerial swath. When the uncertainties in the strike and dip trend of the nodal plane are included, the shape of the swath resembles a bow tie. This swath, representing the intersections of all possible nodal planes with the ground surface, is called a seismo-lineament (Figure 12). The surface trace of a given fault might be found within the seismo-lineament if (1) the nodal plane is coincident with the fault, (2) the fault ruptures the ground surface and (3) it is approximately planar.

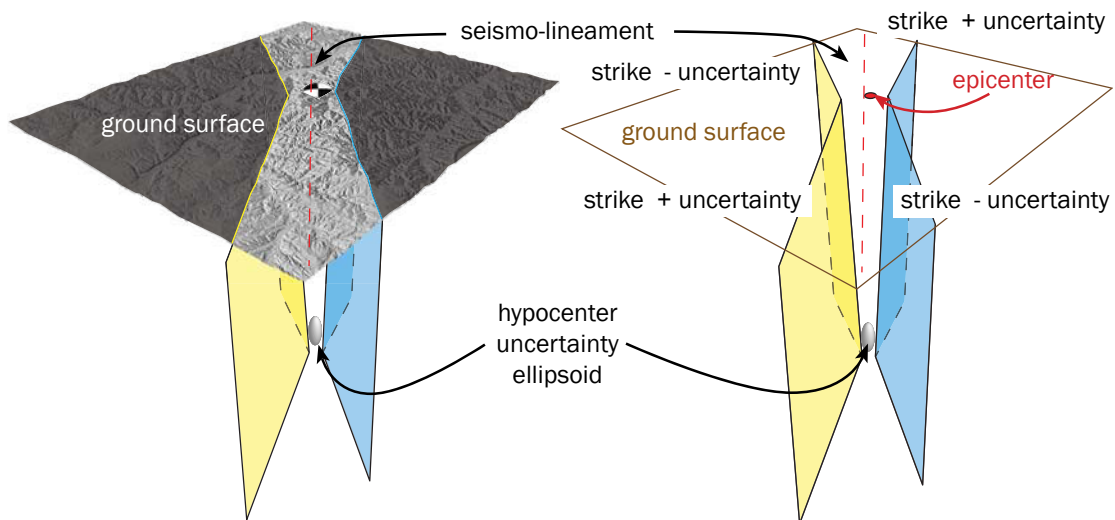


Figure 12. Diagram of the geometry of a seismo-lineament. Adapted from Reed (2013).



### *Event Groupings*

I used a method outlined by Holland (2014) in which I first determined the inter-event azimuth for each pair of events within each cluster using the Line Measure tool in Google Earth. Because of the uncertainty in such measurements, I rounded the figures to the nearest integer. Then I compared the inter-event azimuth with the strikes of each event's FMS. If both FMS have strikes that are within  $10^\circ$  of each other and within  $30^\circ$  of the inter-event azimuth, then I grouped the pair together. I added to the pairs any other events whose inter-event azimuth and FMS strike also fell within the same range. Where two events were very close to each other, their inter-event azimuth was ignored as criteria because they would still be likely genetically related to the same fault.

### *Geomorphic Analysis*

Because faults often form linear features on the ground surface visible in remotely sensed data, I analyzed the geomorphology of the study area using a shaded relief map in ArcGIS, called a hillshade. Lineaments in the topography parallel to a given nodal plane are accentuated if the hillshade is illuminated perpendicular to the strike of that nodal plane, allowing for enhanced identification of features potentially related to faulting. I highlighted key features as potential surface traces of faults and labeled each with the rationale for which it was chosen. Table 4 is a list of such features (Cronin et al., 2008, after Ray, 1960; Miller, 1961; Wesson et al., 1975; Bonilla, 1982; Slemmons and DePolo, 1986; Cronin et al., 1993; McCalpin, 1996; Burbank and Anderson, 2011).

ArcGIS is equipped with several watershed analysis scripts which, when applied to a DEM, produce a vector shapefile of all of the drainages (Appendix A). I used these scripts to produce such a shapefile for the study area. Then, using the ArcGIS Raster Calculator I reproduced the DEM with inverse values and ran the scripts again, resulting in another

shapefile that represents the ridge lines. I ran these shapefiles through another script in ArcGIS called Linear Directional Mean that produces a straight line for each drainage or ridge line segment, representing its mean azimuth, length and geographic center. To aid in the geomorphic analysis, I filtered these new shapefiles for each earthquake based on the nodal plane strike  $\pm 10^\circ$ , which highlights ridges and drainages that might correspond with faults for each event. (Figure 13)

Table 4. Potential geomorphic indicators of faulting.

Description of Feature
Stream channels aligned on opposite sides of a drainage divide
A lower-order (smaller) stream channel aligned across a higher-order stream channel
An anomalously straight segment of a stream channel
Aligned straight segments of one or more stream channels
A lower-order stream channel, the trend of which is directed upstream relative to the higher-order stream it intersects, so water flowing from the smaller stream into the larger stream has to change directions through an obtuse angle
Abrupt changes in gradient along a stream channel
A stream channel that steps down in the direction of flow, indicated by rapids or a waterfall
A stream channel that steps up in the direction of flow, indicated by a pond
Apparent lateral deflection of an incised stream channel or floodplain
Abrupt changes in gradient along a ridge crest
A ridge crest that steps down abruptly in the direction of decreasing elevation
A ridge crest that steps up in the direction of decreasing elevation
A saddle in the ridge crest
Apparent lateral deflection of a ridge crest
Abrupt changes in the gradient of a surface localized along a narrow linear step (fault scarp)
Benches or faceted spurs at the base of ridges that are apparently unrelated to erosion
A set of ridges in an en echelon array
A topographic basin along a linear trough (pull-apart basin, sag pond)
A topographic hill along a linear trough (pop-up, pressure ridge)
A ridge across the mouth of a stream drainage that is not a glacial moraine (shutter ridge)

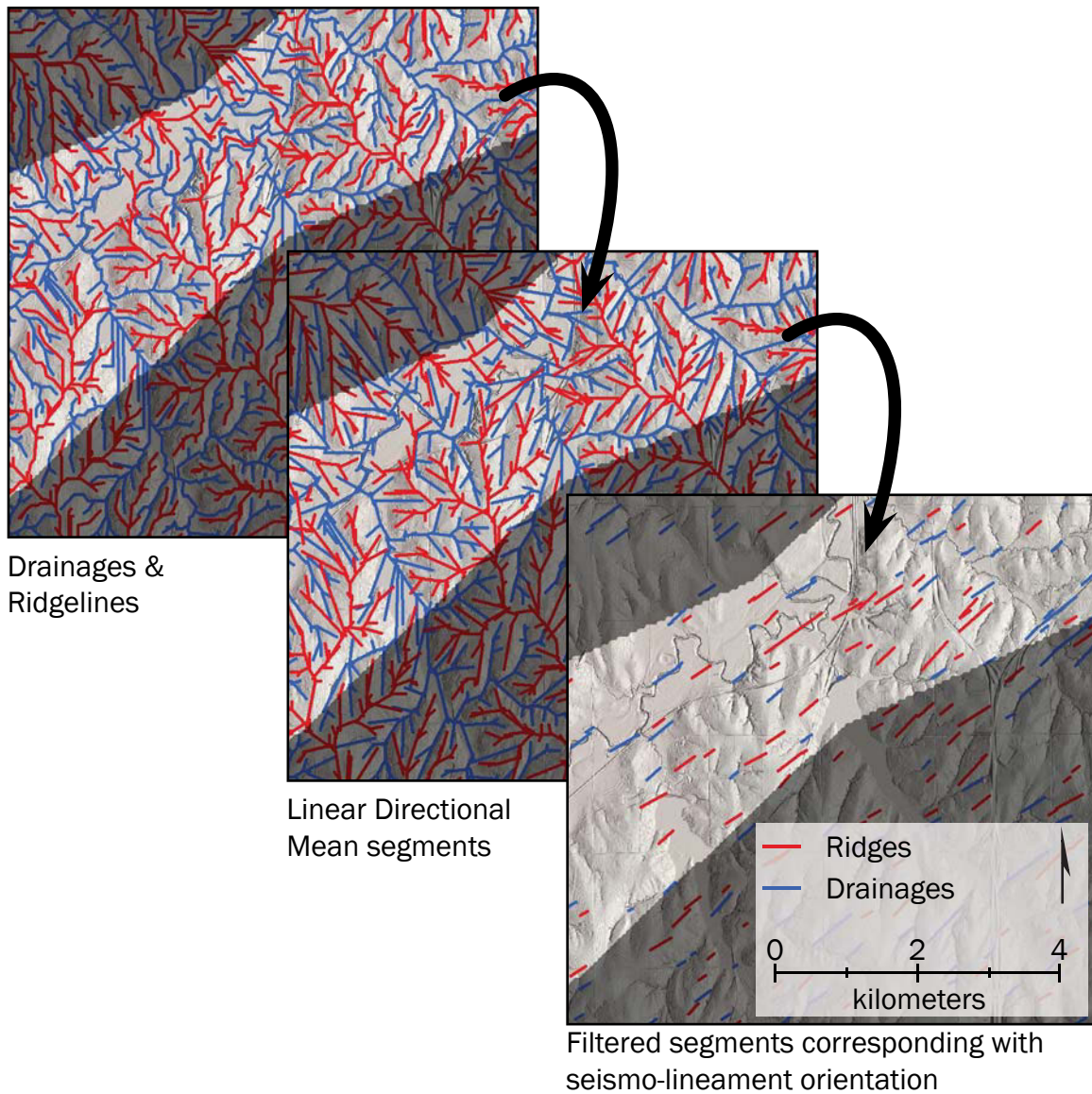


Figure 13. Sample location demonstrating ridgeline and drainage delineation. The Linear Directional Mean script in ArcGIS produces the mean location, length, and orientation of every drainage and ridge segment. The result can be filtered to display segments of a specified range.

### *Field Investigations*

The geomorphic analysis provides testable hypotheses for the location of seismogenic faults. Field work is used to search for physical evidence of faulting in evaluation of these hypotheses. In the case that such evidence is found, observations are documented, including GPS coordinates, physical descriptions of the lithologies on either

side of the lineament, photographs, measurements of the strike and dip of fault planes, measurements of shear striations, measurements of fault offset, and uncertainties for all measurements. These observations are later compared with the focal mechanism and seismo-lineament for each earthquake for correlation.

Based on accessibility to geomorphic lineaments I chose six locations for field investigation. Only lineaments that intersected roads or were within reasonable hiking distance were selected for investigation. Due to the small magnitude of the earthquakes and the lack of any major tectonic activity for 300 million years to disrupt the horizontality of the strata, it is assumed that any ground rupture from recent faulting, and evidence thereof, would be small or non-existent. Therefore, I did not expect to discover any features that a geologist might normally expect to observe in association with recent faulting, such as landslides, springs, differential weathering patterns, or shear striations (Reed, 2013). The features and anomalies that we looked for include fractures with observed displacement, abrupt changes in gradient across dirt roads, abrupt and linear changes in autumn coloring of trees and foliage. All observations were documented and photographs were taken.

### *Three-Dimensional Model*

I modeled all of the hypocenters in the study area in three dimensions in order to more clearly “see” the faults. In ArcScene, 3D modeling software in the ArcGIS Desktop suite, I imported the shapefile containing hypocenter data as well as the DEM and hillshade for the study area. When first imported, all data are assumed to have no z values. Using the Base Heights tab for each dataset, I assigned z values. For the hillshade, the z values are stored in the DEM raster. The elevation values of the hypocenter dataset are stored as positive values in kilometers, whereas the DEM is in meters, so I set its z values to  $\text{Depth}*(-1000)$  to match the DEM. (Figure 14)

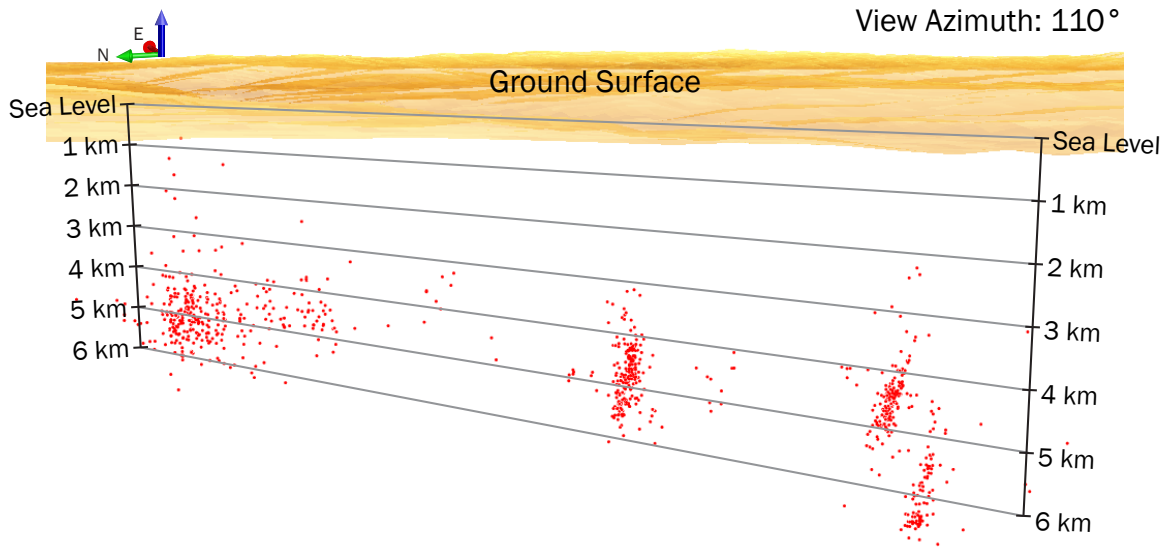


Figure 14. Three-dimensional model of hypocenters in the study area.

#### *Drainage Network Trend Analysis*

In order to determine if there is a preferred orientation for drainages within seismo-lineaments and if that orientation aligns with the nodal planes, I analyzed the orientations of drainage segments. I selected all the linear drainage segments (produced by the Linear Directional Mean ArcGIS script) located within any seismo-lineament from each event group to a maximum distance of 10 km from the epicenters (Figure 15), then organized them into 5° bins based on their azimuth. I generated rose diagrams with the length of each bin wedge indicating the cumulative length of all drainages in that azimuthal range.

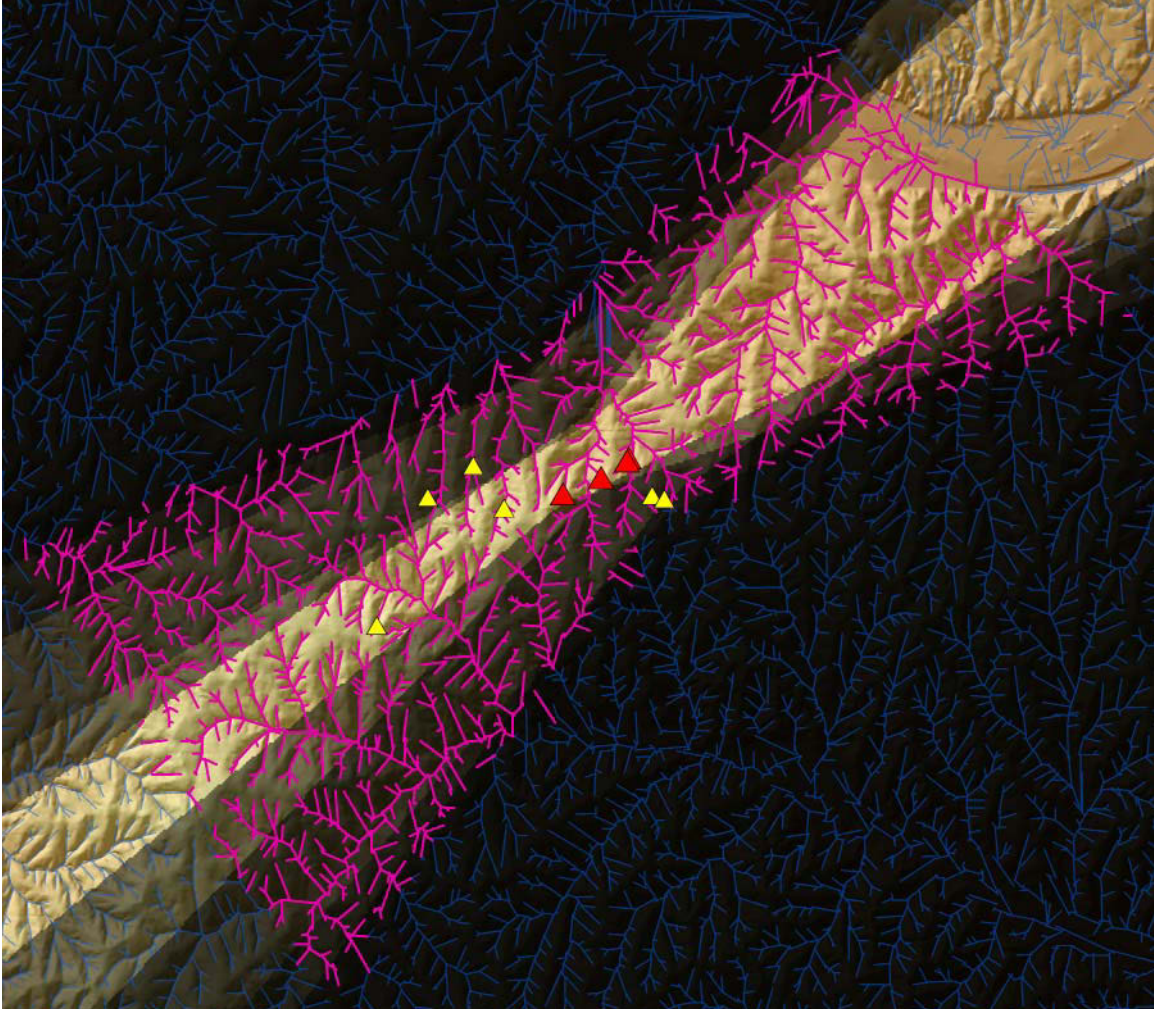


Figure 15. Example of drainage selection for trend analysis from for the NE-A2 even group. The blue lines are all drainages. Magenta lines are those selected for analysis. Yellow triangles are epicenters in this thesis. Red triangles are the events in this group (NE-2, NE-4, NE-5, and NE-6).

## CHAPTER FOUR

### Results

#### *Seismo-lineaments*

For each cluster, most of the seismo-lineaments produced by the *Mathematica* code were very similar to each other; initial observations are described below. There were, however, a few notable exceptions, also described below.

#### *Southwest and Middle Clusters*

There are no obvious fault-related lineations in the SW or the M clusters. The few potential lineations align with the northeast-trending seismo-lineaments rather than along the southeast-trending ones where we would expect to find them based on the spatial distribution of epicenters in the cluster. (Figure 16, Figure 17)

#### *NE Cluster*

Most of the lineations appear to approximately align with the directional trend of the distribution of epicenters in the NE cluster. However, as was the case in the previous clusters, none of the lineations appear to be obviously related to faulting. (Figure 18)

#### *Anomalous Seismo-Lineaments*

Most of the earthquakes in this study have steeply-dipping strike-slip focal mechanisms. But the SW-4 event, nodal plane A has a dip angle of  $51^\circ$  (Figure 19) and the M-8 event, nodal plane B has a dip angle of  $51^\circ$  (). Event NE-3 has a primarily normal focal mechanism with a slight strike-slip component (Figure 21). One nodal plane dips  $36^\circ$  and the other  $66^\circ$ .

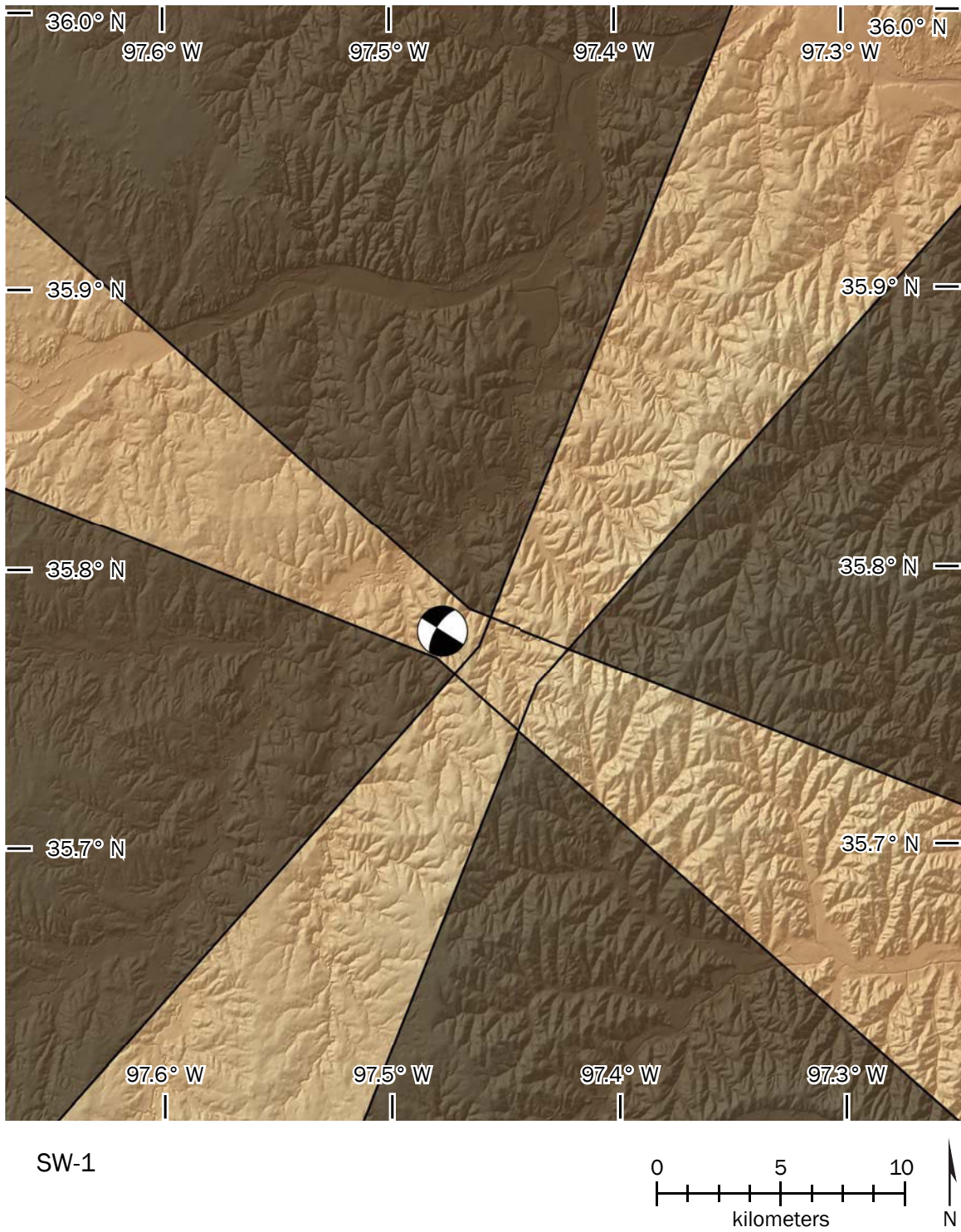


Figure 16. Characteristic seismo-lineaments for the SW Cluster.



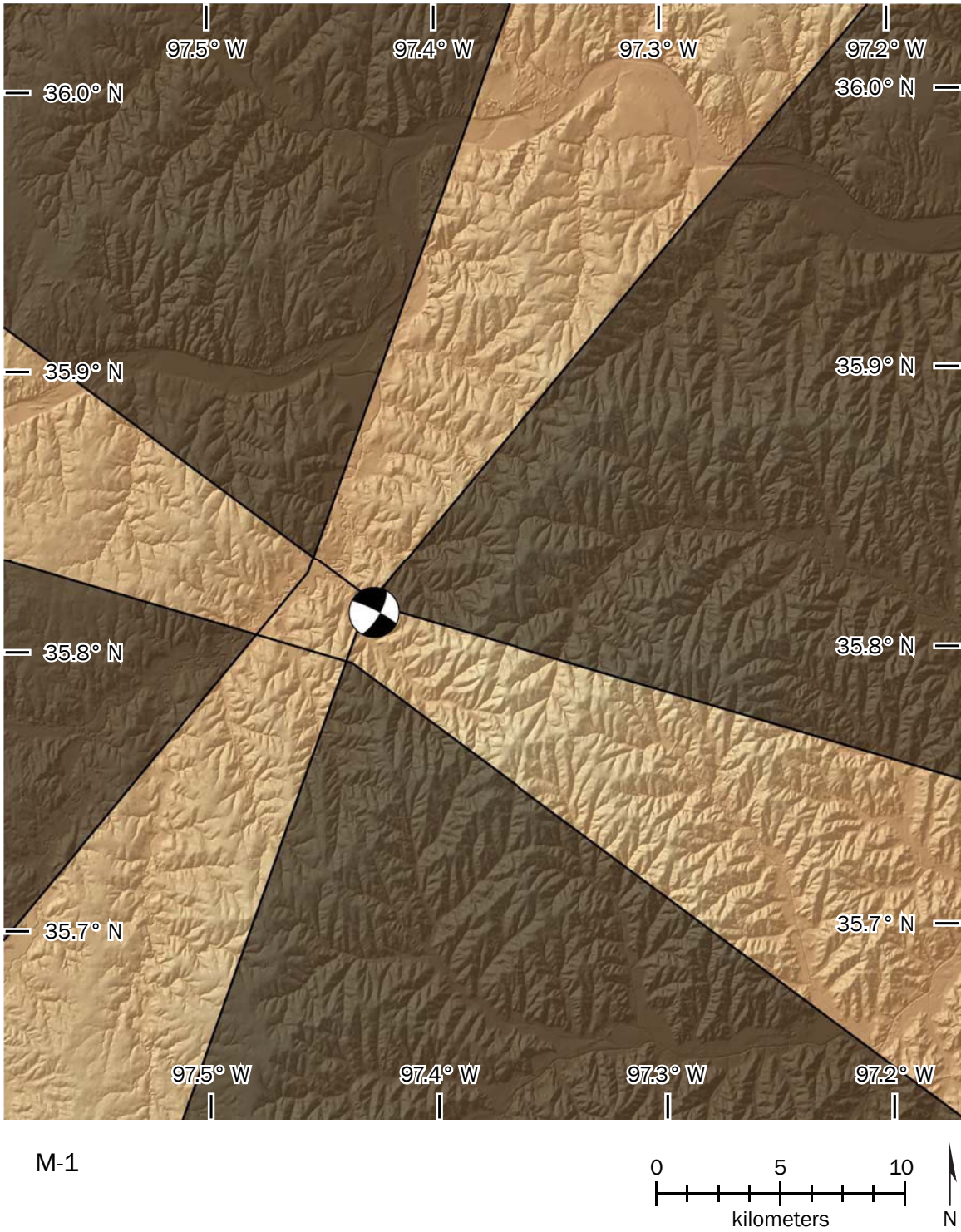


Figure 17. Characteristic seismo-lineaments for the M Cluster.

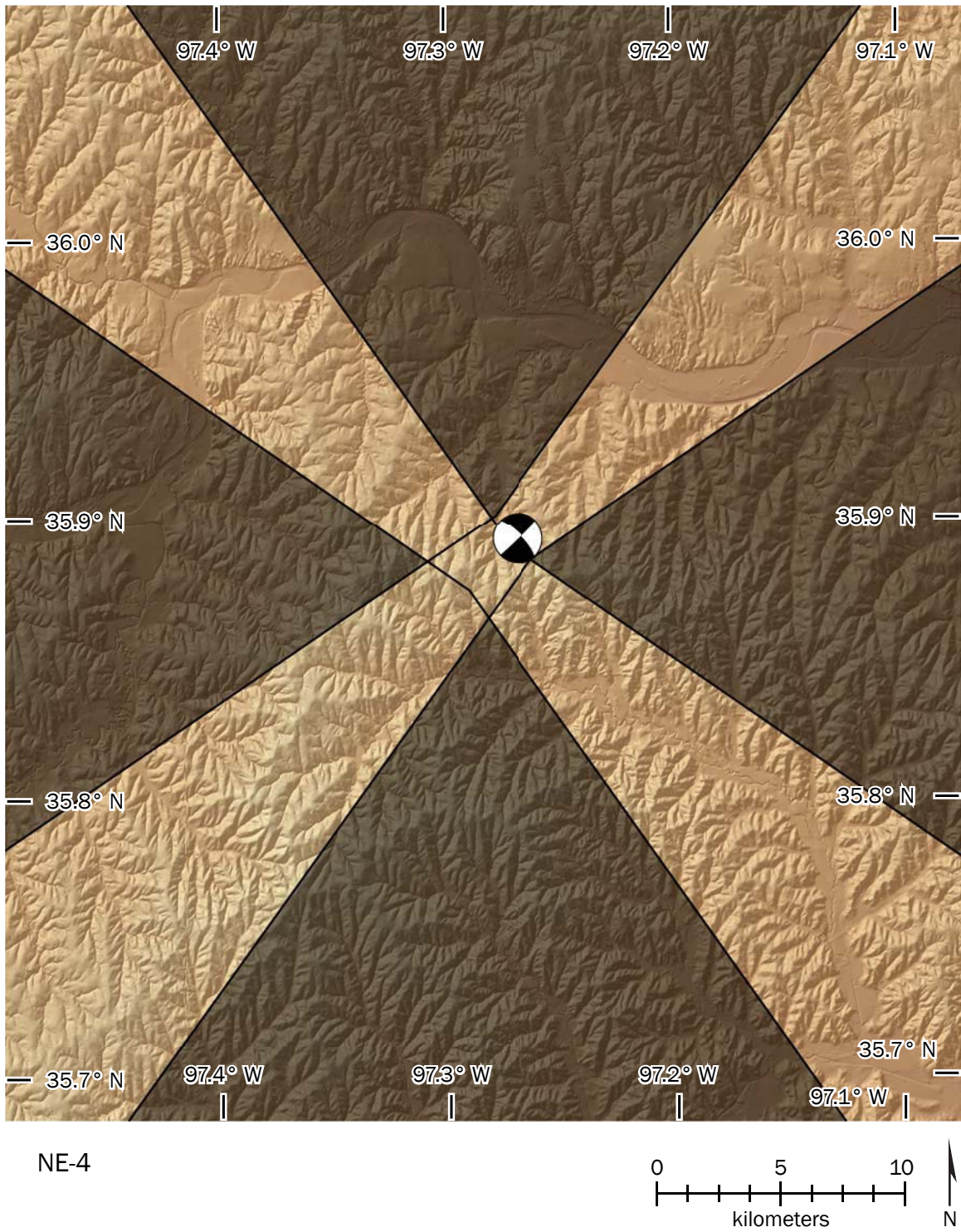


Figure 18. Characteristic seismo-lineaments for the NE Cluster.

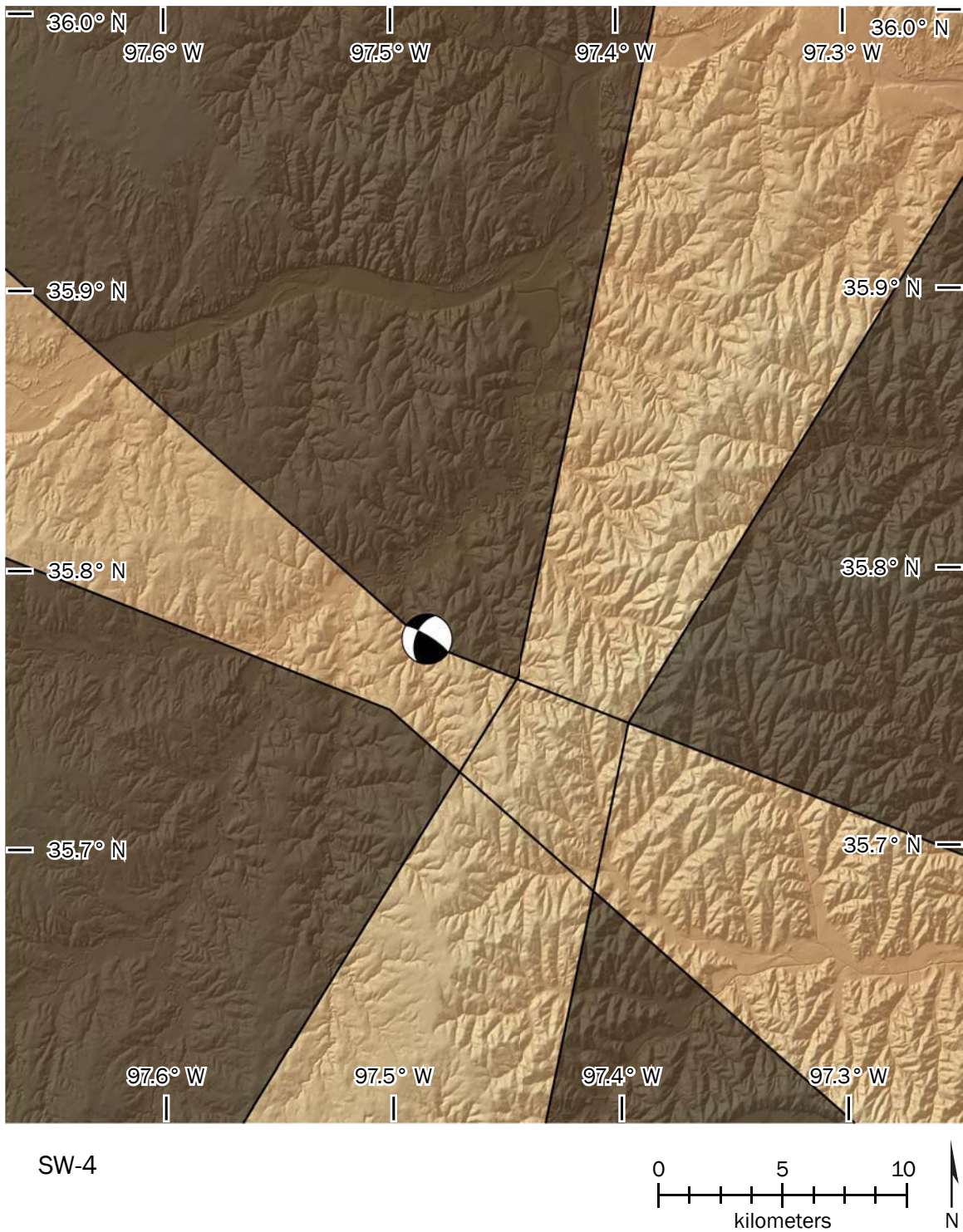


Figure 19. Seismo-lineaments for the event SW-4. The NE-trending nodal plane has a dip angle of  $51^\circ$ .

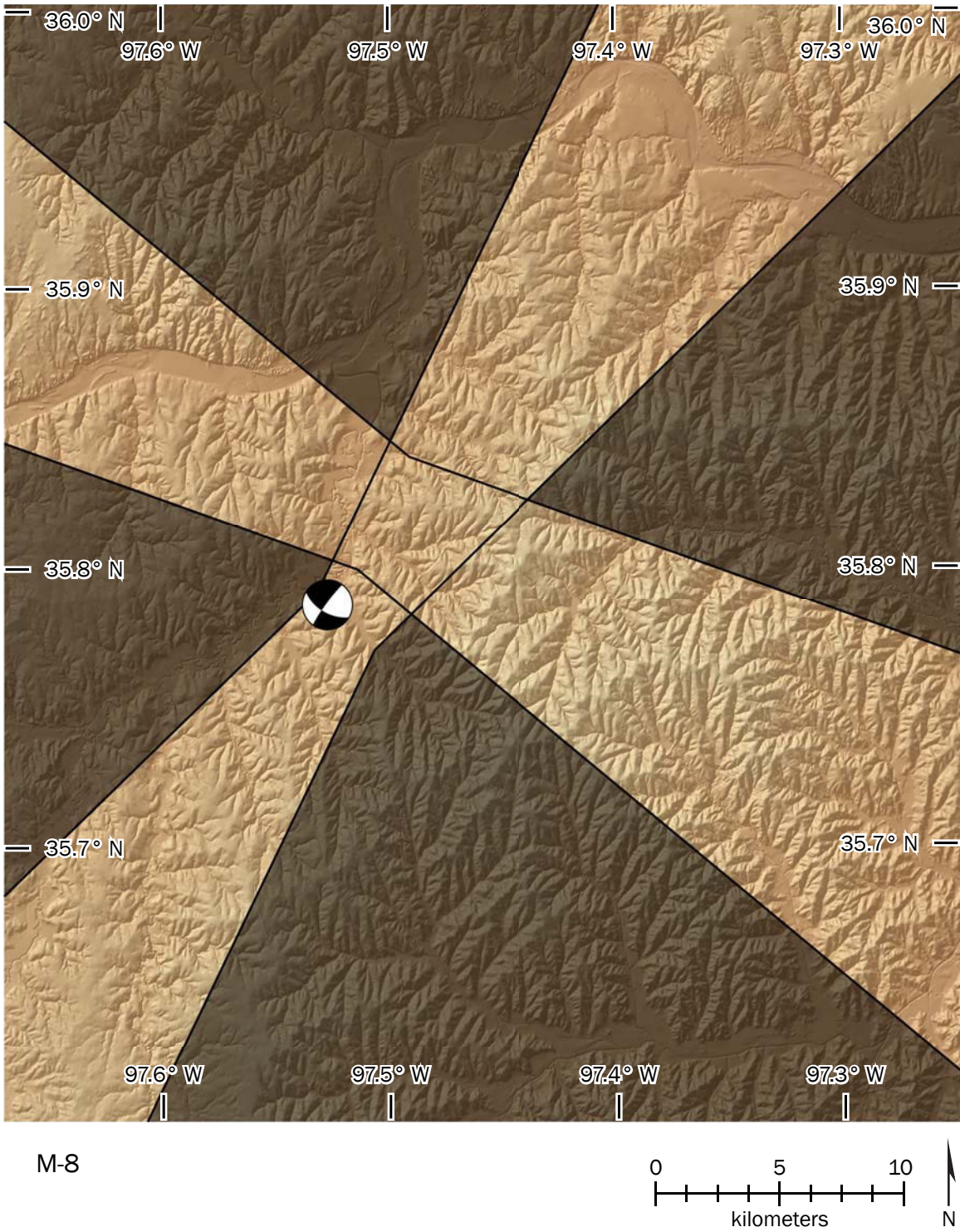


Figure 20. Seismo-lineaments for the event M-8. The NW-trending nodal plane has a dip angle of  $55^\circ$ .

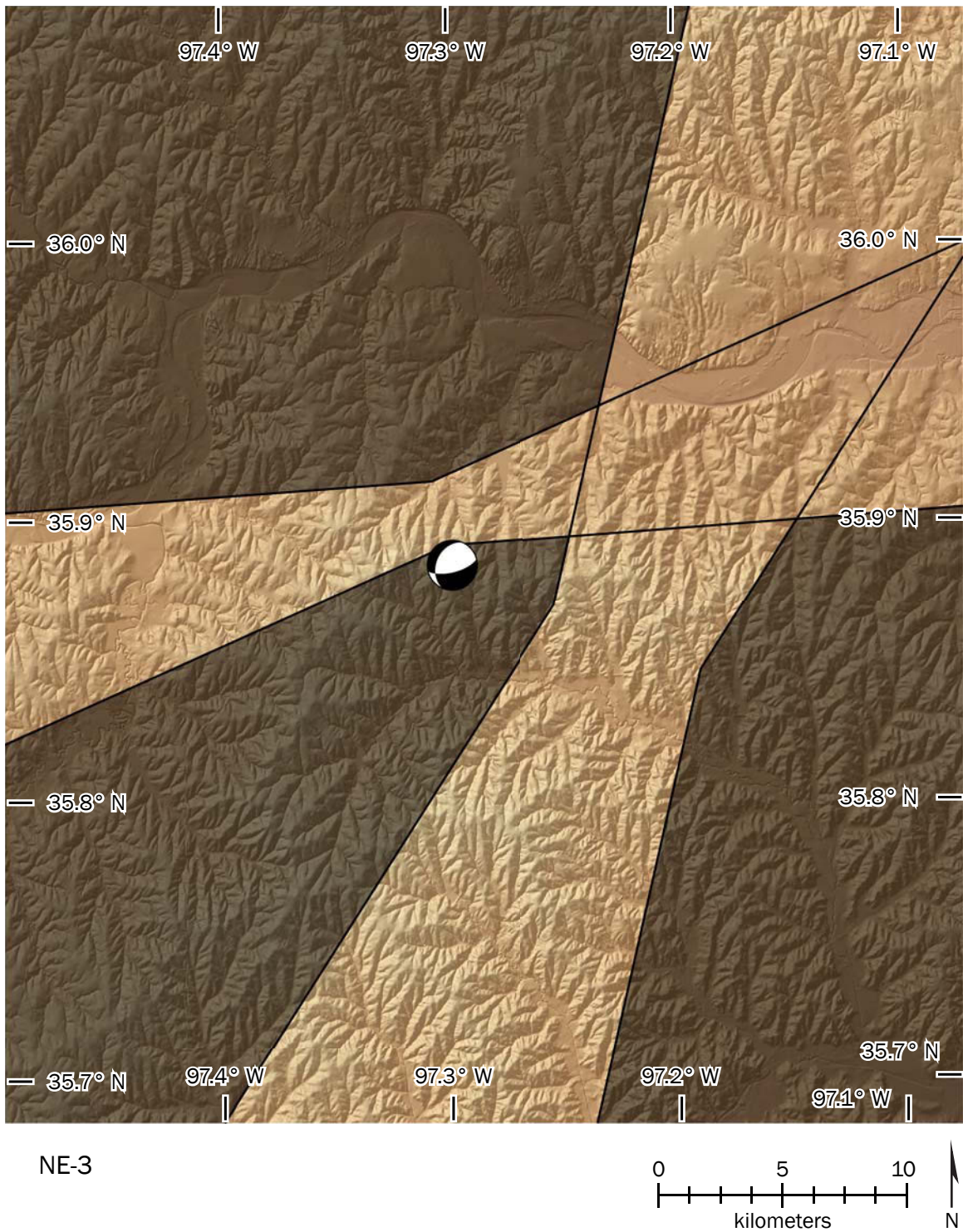


Figure 21. Seismo-lineaments for the event NE-3 which has a strong normal fault component rather than mostly strike-slip like the majority of the others.

### *Event Groupings*

Most events grouped with at least one other event. Figure 22 shows these groups and the relevant geomorphic lineaments within the overlapping seismo-lineaments. However M-8 and NE-3 were not able to be grouped. In the case of NE-3, the inter-event azimuth was not coincident with the strike of either focal mechanism solution. In the case of M-8, even though its seismo-lineament did match up well with that of M-1, M-2, and M-3, giving the impression that they can be grouped because they nearly intersect at the ground surface; however, their dip vectors are in opposite directions, meaning they diverge at depth.

### *Geomorphic Analysis*

Figure 23 shows the lineaments discovered in the geomorphic analysis and Table 5 gives the rationale for each. None of the lineaments are an obvious geomorphic expression of faulting; however, the most promising one is along an apparently offset stream bed, consistent with what one would expect of a right-lateral strike slip fault in this orientation (Figure 21.J). If evidence can be found to verify this, then it means that such faulting has occurred in the distant past as well as in the present. The magnitude of current events is far too small to have produced the ~200 meters of displacement seen here.

During the writing of this thesis, after the field work had already been conducted, I found two additional geomorphic lineations align with and are located within seismo-lineaments. It was too late in the process to return to the field to investigate these. However, they might be investigated in future work related to this work. These lineaments are identified with an asterisk (\*) in Table 5.

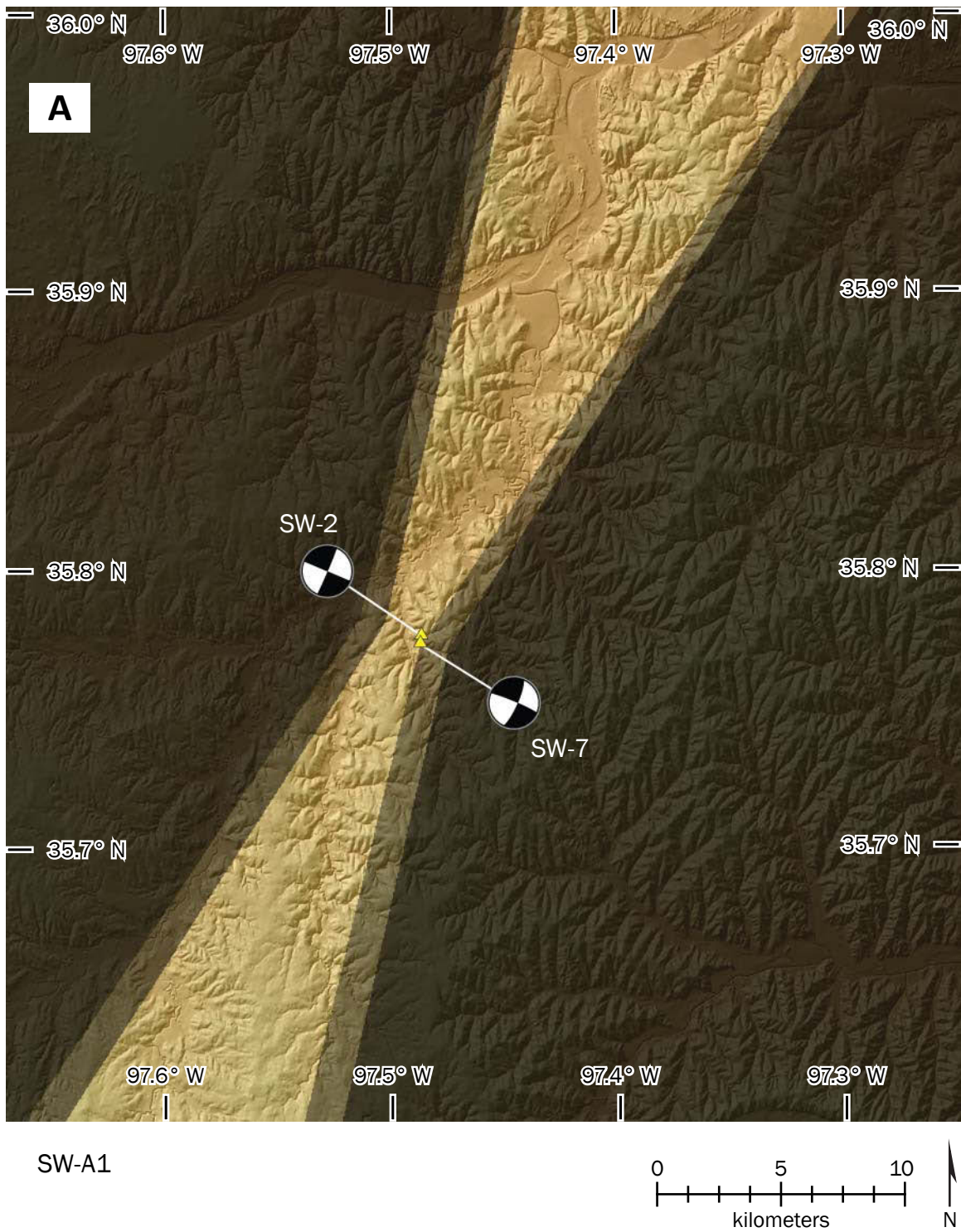
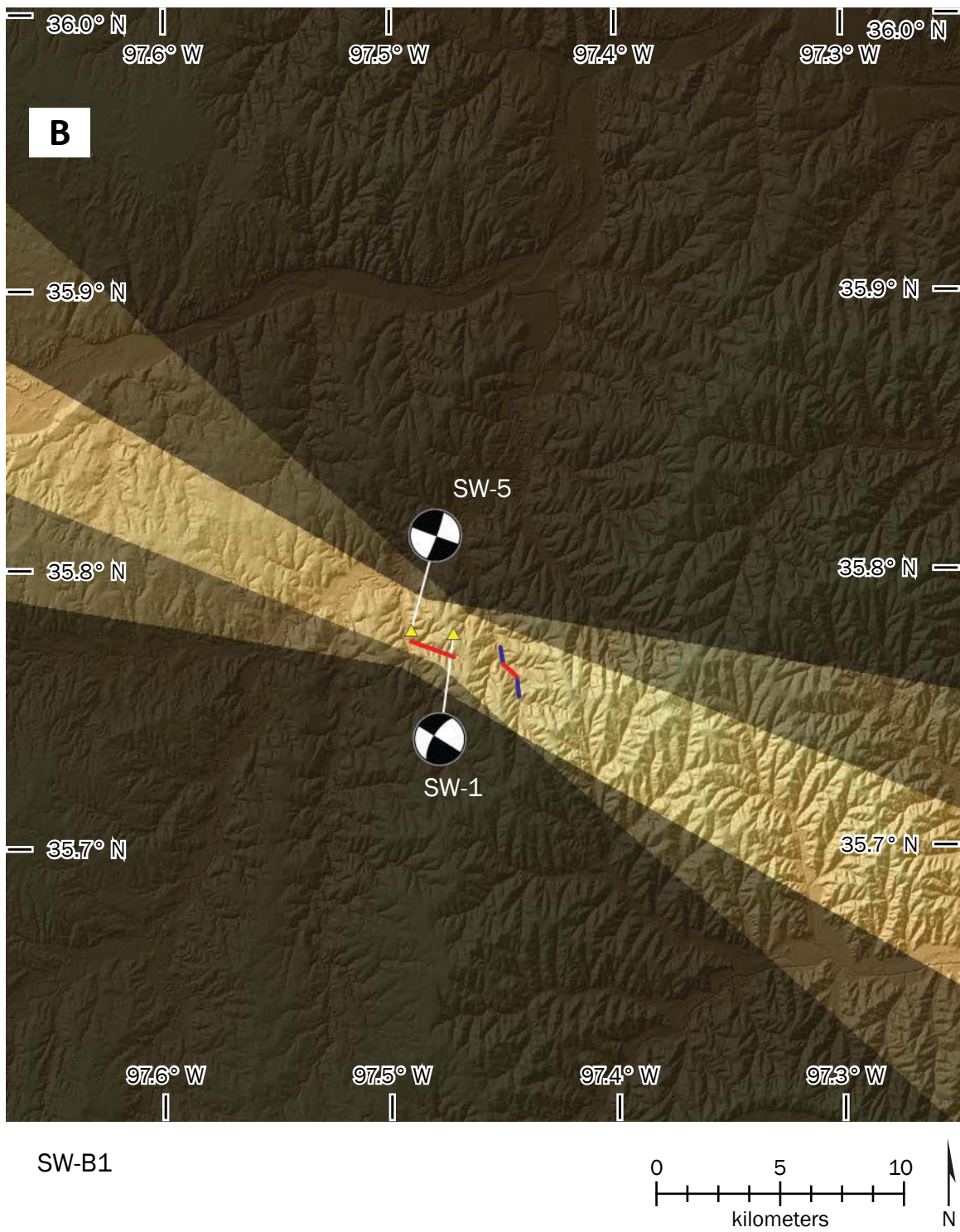
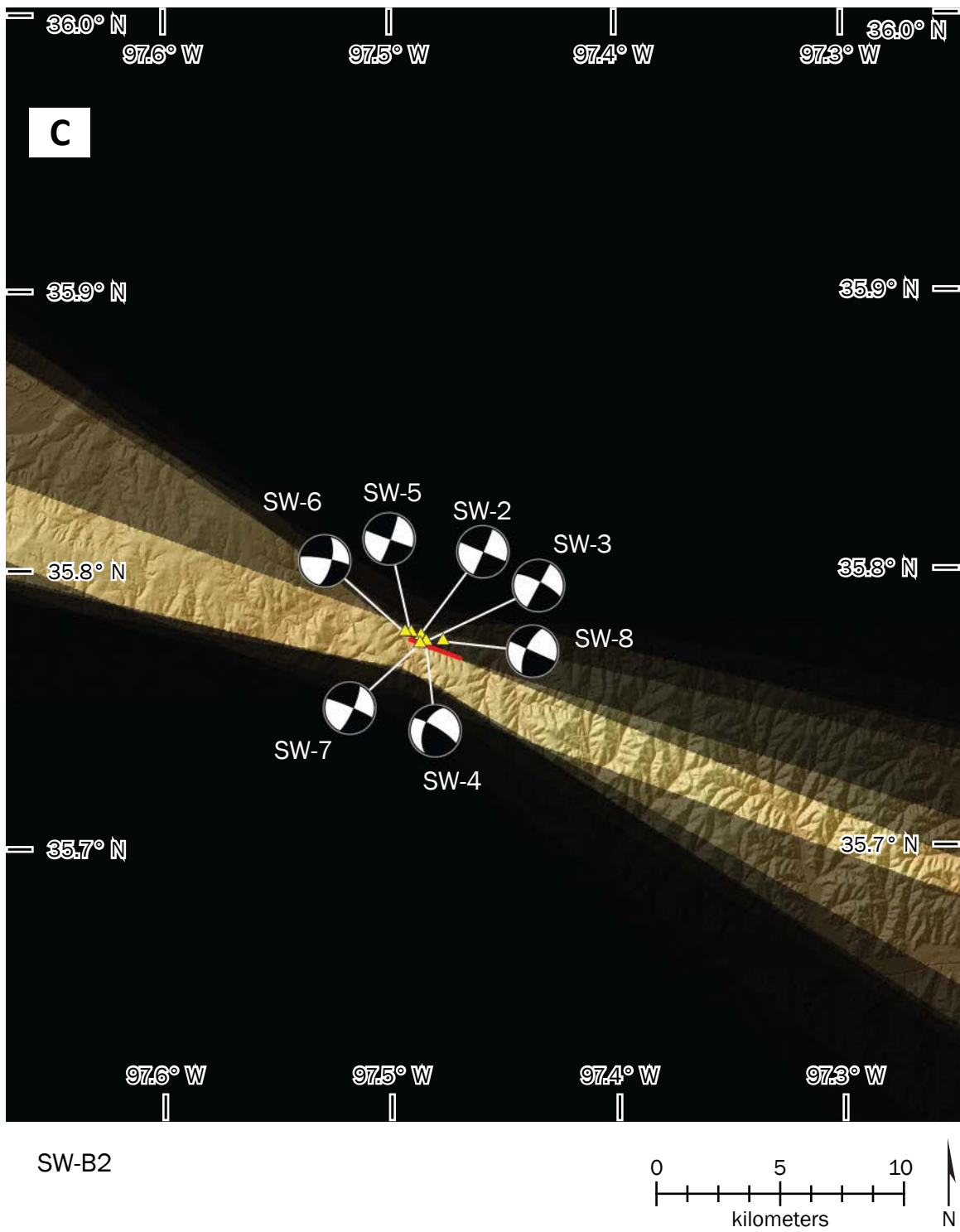
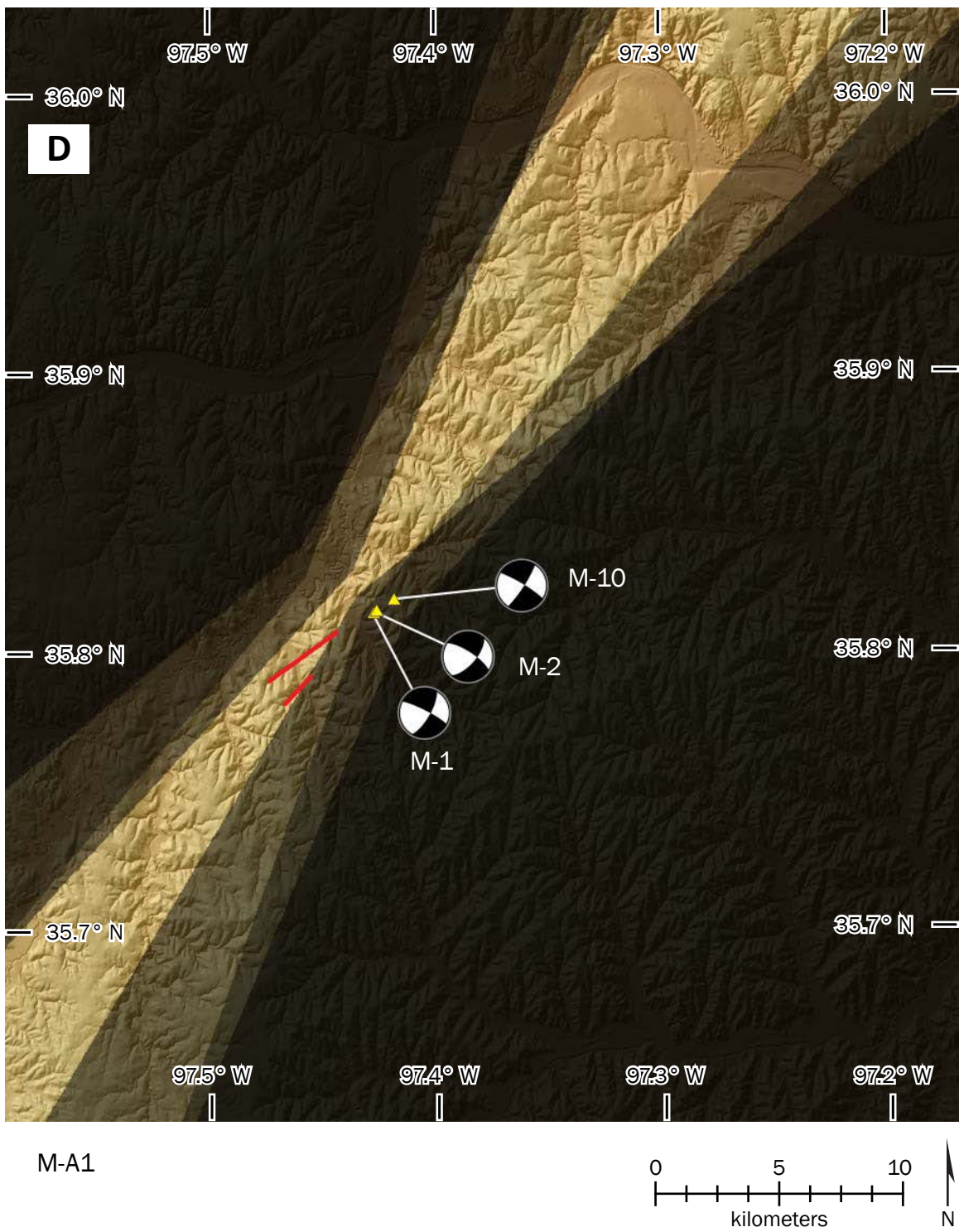


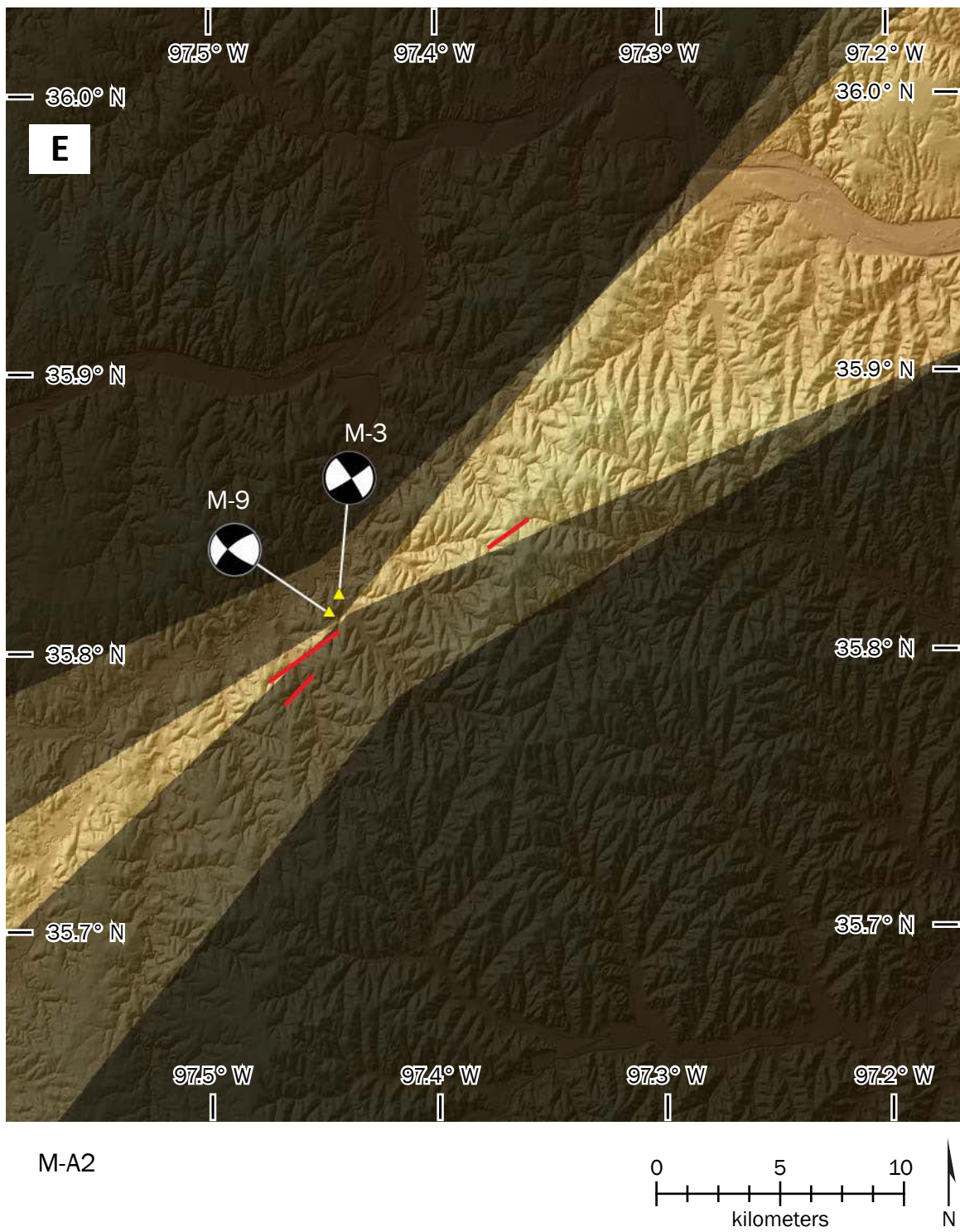
Figure 22. A–K. Overlapping seismo-lineaments for event groups. Focal mechanism diagrams are represented, pointing to yellow triangles that indicate the epicenters for each group. Where visible, red lines represent the relevant geomorphic lineaments and blue lines show apparently offset drainages.

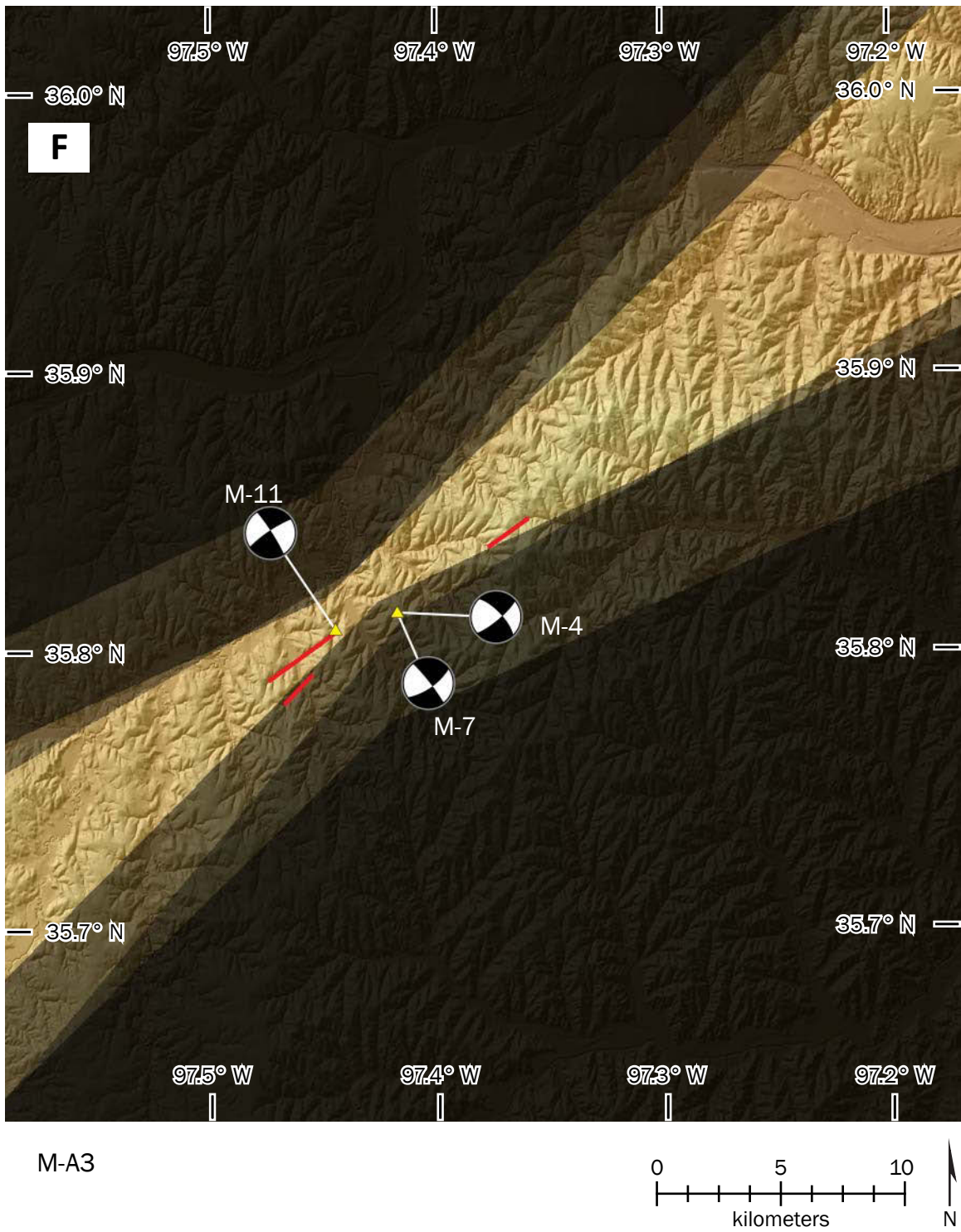


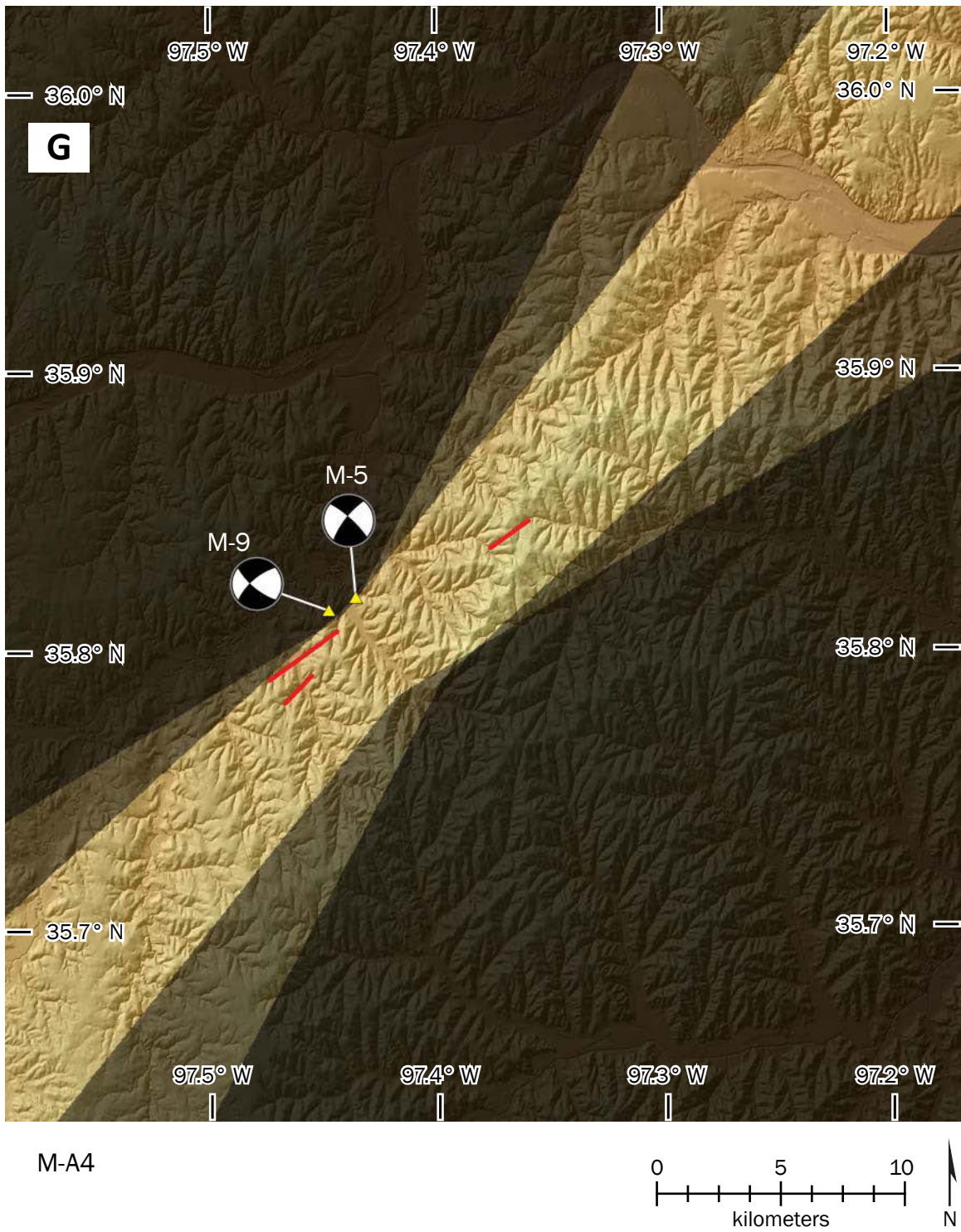


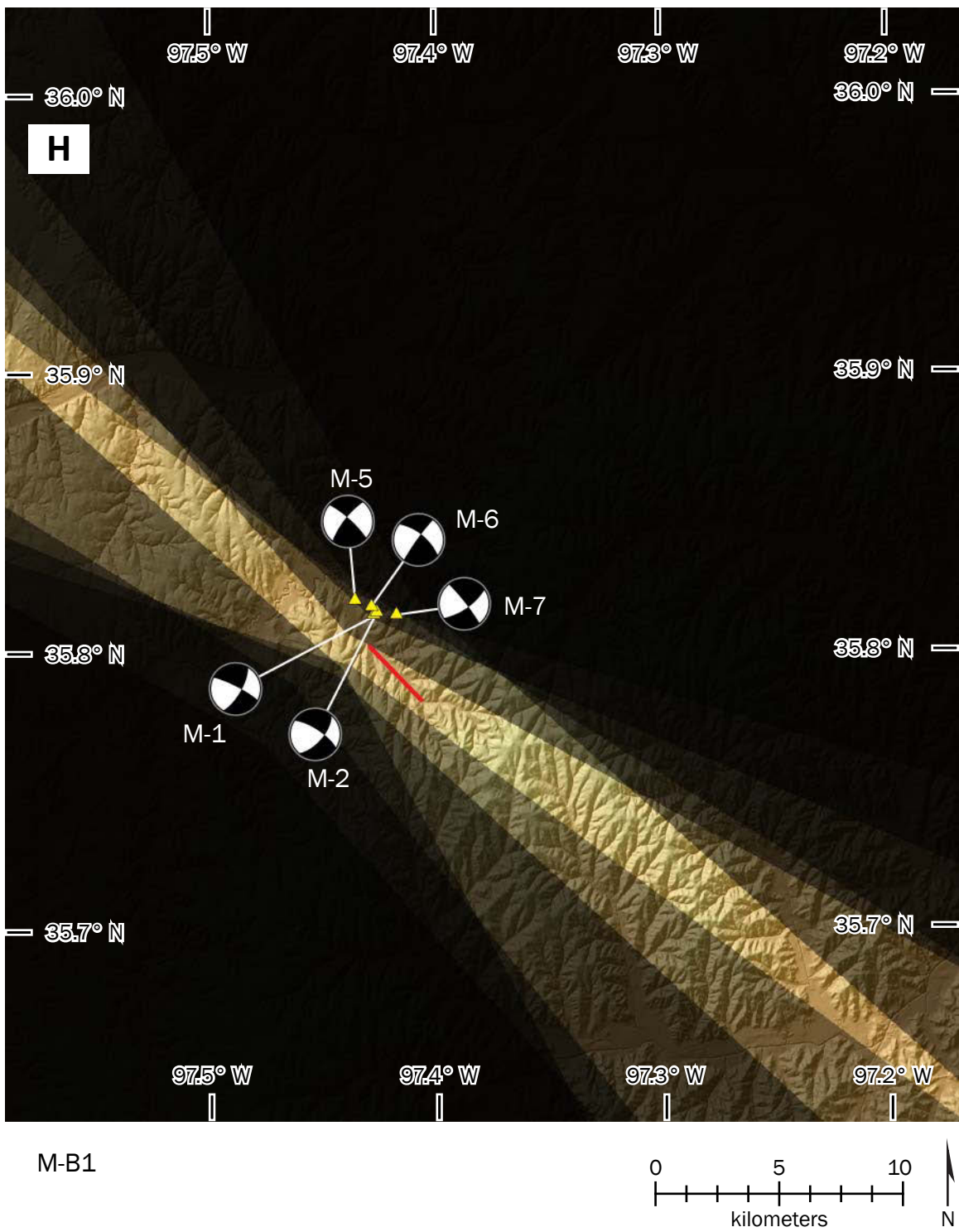


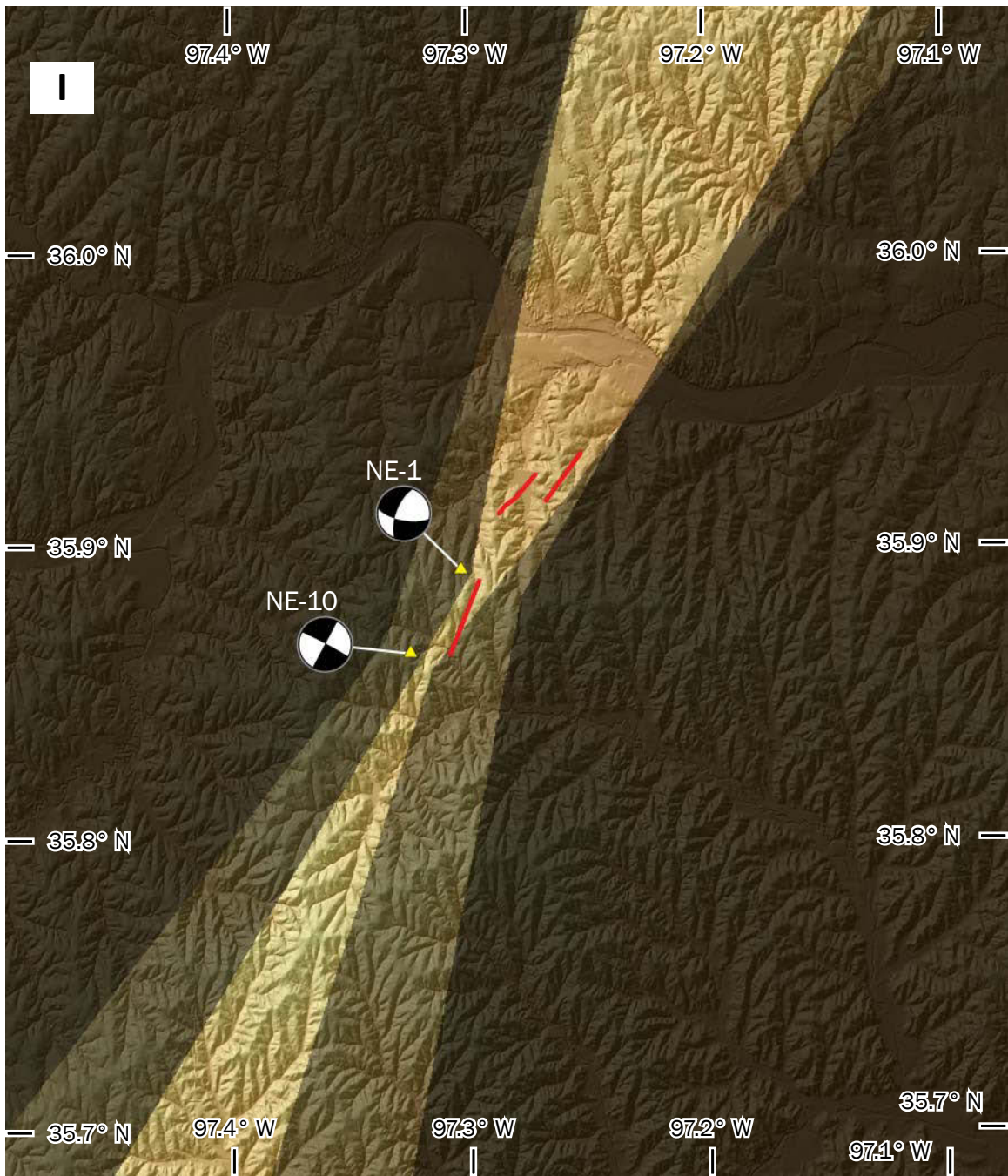




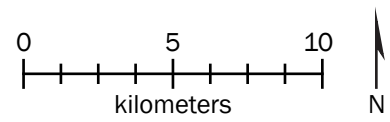


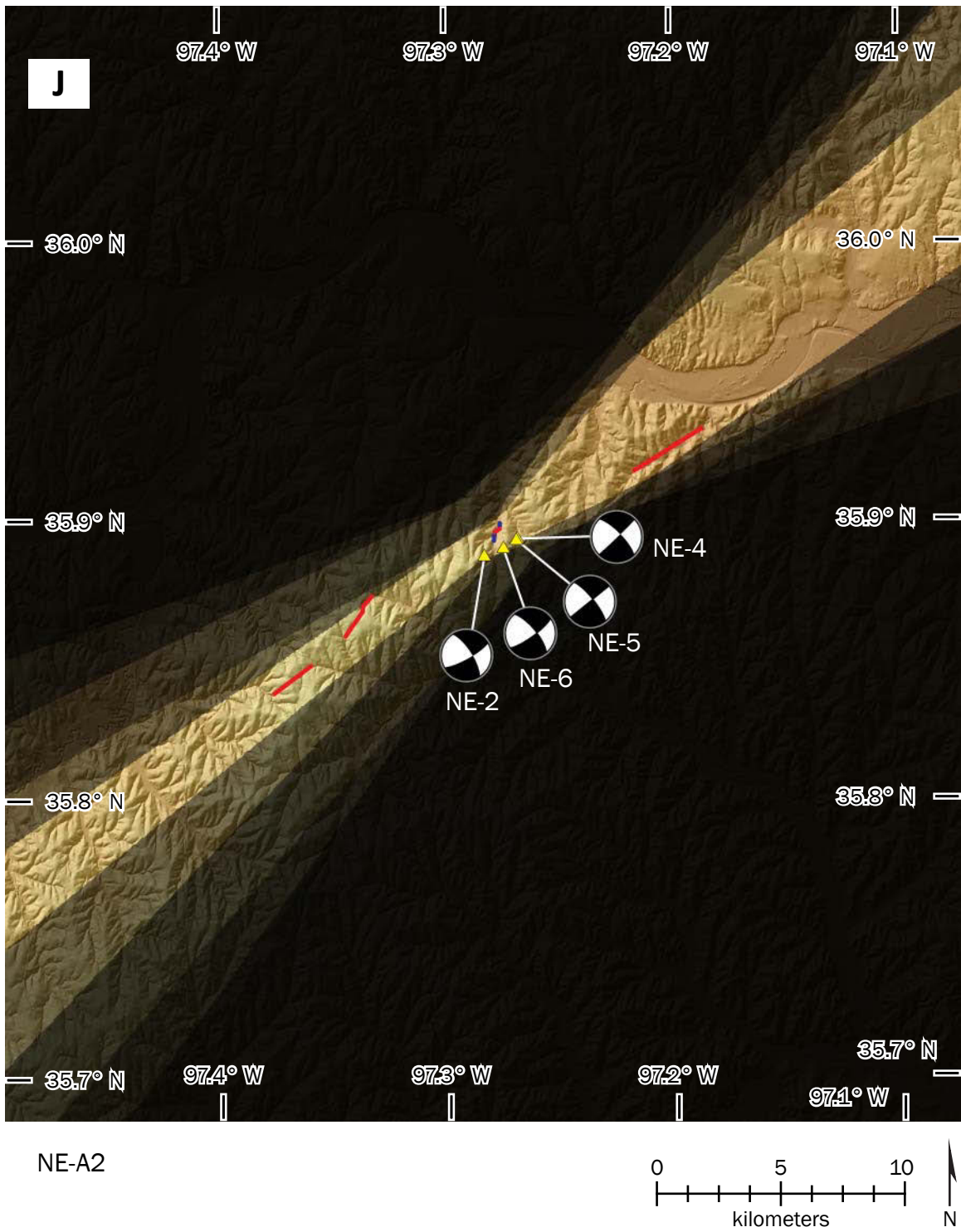




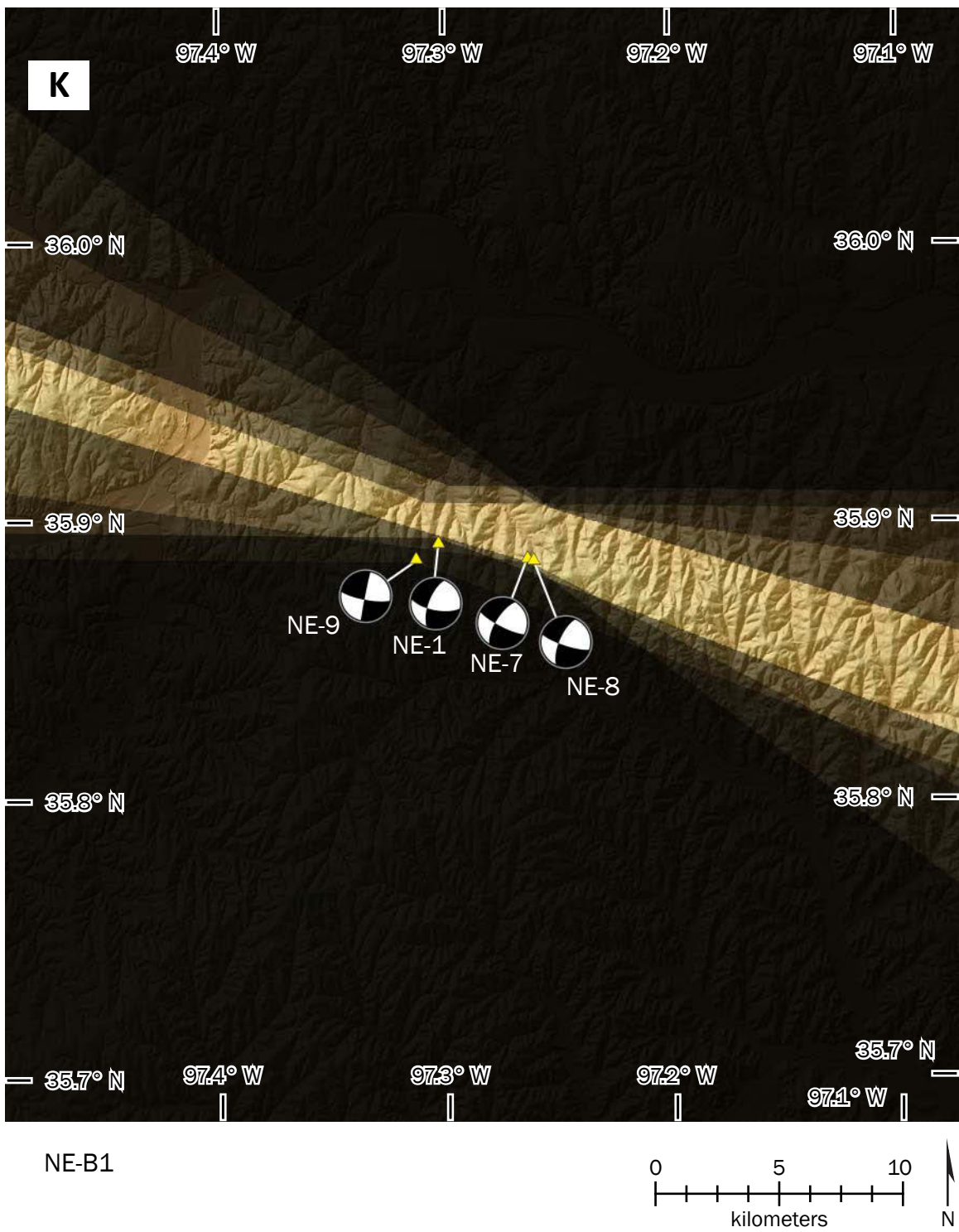


NE-A1









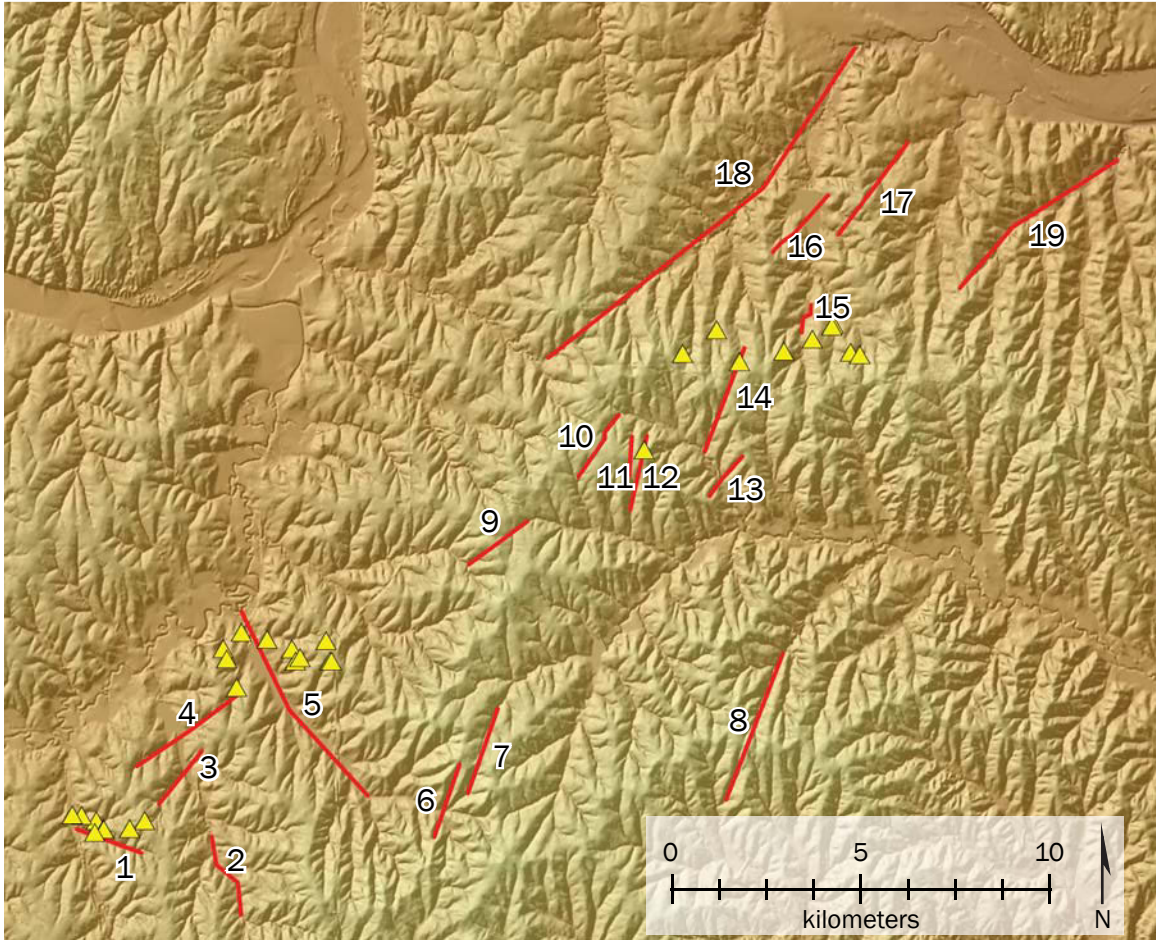


Figure 23. Geomorphic lineaments throughout the study area. Numbers correspond with Table 5.

Table 5. Geomorphic lineations and the rationale for choosing each one.

Number	Rationale (Description of Feature)
1	Anomalously straight segment of stream channel
2	Apparent lateral deflection of incised stream channel
3	Lower-order stream channels aligned across a higher-order stream channel
4	Stream channels aligned on opposite sides of a drainage divide; Lower-order stream channels aligned across a higher-order stream channel
5	Anomalously straight segment of stream channel
6	Lower-order stream channels aligned across a higher-order stream channel
7	Stream channels aligned on opposite sides of a drainage divide
8	Lower-order stream channels aligned across a higher-order stream channel
9	Stream channels aligned on opposite sides of a drainage divide; Aligned straight segments of one or more stream channels
10	Stream channels aligned on opposite sides of a drainage divide; Aligned straight segments of one or more stream channels
11	Stream channels aligned on opposite sides of a drainage divide
12	Stream channels aligned on opposite sides of a drainage divide
13	Lower-order stream channels aligned across a higher-order stream channel
14	Stream channels aligned on opposite sides of a drainage divide
15	Apparent lateral deflection of incised stream channel
16	Stream channels aligned on opposite sides of a drainage divide; Lower-order stream channels aligned across a higher-order stream channel
17	Stream channels aligned on opposite sides of a drainage divide; Aligned straight segments of one or more stream channels
18*	Stream channels aligned on opposite sides of a drainage divide; An anomalously straight segment of a stream valley
19*	An anomalously straight segment of a stream valley

*Field Investigations*

Thick soil, dense foliage, high water, private property, or a combination of these prevented me from seeing much bedrock. In every location I investigated, no discernible evidence of faulting or surface disturbance was found. Figure 24 is a map of the locations of the photographs for each field stop.

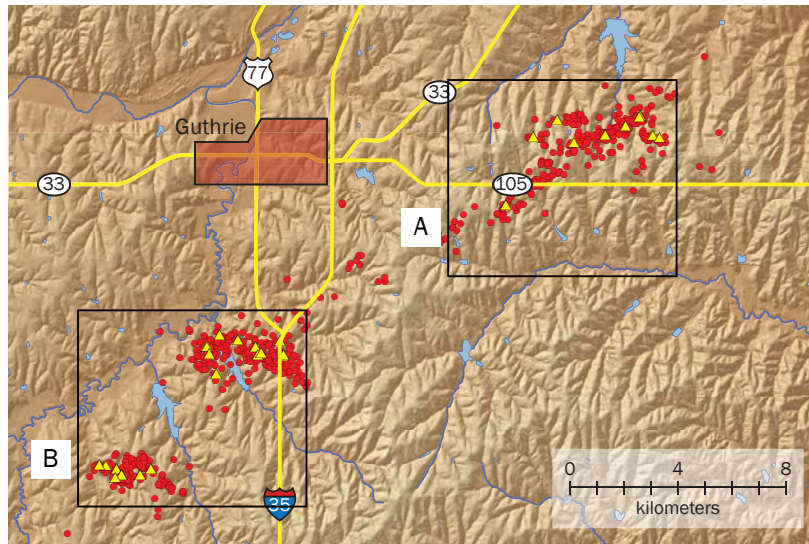
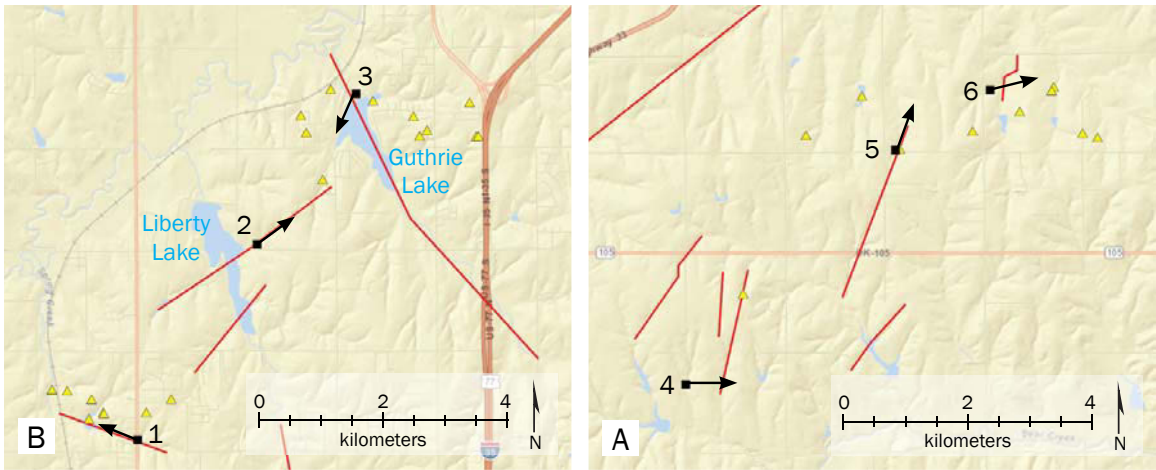


Figure 24. Map of locations of field stops and photos. Black squares are photo locations and the black arrows indicate the direction the camera was facing. Yellow triangles show epicenters for the events in this study. Red lines are suspect geomorphic lineaments. Red circles in the bottom map show all epicenters  $M \geq 2$ .

Table 6. Locations of field investigations. Numbers correlate with numbers in Figure 24.

Number	Location Name
1	Cottonwood Creek
2	Liberty Lake
3	Guthrie Lake
4	Westminster Blvd.
5	College Avenue
6	Henry Road

### *Cottonwood Creek*

This lineament follows the trend of Cottonwood Creek, which intersects South Broadway Street southwest of city of Guthrie. Except where it intersects the road, the entire length of the lineament is located on private property. The soil cover was deep enough to obscure all bedrock. No sign of fault movement was found. (Figure 25)

### *Liberty Lake*

This lineament intersects Liberty Lake, located southwest of Guthrie, and extends along two drainages that flow into the lake, along a SW-NE trend. The northeast drainage intersects a gravel road very near the lake shore. As it extends away from the lake, it enters into increasingly dense foliage with deep soil cover. The length of the southwest drainage is located on private property. No sign of faulting could be discerned along either drainage. (Figure 26)

### *Guthrie Lake*

The lineament at Guthrie Lake extends along the primary inlet stream, and along the length of the elongated reservoir, and intersects the dam. The inlet stream was located mostly on private property, and the length that was not was surrounded by such dense vegetation that it was impossible to hike through. Moreover, the stream was flowing, inhibiting any investigation of its bed. I traversed the earthen dam and walked along the road located at its crest, but there were neither cracks nor misaligned features along its entire length. (Figure 27)



Figure 25. Photo of Cottonwood Creek lineament. Red dashed line shows geomorphic lineament. Blue curve shows stream bed.



Figure 26. Photo of Liberty Lake lineament. Red dashed line shows geomorphic lineament.

### *Westminster Blvd.*

One of the lineaments at this location was a drainage that followed along the side of the road for about 800 meters. I walked as much of its length as possible, but found no sign of faulting. The foliage here was very dense and obstructed most of the drainage. The other lineament extends along a drainage that intersects the road, but was far too overgrown for any amount of investigation at the intersection. The rest of it was located on private property. (Figure 28)

### *College Avenue*

This lineament is along two straight drainage segments aligned on either side of a divide and intersects three roads: University Ave, N 3200 Rd., and College Ave. At the University Ave intersection, the vegetation was too dense for any investigation. At the N 3200 Rd. intersection, the lineament also crosses a man made dike, but no evidence of faulting could be found. The dike did not appear even slightly disturbed. At the College Ave intersection I was able to hike along the stream bed into the forest for ~150 meters but found no sign of ground movement. The lineament might have crossed through the stream's cutbank at a curve in the stream bed, but no evidence of faulting was found. (Figure 29)

### *Henry Road*

This lineament seemed to be the most promising because it is along an apparently offset stream bed, consistent with what we would expect of a right-lateral strike slip fault in this orientation. However, the foliage was far too dense to penetrate, and the lineament itself is located on private property. (Figure 30)



Figure 27. Photo of the dam at Guthrie Lake. Red dashed line shows geomorphic lineament.



Figure 28. Photo of the ditch along Westminster Blvd.. Red dashed line shows geomorphic lineament.





Figure 29. Photo of the cutbank in the stream bed along the College Avenue lineament. Red dashed line shows geomorphic lineament.

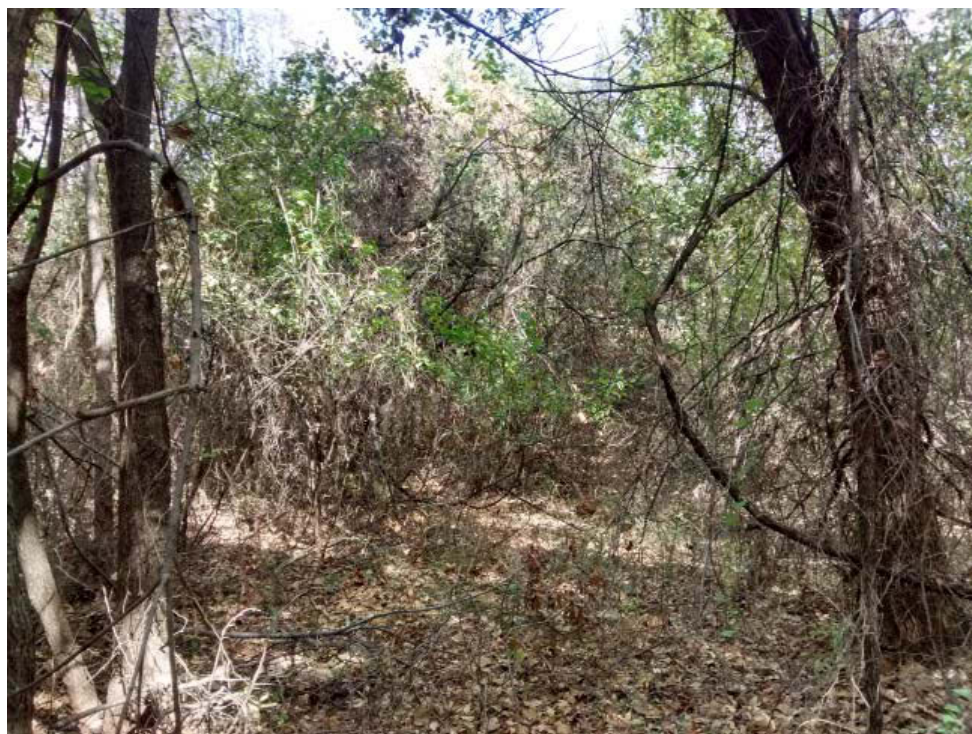


Figure 30. Photo of the dense foliage en route to reach the Henry Road lineament.

### *Three-Dimensional Model*

I modeled the hypocenter locations in three dimensions to better understand their spatial distribution at depth. Figure 14 in Chapter Three shows a stereographic image of this model, but without the aid of a stereoscope, adequately displaying a three dimensional model of points is near impossible. Instead Figure 31 shows a map of the hypocenters symbolized by depth. It is clearly seen, by the difference in colors, that hypocenters cluster not only horizontally, but with depth as well. This is apparent in the SW cluster which I had previously thought represented only one fault, when there are evidently at least two. There are likely at least two faults in the NE cluster, possibly more. Due to the dip of the faults the epicenters cluster together and disguise the distinction. But in three dimensions it is obvious that there are actually two clusters at different depths.

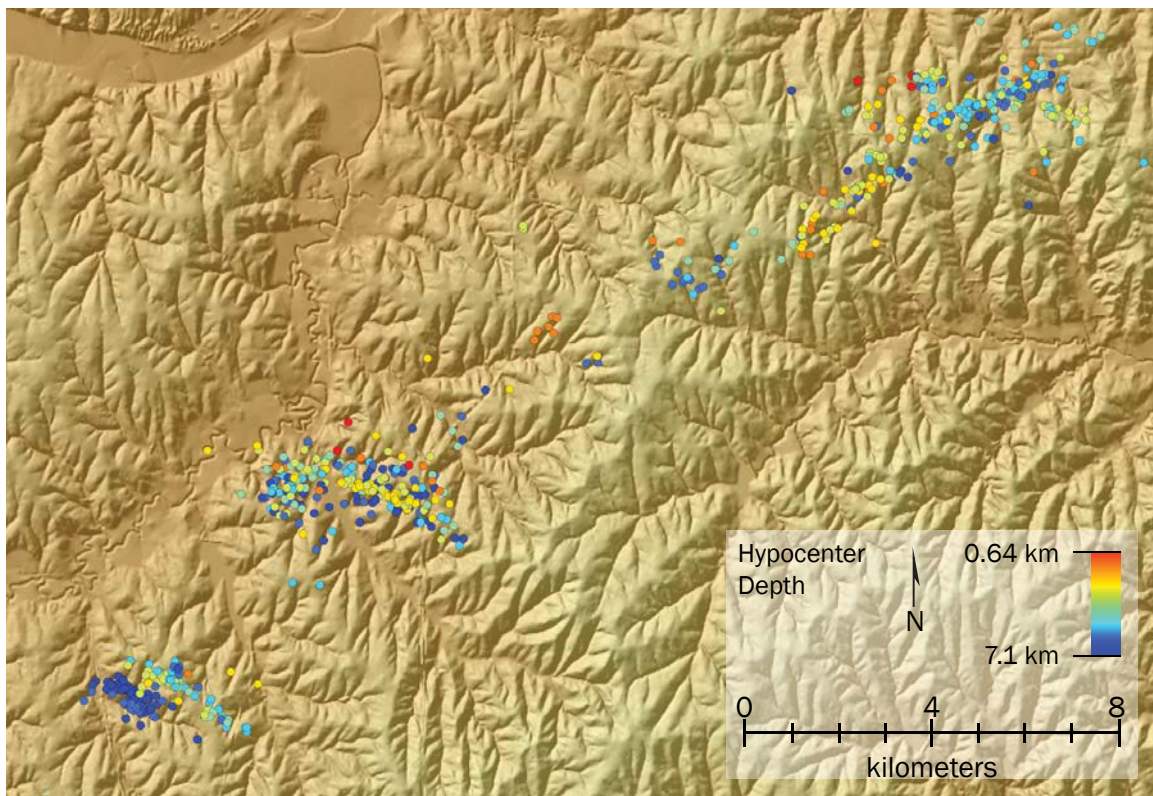


Figure 31. Epicenters colorized by depth.

### *Drainage Network Trend Analysis*

I generated rose diagrams for the cumulative drainage segment lengths in  $5^\circ$  bins for each event group (Figure 32). From this analysis there appears to be no correlation between the orientation of drainages and the orientation of overlapping seismo-lineaments in the groups. Below are two rose diagrams per cluster, one for an event group with a NE-SW nodal plane trend and one for an event groups with a NW-SE nodal plane trend. Each wedge represents the cumulative length of drainage segments in a given orientation. The red wedges represent the orientation of the overlapping seismo-lineaments in that event group.

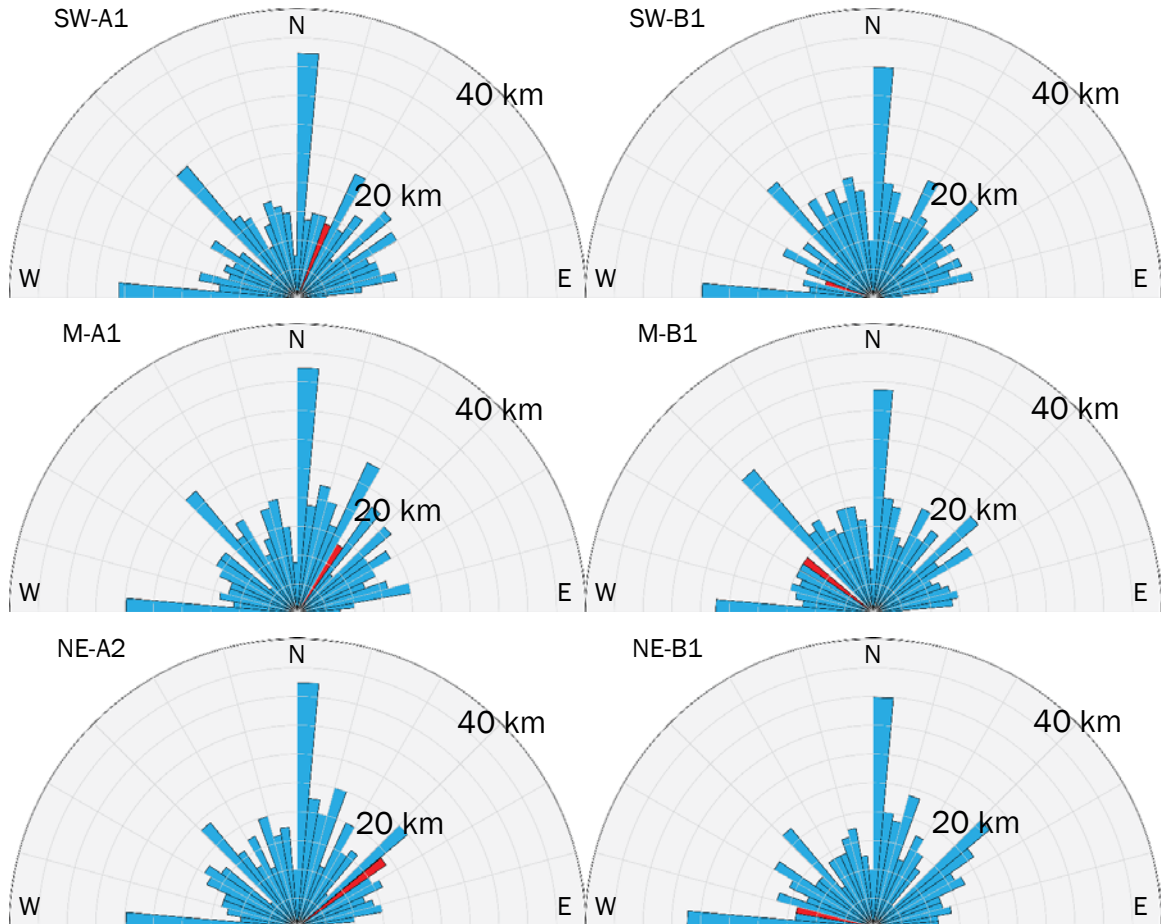


Figure 32. Rose diagrams for drainage trend analysis. Red wedges are the orientations of the event groups.

## CHAPTER FIVE

### Discussion & Conclusions

The purpose of this study was to correlate recent earthquakes with seismogenic faults and determine if they have ruptured the ground surface. Due to the lack of geomorphic expression and the depth of the hypocenters, I conclude that none of the faults in the study area have ruptured the ground surface. It appears that virtually all of the events of  $M \geq 2$  occurred at crystalline basement depths, below the  $\sim 2$  km thick sedimentary cover. Due to the lack of evidence from field investigations, an apparent lack of any preferred orientation for drainages in the area, and a lack of published maps of basement faults, it is not possible to map precisely where each fault is located without detailed geophysical analysis. Even with the aid of geophysical data, it may prove very difficult due to the high angle of the faults as indicated by the focal mechanisms.

The Nemaha system was likely formed as part of the Ancestral Rocky Mountain orogenesis in the Late Paleozoic Era, based on the limited data and models available. I infer that the faults responsible for the earthquakes in this thesis are part of the Nemaha system, based on their proximity to the southern end of the Nemaha structure, the orientations of the nodal plane trends, and the steep dip angles from the 29  $M \geq 3.5$  events. I have mapped seven broad swaths wherein I infer at least one seismogenic fault would intersect the ground surface if it was emergent at the ground surface (Figure 33), which are broadly coincident with the findings reported by Darold and Holland (2015).

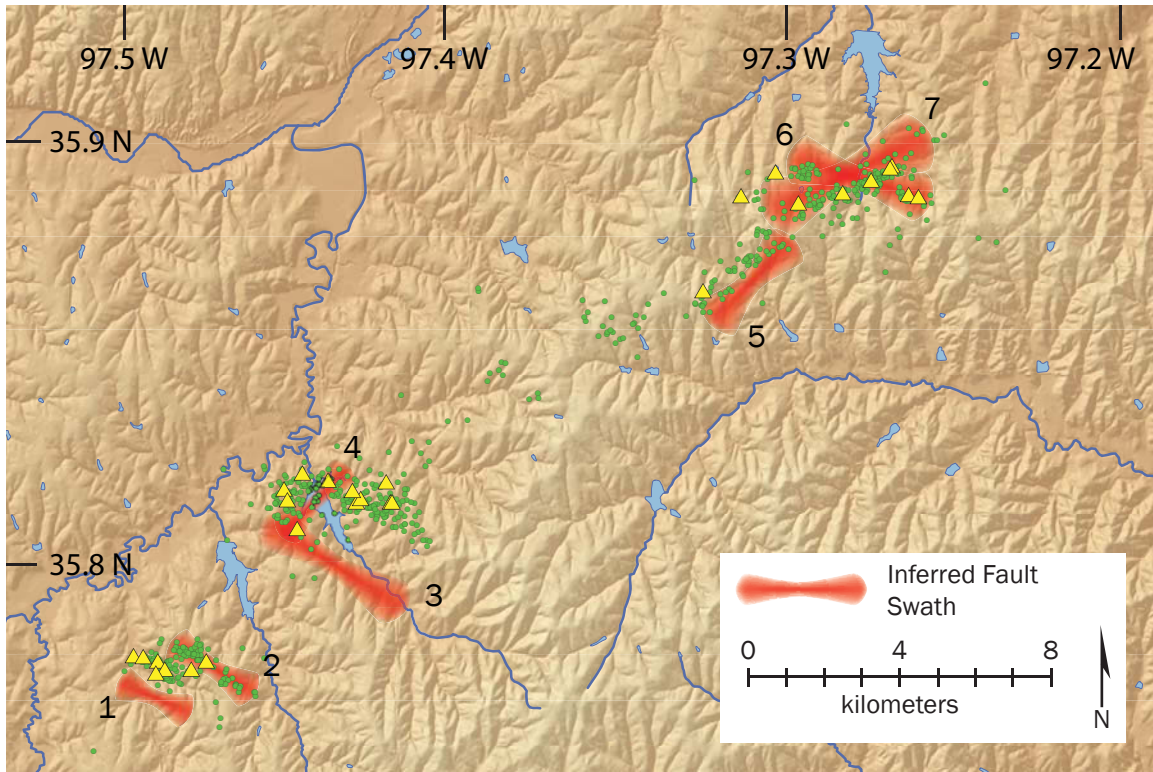


Figure 33. Inferred fault swaths from synthesis of event groups and 3D model of hypocenters. Numbers refer to event groups used to define the respective swaths. Specific figures for event groups are referenced in Table 7.

Table 7. Event groups that correlate with fault swaths in Figure 33.

Number	Event Group	Page Number
1	SW-B2	34
2	SW-B1	33
3	M-B1	39
4	M-A1, A2, A3, A4	35-38
5	NE-A1	40
6	NE-B1	42
7	NE-A2	41

### *Suggestions for Future Work*

Toward the end of the process I found an online source for LIDAR data of central Oklahoma, including the study area for this work (OCC, 2015). However the data were unprocessed and the file sizes were very large and it was too late for a profitable effort to be made in accessing and processing the data. Future work expanding on the inferences made in this thesis could be made with the LIDAR. It is possible that higher resolution data might enable the identification of fault-related geomorphic features that were not visible with the data available at this time.

## APPENDICES

## APPENDIX A

### ArcGIS Scripts and Workflow

The workflows to produce seismo-lineament swaths and delineations of drainages and ridgelines in ArcGIS involves several scripts and iterative models built with the ArcGIS Model Builder. These models and scripts are explained in detail in this appendix.

#### *Model 1: Creating Polylines of Seismo-Lineament Swaths*

This model iterates each step over every file in the directory, so all of the output files (and only those files) from the modified SLAM code were located in the same directory on the hard drive. I used a naming convention for these files with an event identifier as well as a nodal plane identifier (e.g., *SW1\_NP2*). The tools and scripts used in Model 1 are described below (Figure A.1):

ASCII to Raster: Creates a raster dataset in ArcGRID format from an ASCII file, in this case from the plain text file exported by the *Mathematica* SLAM code. The output file is given the same name as the input file, as indicated by *%Name%* in Figure A.1.

Define Projection: The new raster dataset has spatial coordinates, but no projection information to define the origin and units for them. This tool allows the user to select the appropriate coordinate system. Because the SLAM code requires the inputs to be in UTM coordinates, I used UTM Zone 14N.

Contour: Each output text file from the modified SLAM code (Cronin and Rasaka, 2015) is a DEM, but instead of representing the elevation in the region, each cell has a value of either +1 or -1, for cells within and without the seismo-lineament swath, respectively.

The Contour tool creates a polyline shapefile of contour lines based on an input DEM, in



specified intervals. In the model, the interval is two map units so that the contours outline the seismo-lineament swath. The output cannot have the same name as its input, so I added the prefix *C\_* to *%Name%*, resulting in *C\_SW1\_NP2* for the example from above.

Feature Class to Geodatabase: This step is not vital, but is preferred. A geodatabase is a way of storing GIS data in a database that enhances data management. This tool creates a feature class of the shapefile inside the geodatabase, but leaves the original shapefile.

Delete: This step is not vital, but is preferred. After the contour shapefile has been created, the raster dataset (output from the ASCII to Raster tool) is no longer needed. Also, after the contour has been imported into the geodatabase, the original shapefile is no longer needed. These files are deleted to free space on the disk and to reduce clutter. However, the Delete tools will not run until the Contour tool and the Feature Class to Geodatabase script have run, respectively, as indicated by the dashed lines in Figure A.1.

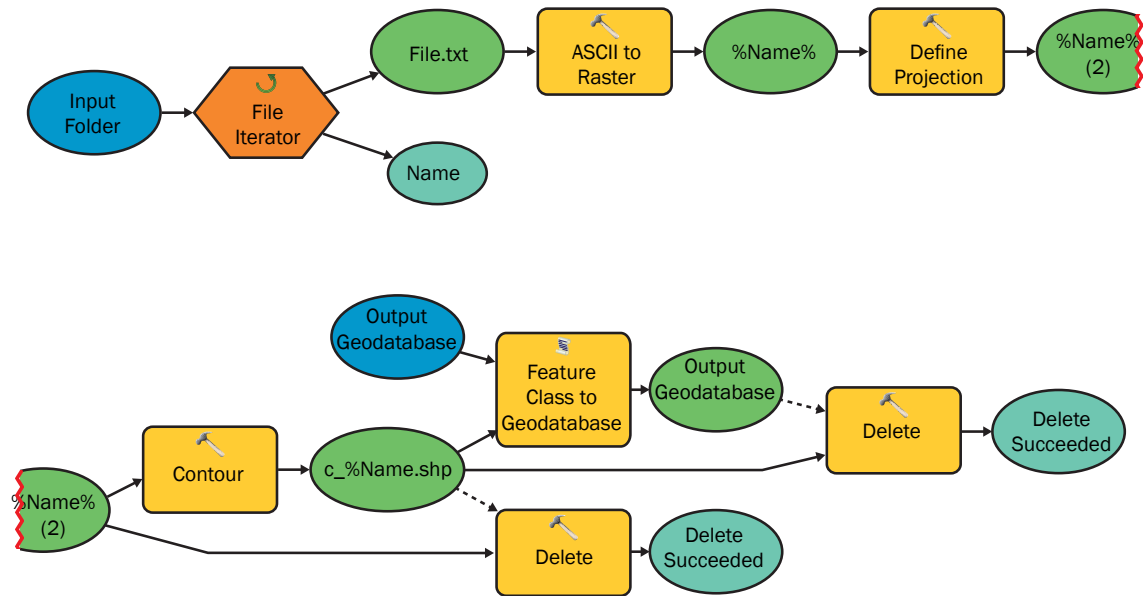


Figure A.1. Model 1 workflow from the ArcGIS Model Builder.

### *Model 2: Creating Polygons of Seismo-Lineament Swaths*

Before this model can be run, I had to manually edit the contour feature class from Model 1 because there are extraneous and unclosed lines (Figure A.2a). The polyline must be fully enclosed in order for the Feature to Polygon tool to work properly (Figure A.2b).

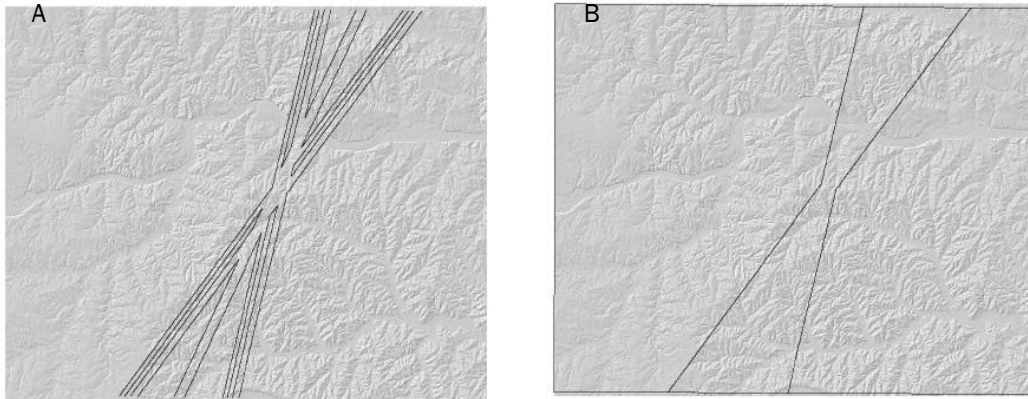


Figure A.2. Screenshots of a seismo-lineament contour shapefile. (A) This shows the shapefile as it is immediately after the model is run. (B) All extraneous lines have been deleted and a box has been drawn to enclose the entire polyline.

Similar to Model 1, this model iterates over each file, but in the geodatabase instead of a directory. For each feature class, the following tools are applied (Figure A.3):

Feature to Polygon: Creates a feature class of polygons from the enclosed polyline feature class. If the lines are not enclosed, no polygon will be created. The output is given the name *P\_ %Name%* which, using the naming example from above, results in *P\_C\_SW1\_NP2*.

Add Field: This adds a new attribute field to the polygon feature class. The purpose of this field is for symbolizing the polygons based on whether it is within or without the seismo-lineament swath. The name of the new attribute field is *Region* and is assigned to be a SHORT INTEGER field.

After Model 2 was run, I selected the three regions in each polygon feature class and assigned them either a +1 or a -1 in the Region field to represent the region within or without the seismo-lineament swath, respectively. Then I gave the region within 100% transparency, and the region without I made black with 50% transparency.

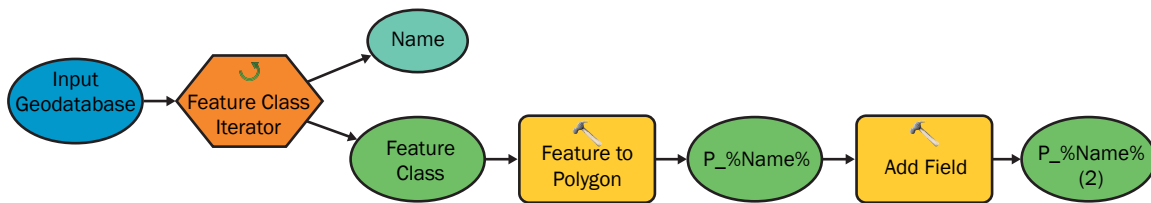


Figure A.3. Model 2 workflow from the ArcGIS Model Builder

### *Model 3: Drainage and Ridgeline Delineation part 1*

The following two models were run twice. For the first run I used a DEM from the USGS. Prior to the second run, I created a new DEM from the first by using the ArcGIS Raster Calculator tool. This applies a given mathematical function to every cell in the dataset. In this case, I simply multiplied each cell by -1, resulting in an inverse DEM of the region, such that the highest elevation is now the lowest, and vice versa. The second run of these two models used the inverse DEM to delineate the ridgelines. Delineating the drainages in a given region does not require a custom-built model, but because some of the tools can take a long time to run, a model automates the entire process. The tools in this model are as outlined below (Figure A.4).

**Fill:** In the case that a DEM contains data artifacts that result in unnatural pits, or sinks, this tool fills them in. Because of the algorithm that is used, a sink artifact will result in all drainages flowing to them in the final output instead of where they actually flow.

Flow Direction: Creates a new raster with each cell indicating the direction to its steepest downhill neighbor.

Flow Accumulation: Creates a new raster with each cell representing accumulated flow, based on the Flow Direction raster. Cells that are in the downhill path from many other cells will have a higher value than cells at higher elevations or cells that are at equal or lower elevation but that do not have as many cells in an uphill path. Unlike the Flow Direction raster, the Flow Accumulation raster actually has the appearance of streams (Figure A.8b).

Stream Order: Creates a new raster with a numeric order to the cells, representing a hierarchy of network branches. There are two available methods of ordering streams: the Strahler method and the Shreve method. The Strahler method (Strahler, 1952) increases stream rank only when they intersect other streams of the same order. The Shreve method (Shreve, 1967) increases stream rank in an additive manner, starting with streams having no tributaries given a rank of one. I used the Strahler method, which is the default in ArcGIS, because the Shreve Method results a much wider range of values, making it difficult to determine an appropriate threshold in the steps below.

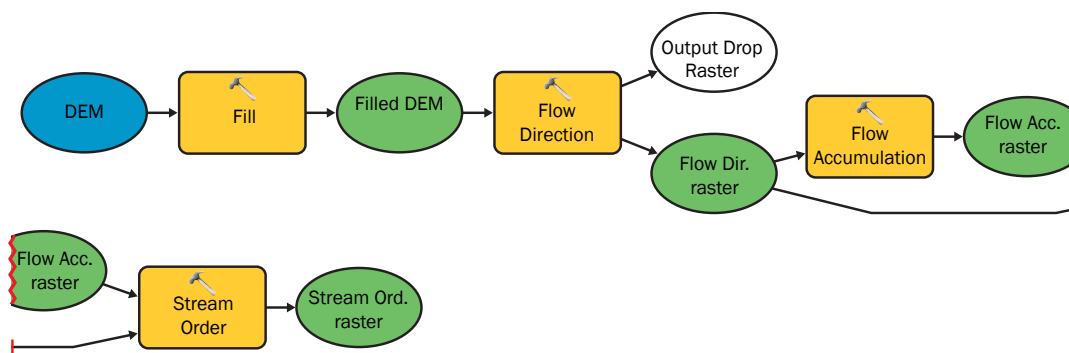


Figure A.4. Model 3 workflow from the ArcGIS Model Builder

*Model 4: Drainage and Ridgeline Delineation part 2*

The Stream Order tool from Model 3 assigns every cell a value based on its stream order. But in reality not every cell of ground is a stream. The Con tool is the first in Model 4 and will create a new raster that excludes cells of a certain value. Before running Model 4 (Figure A.5), I manually determined 2 to be an appropriate threshold. Hence, all cells with a stream order value of 2 or less were excluded from the output raster.

Con: Creates a new raster that evaluates a boolean statement for each cell in the input raster. In this model, the input is the Stream Order raster from Model 3. An SQL statement is required for the boolean evaluation. In this case, the statement was “Value > 2” to include any cell with a value greater than 2.

Stream to Feature: Vectorizes the stream output raster from the Con tool by creating a polyline shapefile. Although another tool exists to vectorize any raster (Raster to Polyline), Stream to Feature uses the Flow Direction raster in its algorithm to optimize vectorization when clusters stream order cells have the same value (Figure A.6).

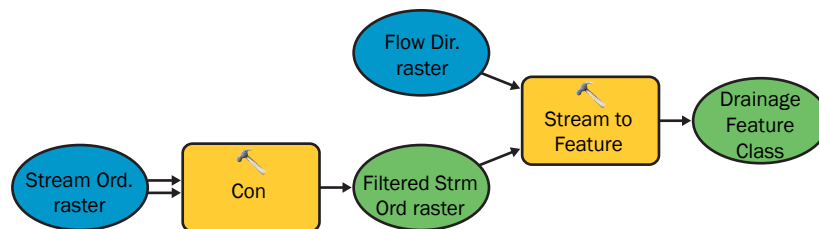


Figure A.5. Model 4 workflow from the ArcGIS Model Builder

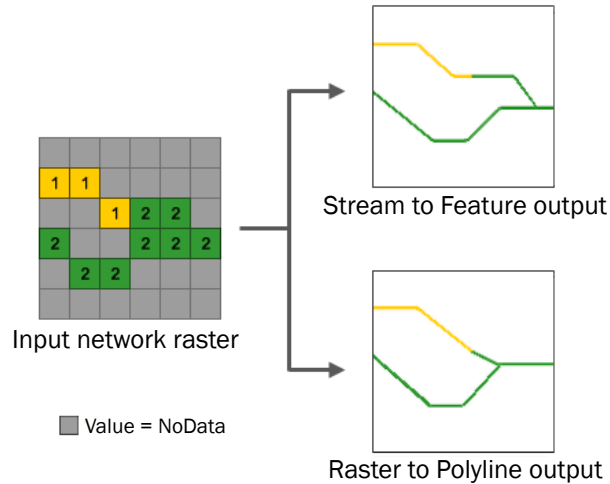


Figure A.6. Comparison of Stream to Feature tool versus Raster to Polyline tool. Image from ESRI (2015)

#### *Model 5: Linear Directional Mean*

This is another model in which not all the tools are necessary but are useful. The end result of this model is a feature class of straight segments representing the mean location and orientation of every stream segment (Figure A.7). In this case a stream segment is defined as a length of the stream or drainage from one confluence to another. This linear directional mean shapefile has an attribute field for each segment containing that segment's azimuth, limited to the range of 0°-180°. Using an SQL definition query, this shapefile can be filtered to show segments in a defined range of azimuths, aiding the geomorphic analysis.

**Linear Directional Mean:** By default, this script identifies the mean geographic center and vector of a set of lines and produces a shapefile of a single vector. However, by using either the *from\_node* or the *to\_node* attribute field as a Case Field, it identifies the mean center and vector of each line in the set.

**Add Field:** This adds a new attribute field to the output from Linear Directional Mean. The purpose of this field is to constrain the range of azimuths to 0°-180° for simplified definition queries. For example, if the desired range was 45° ±10°, then

the definition query would have to be “CompassA >=35 AND CompassA <=55 OR  
CompassA >=215 AND CompassA <=235” to include the range of  $225^{\circ} \pm 10^{\circ}$  (CompassA  
is the default name for the attribute field containing azimuthal directions. This can get  
cumbersome when analyzing several different ranges.

Calculate Field: Adding a new field simply adds a blank field. Calculate Field then  
names it and assigns values to the field based on values in other fields. In this example,  
I named the field *LimitAz* and used the following VB script with an assigned *azimuth*  
expression to populate the field:

```
If [CompassA] > 180 Then  
azimuth = [CompassA] - 180  
  
elseif [CompassA] <= 180 Then  
azimuth = [CompassA]  
  
end if
```

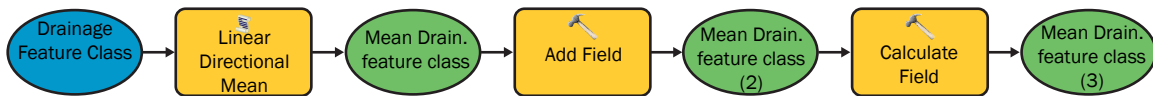


Figure A.7. Model 5 workflow from the ArcGIS Model Builder

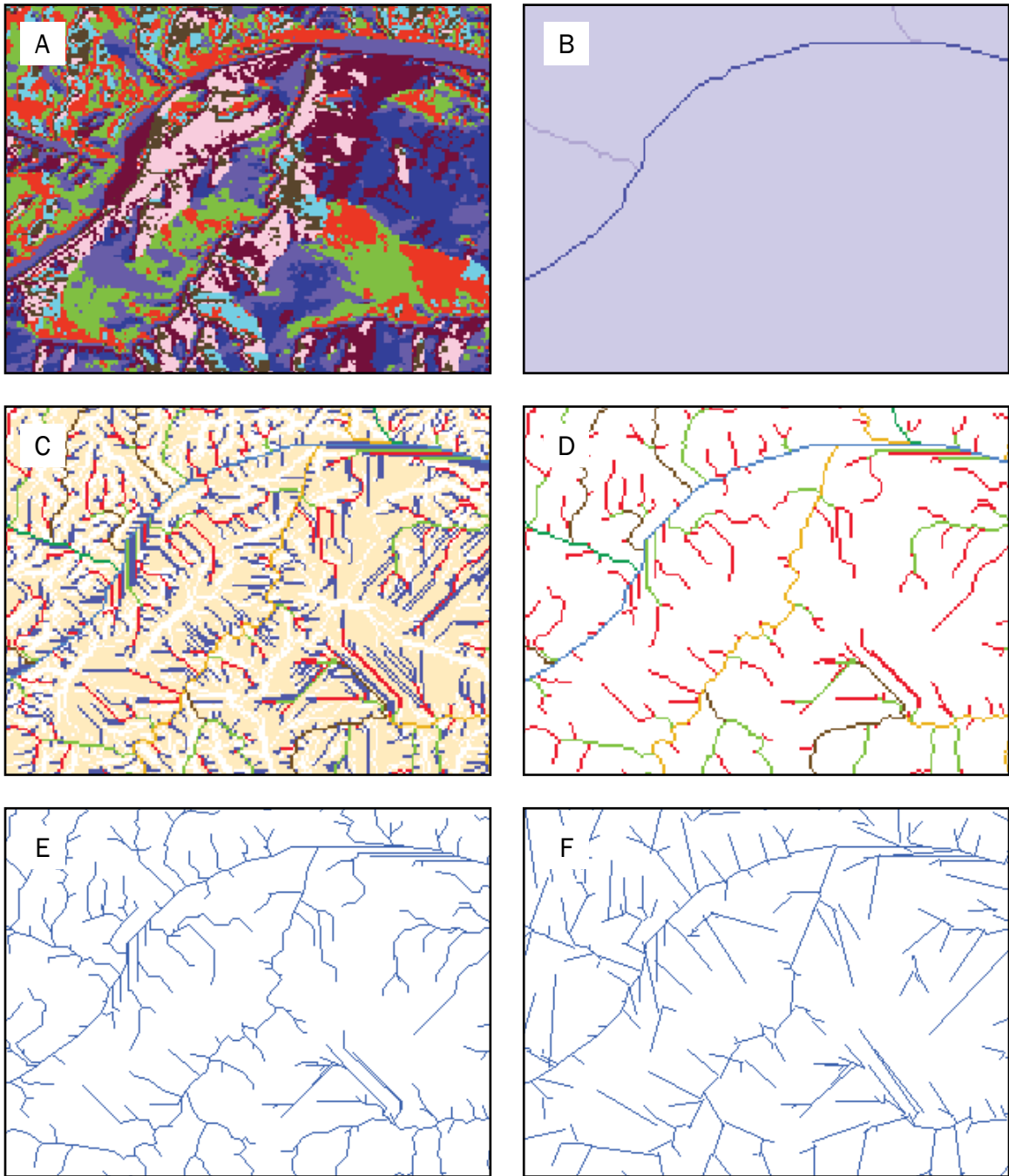


Figure A.8. Intermediate rasters and final vector shapefiles produced by Models 3–5. Each image is of the same sample area, in order to demonstrate the differences. (A) Flow Direction raster. Each color represents each of eight cardinal directions to the steepest downhill neighbor; (B) Flow Accumulation raster. Each color represents a classification of accumulation of flow. The darker the color, the more the accumulation (i.e., the larger the stream); (C) Stream Order raster. Each color represents a stream rank, based on the Strahler Method; (D) Stream Order raster, filtered with the Con tool; (E) Stream to Feature vector shapefile; and (F) Linear Directional Mean vector shapefile.



## APPENDIX B

### Seismo-Lineaments for all Events

The seismo-lineaments for the most representative and unusual events in each cluster are located in Chapter Four. The seismo-lineament swaths for all 29 events are located here.

Figure B.1 shows a map of the location of the epicenters for all 29 earthquakes.

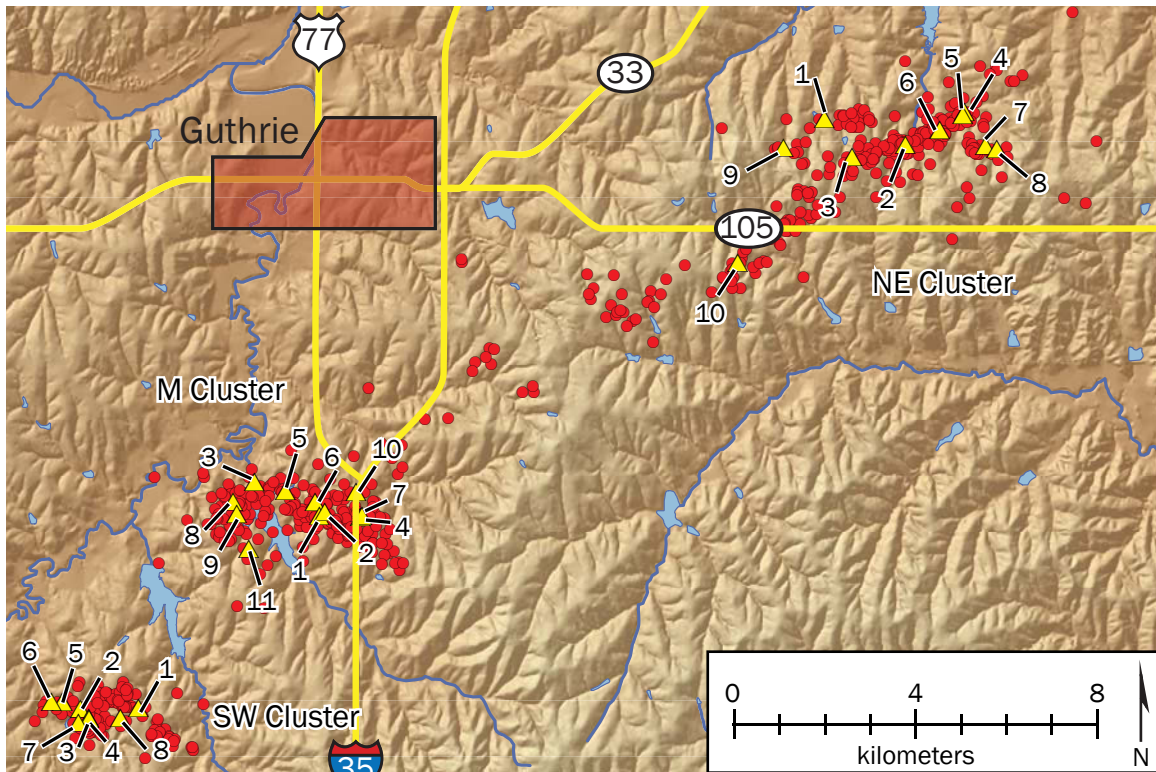


Figure B.1. Location of the study area. The city of Guthrie is approximately 40 km north of Oklahoma City. Yellow triangles mark those seismo-lineaments are shown below. Red circles are all epicenters  $M \geq 2$ .

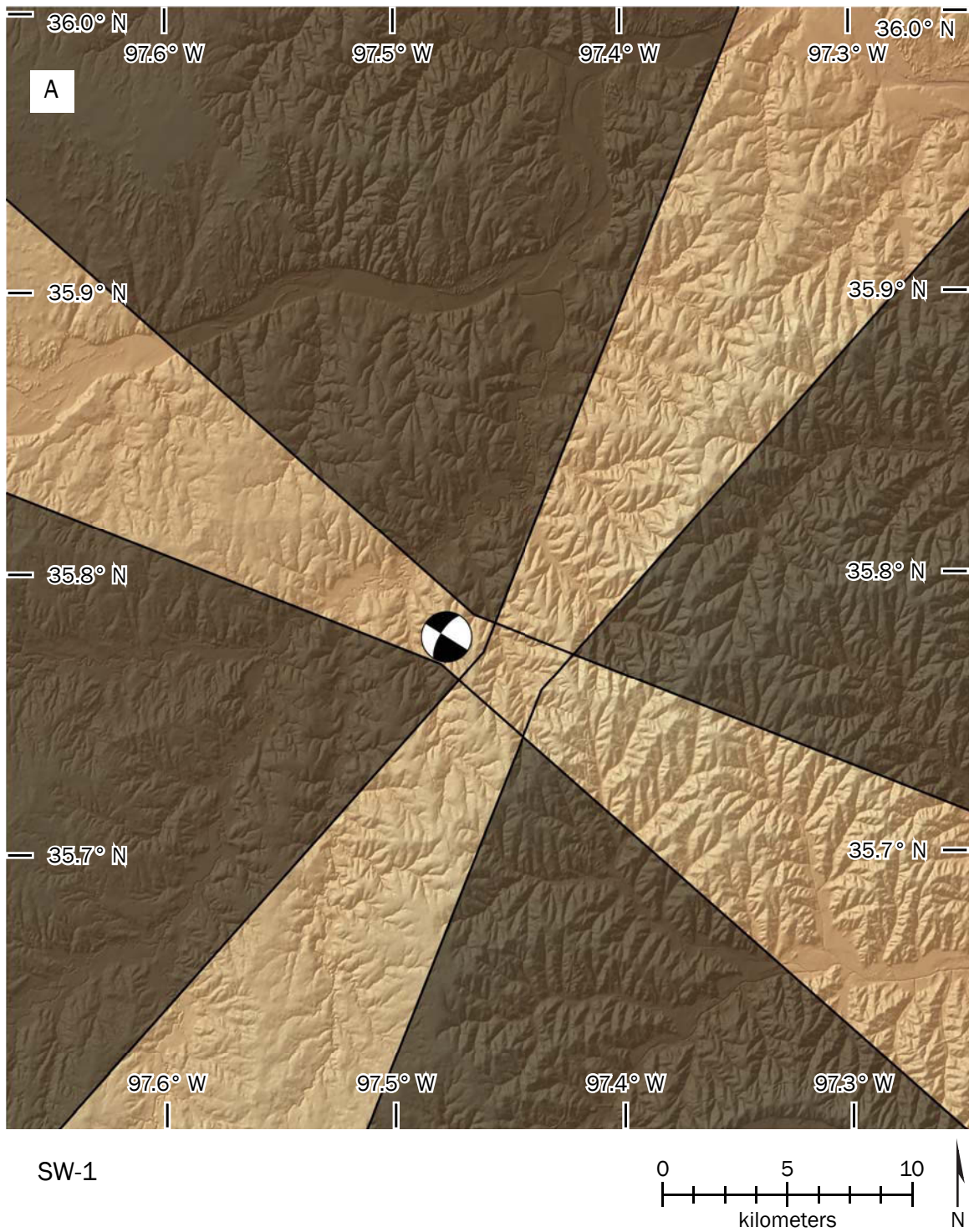
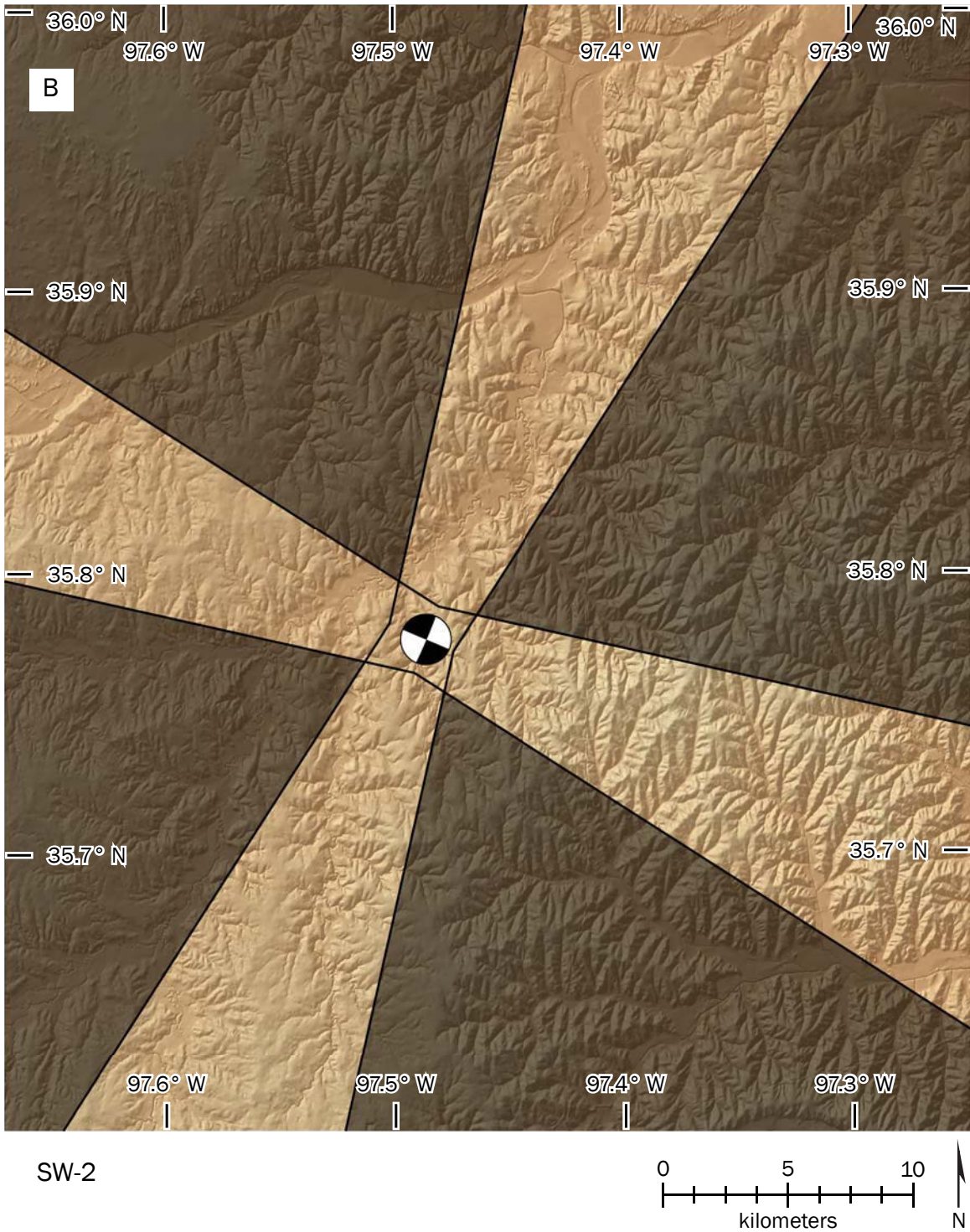
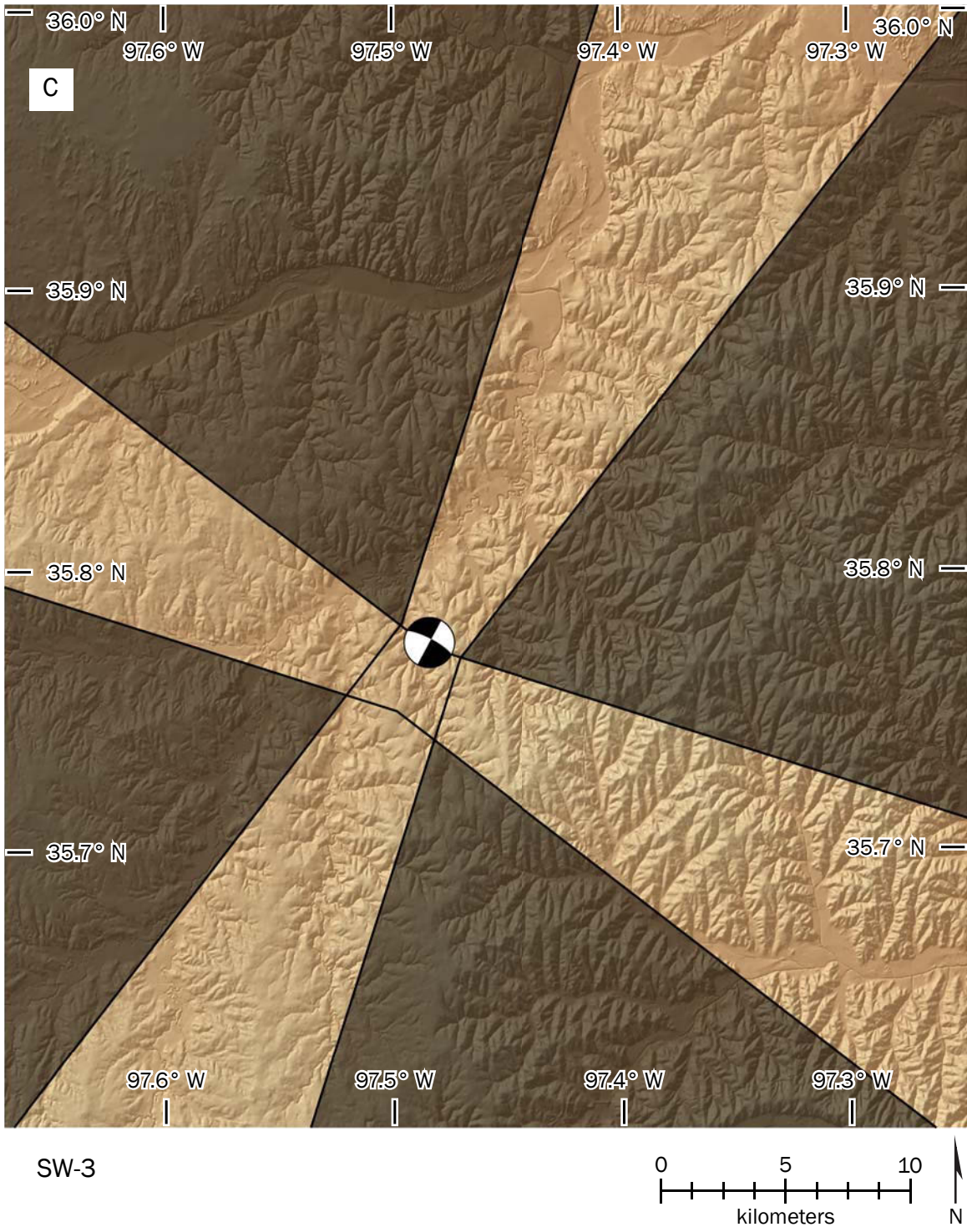
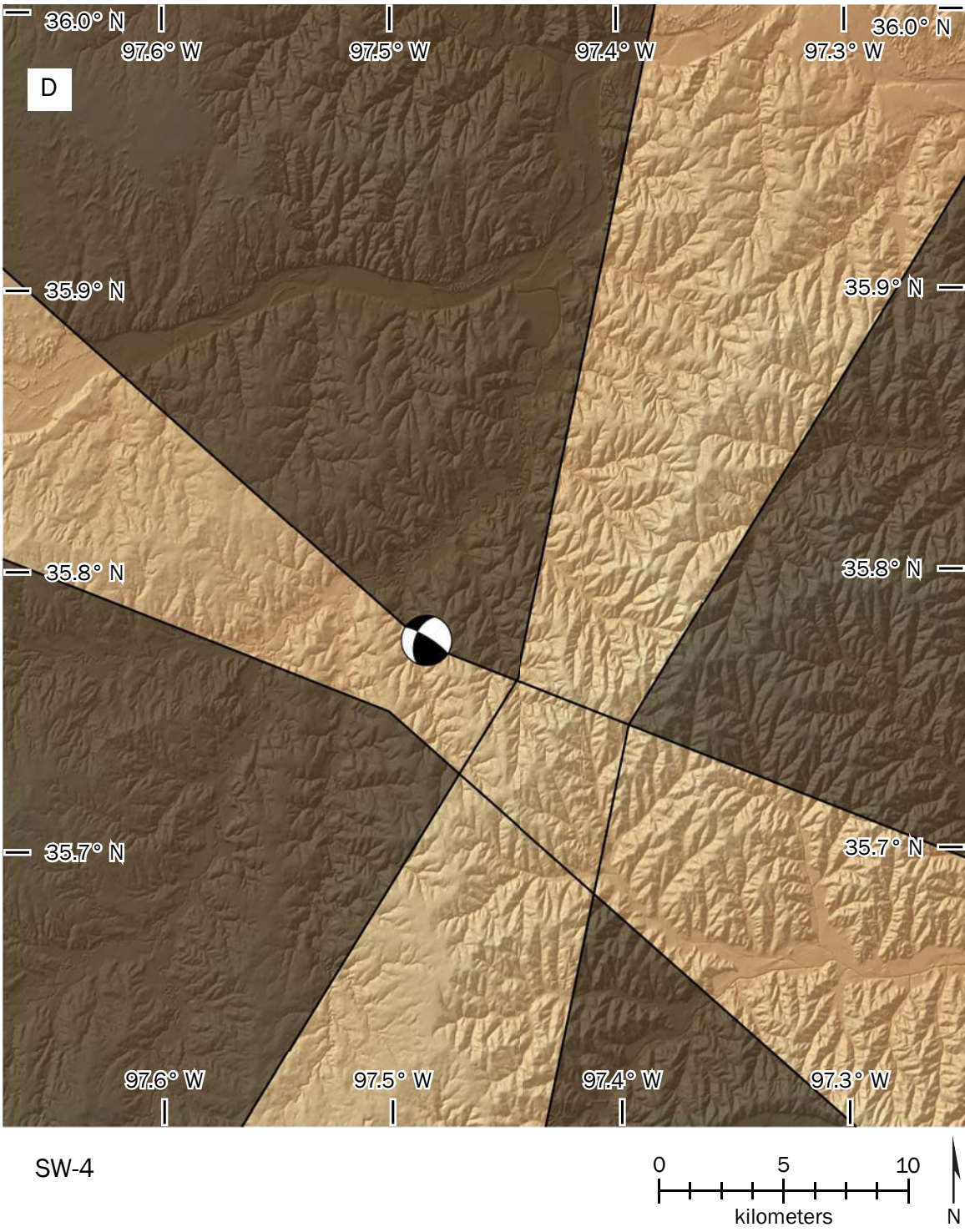
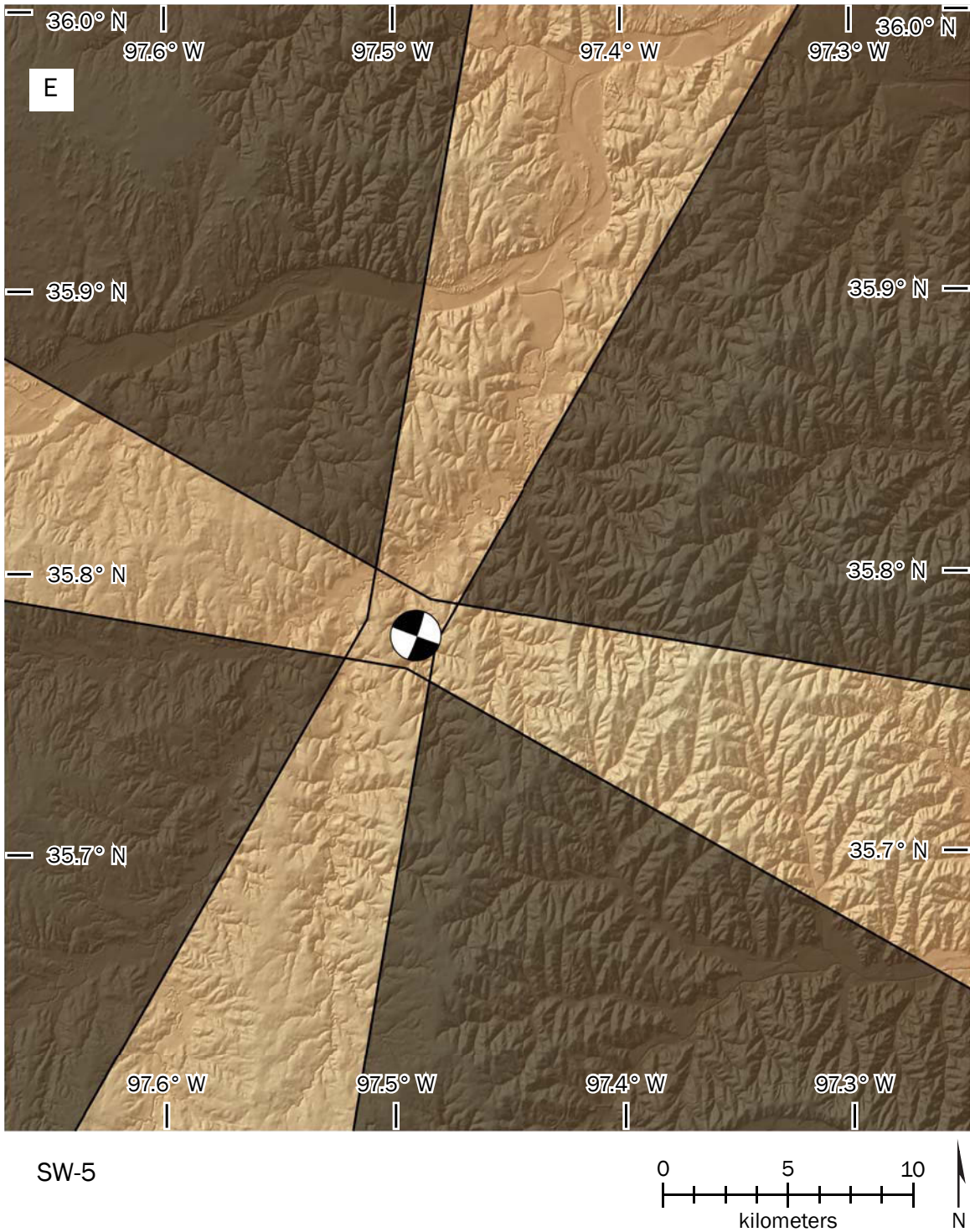


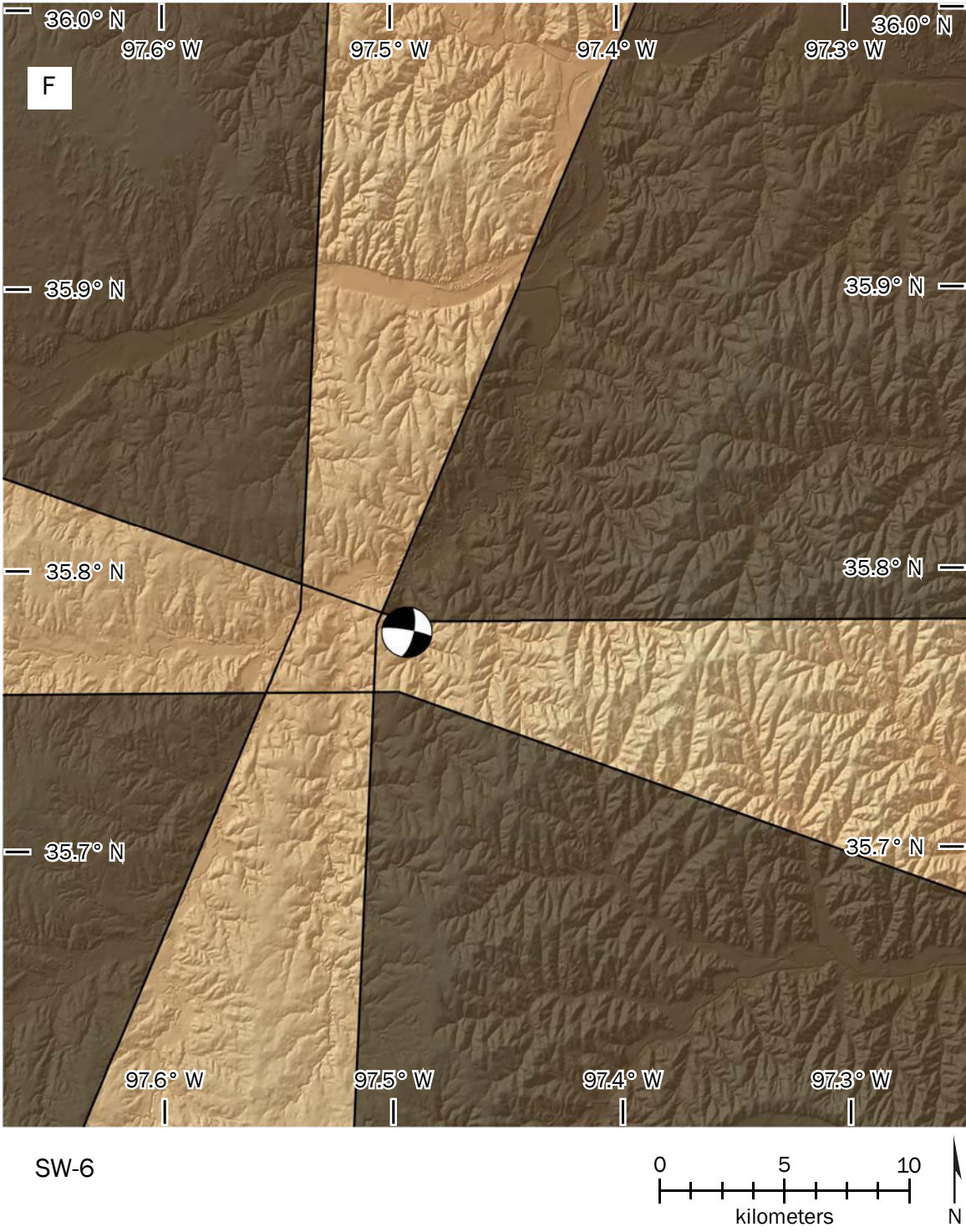
Figure B.2. A-AC. All seismo-lineaments from this study.

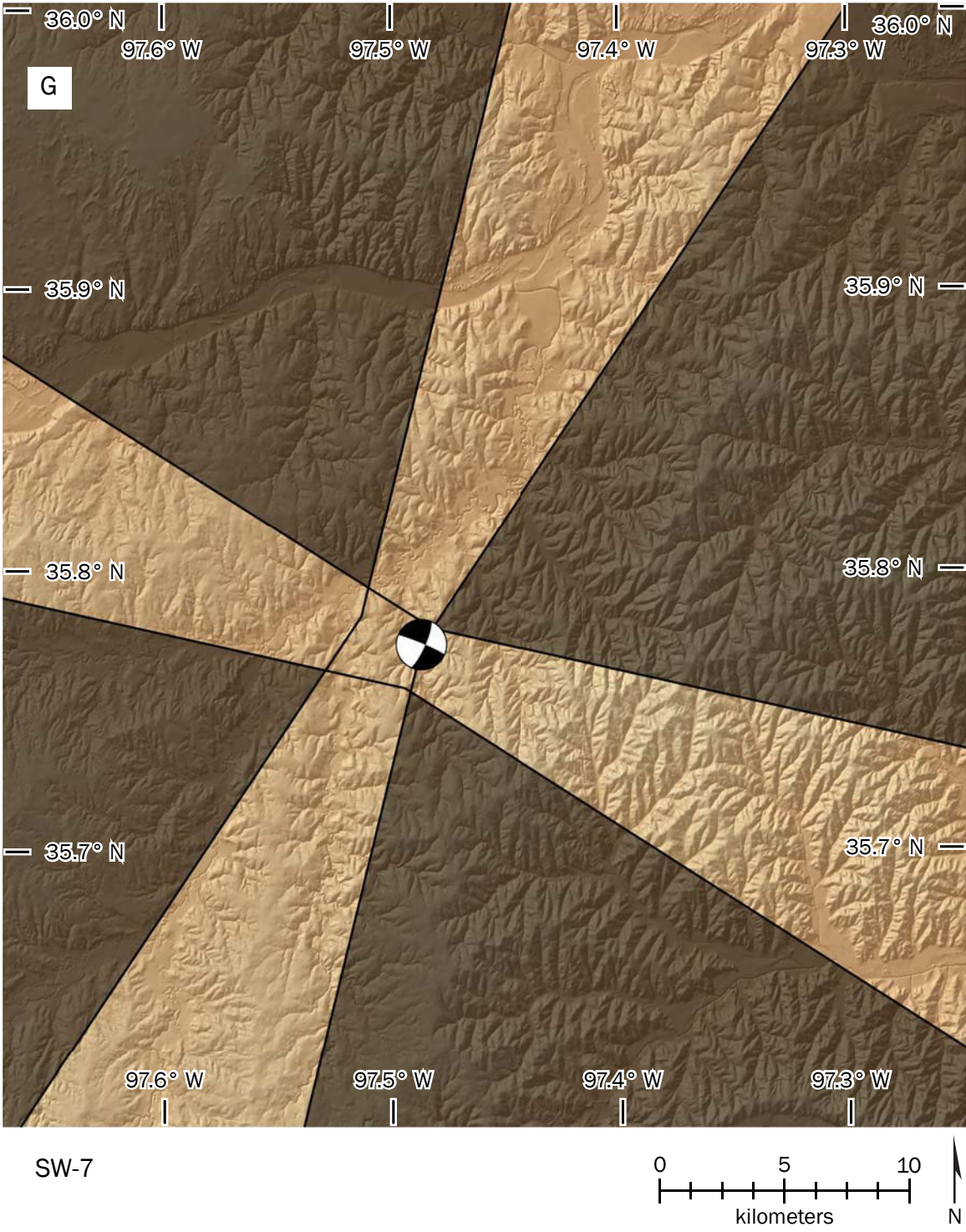




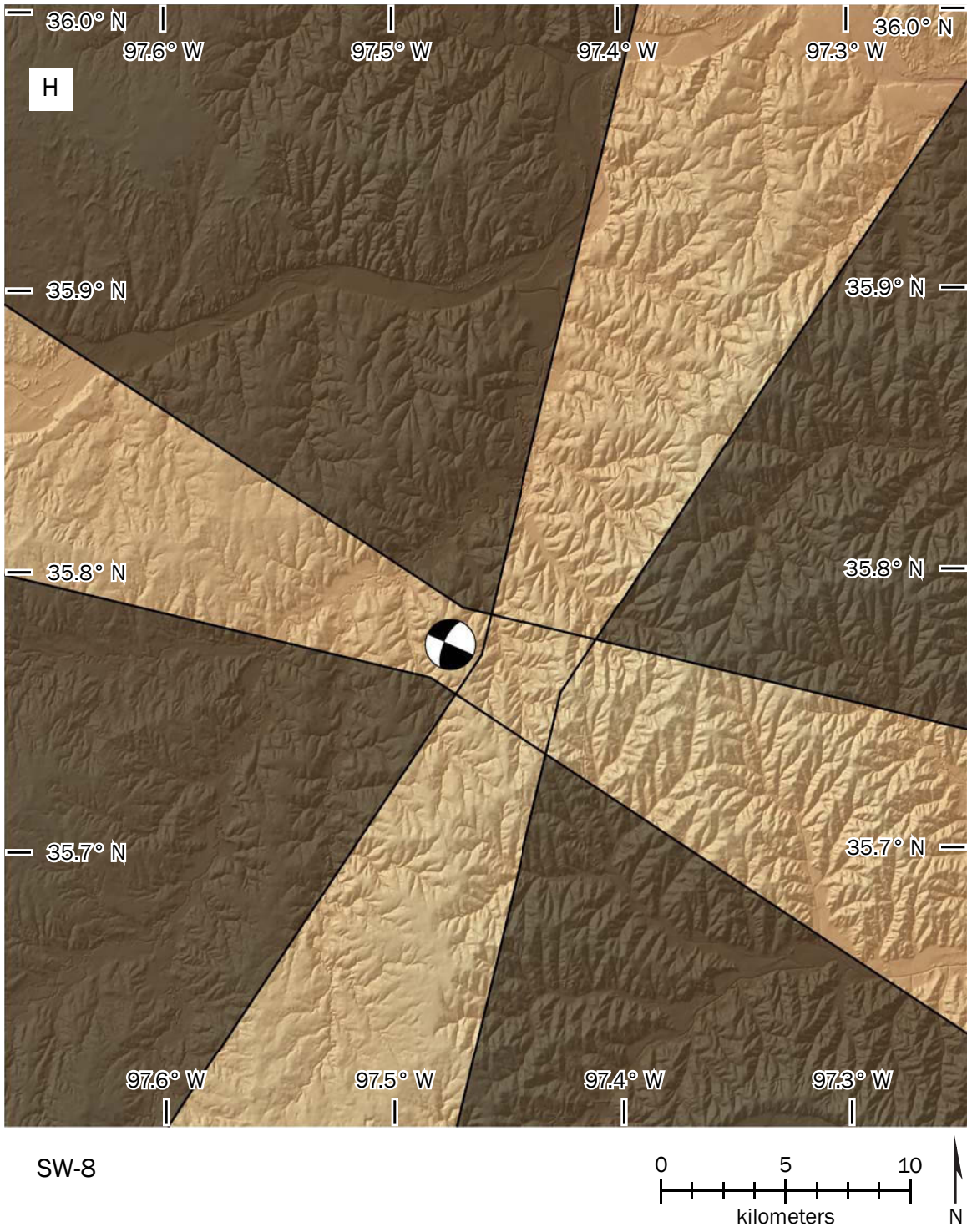


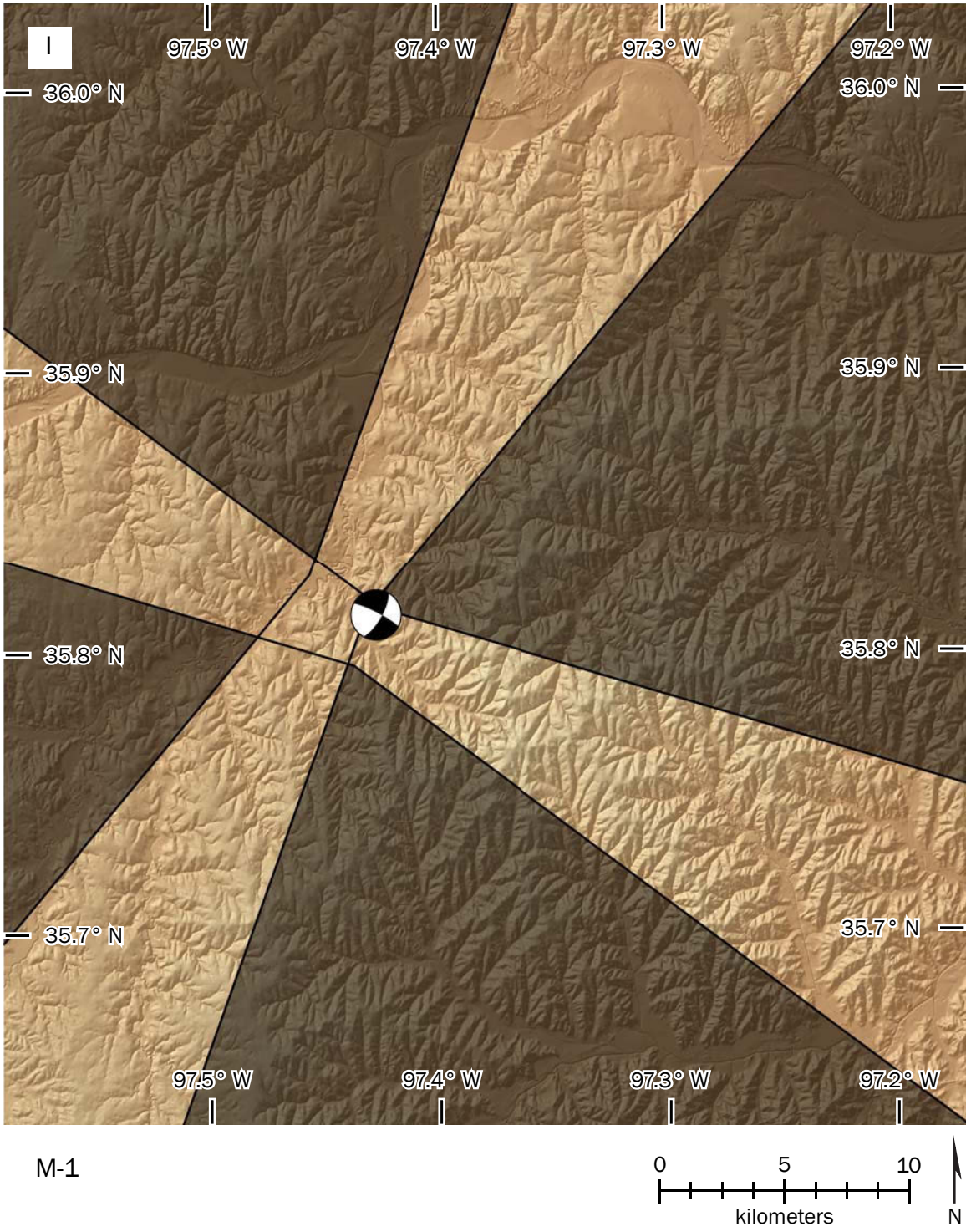


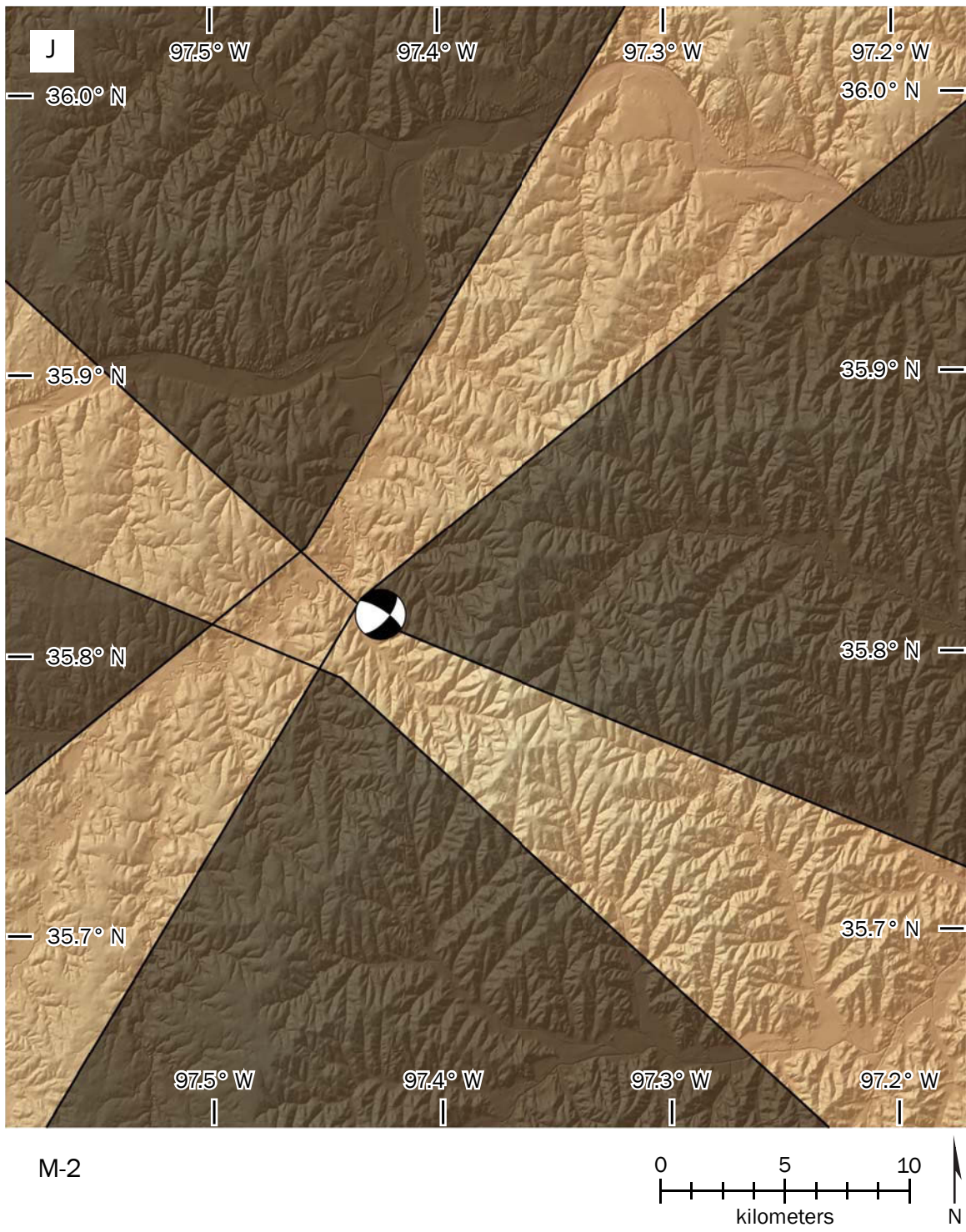


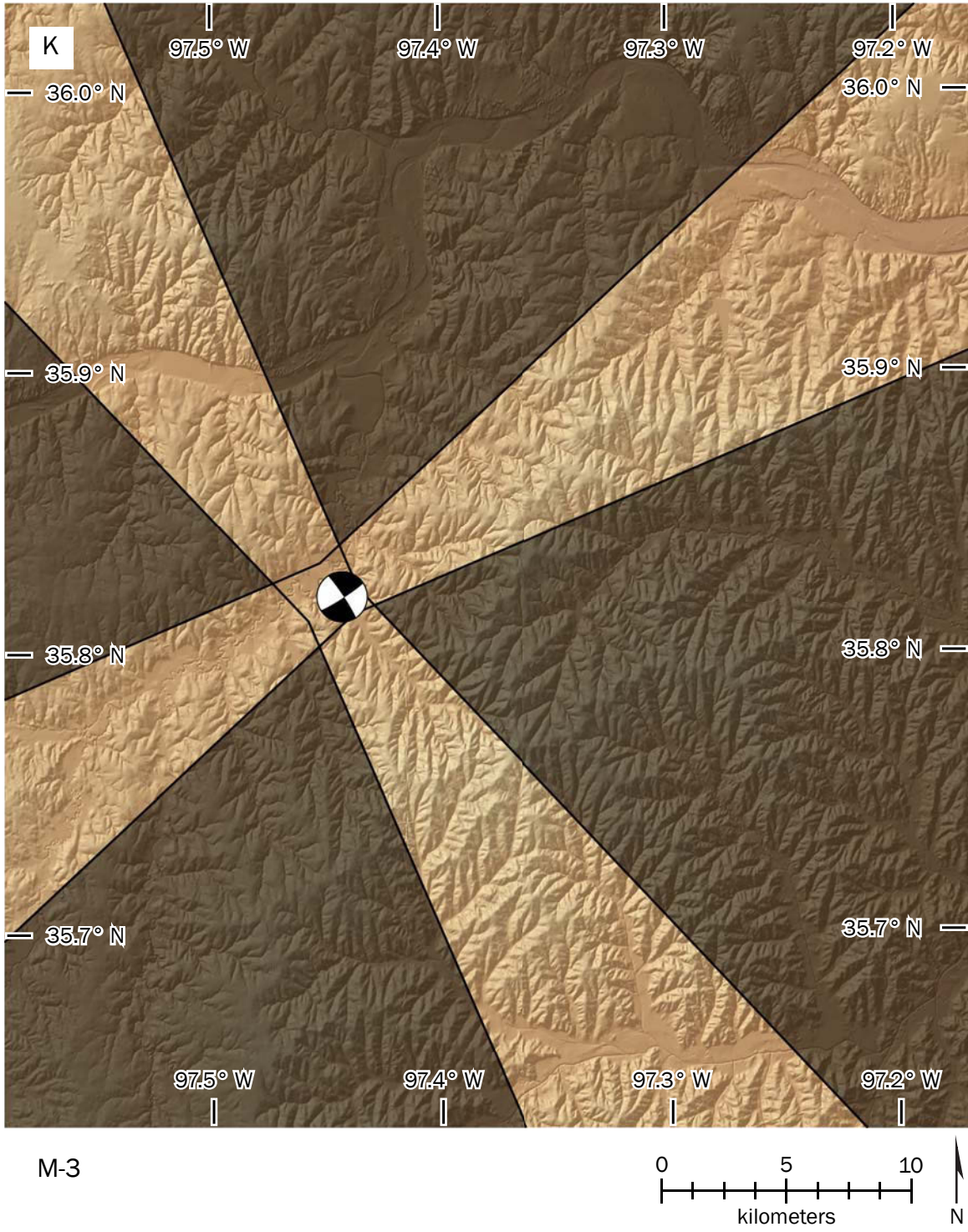


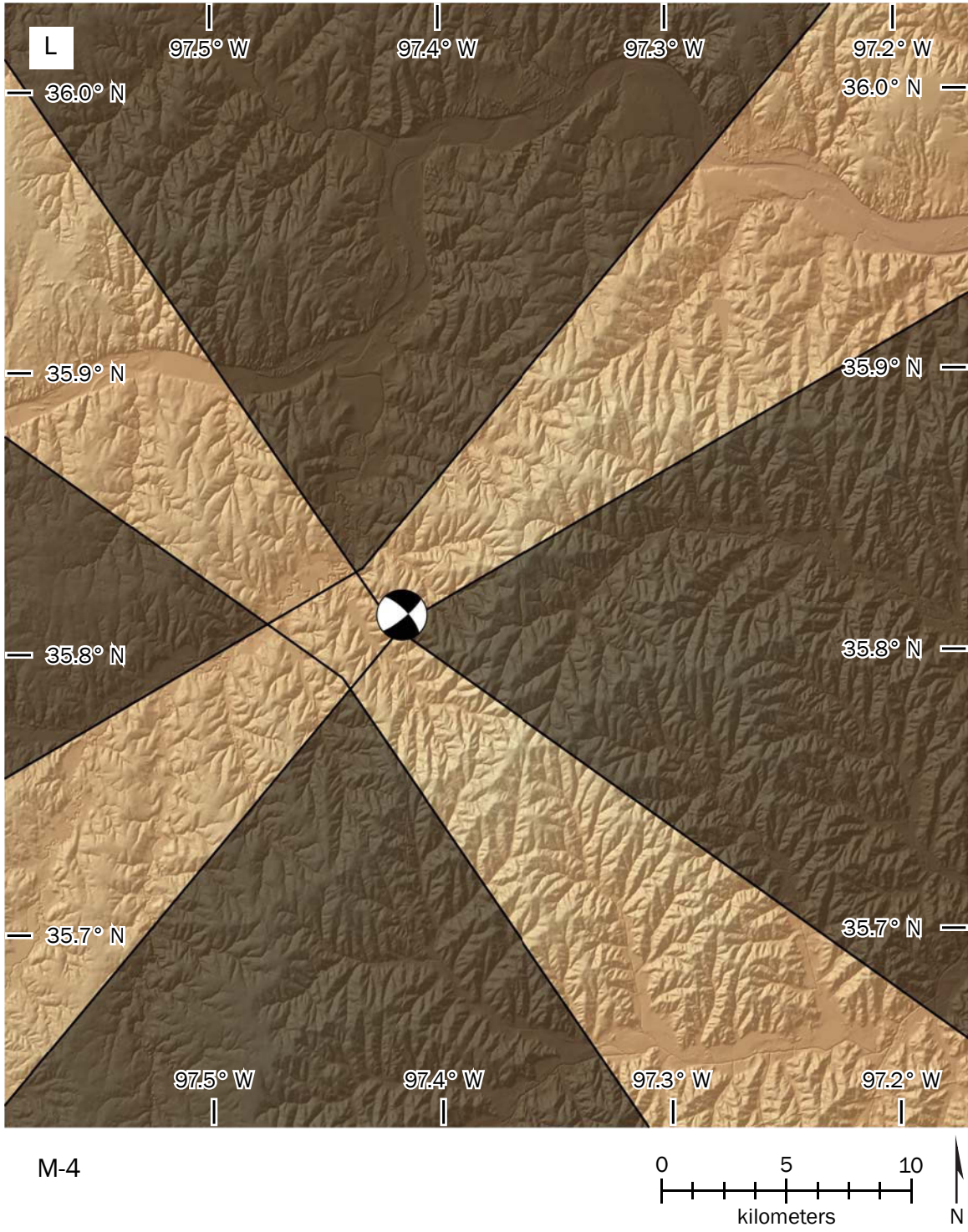


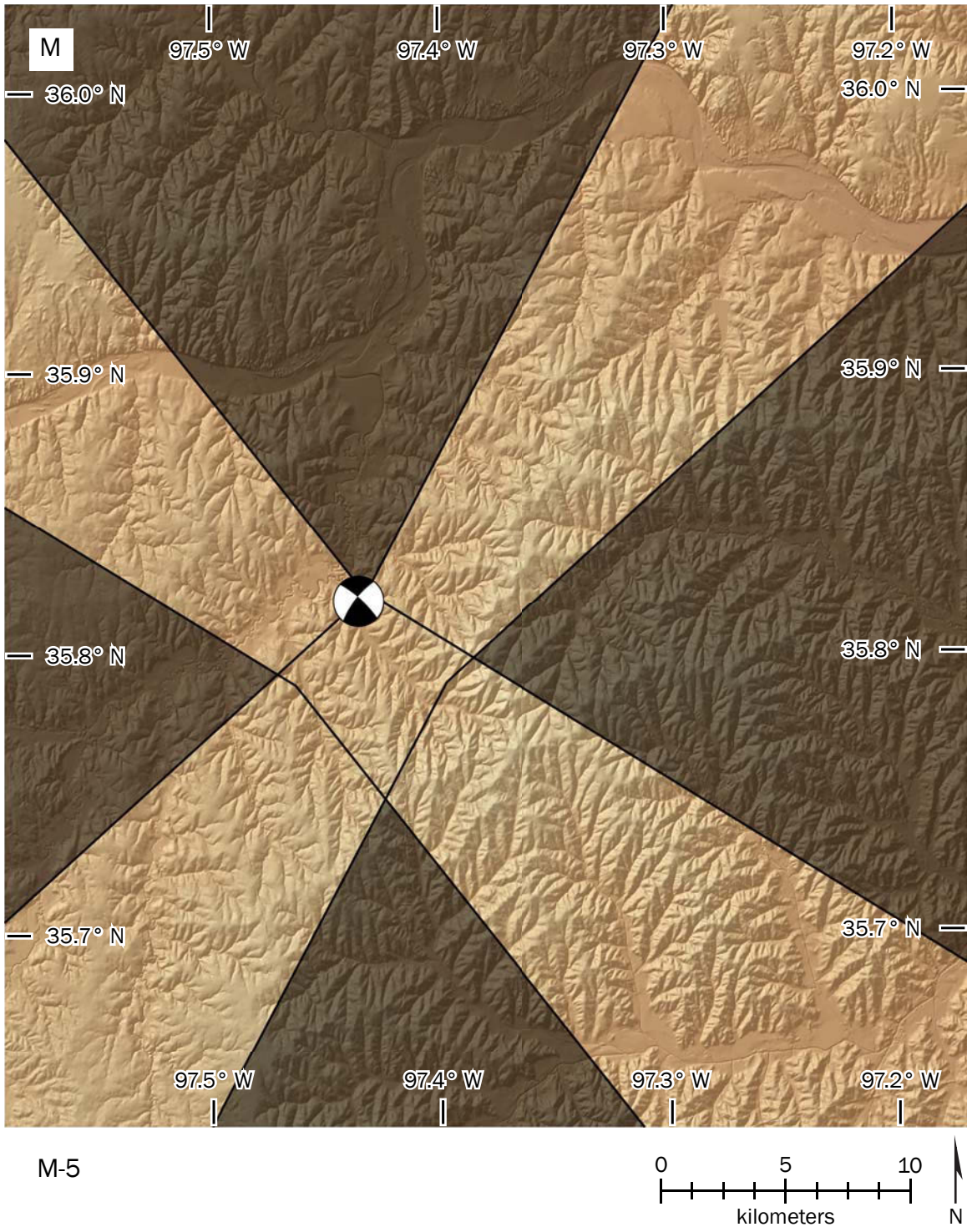


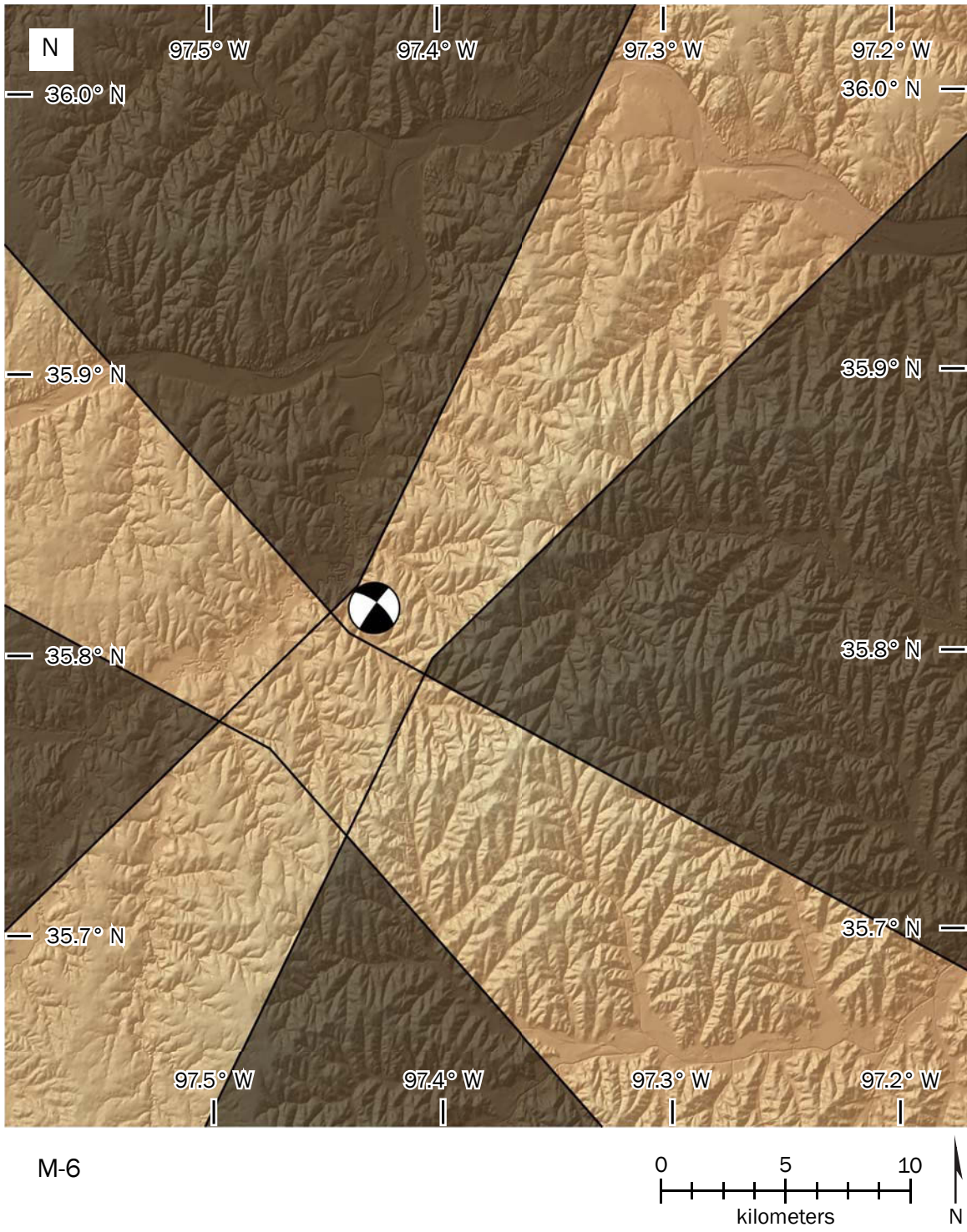


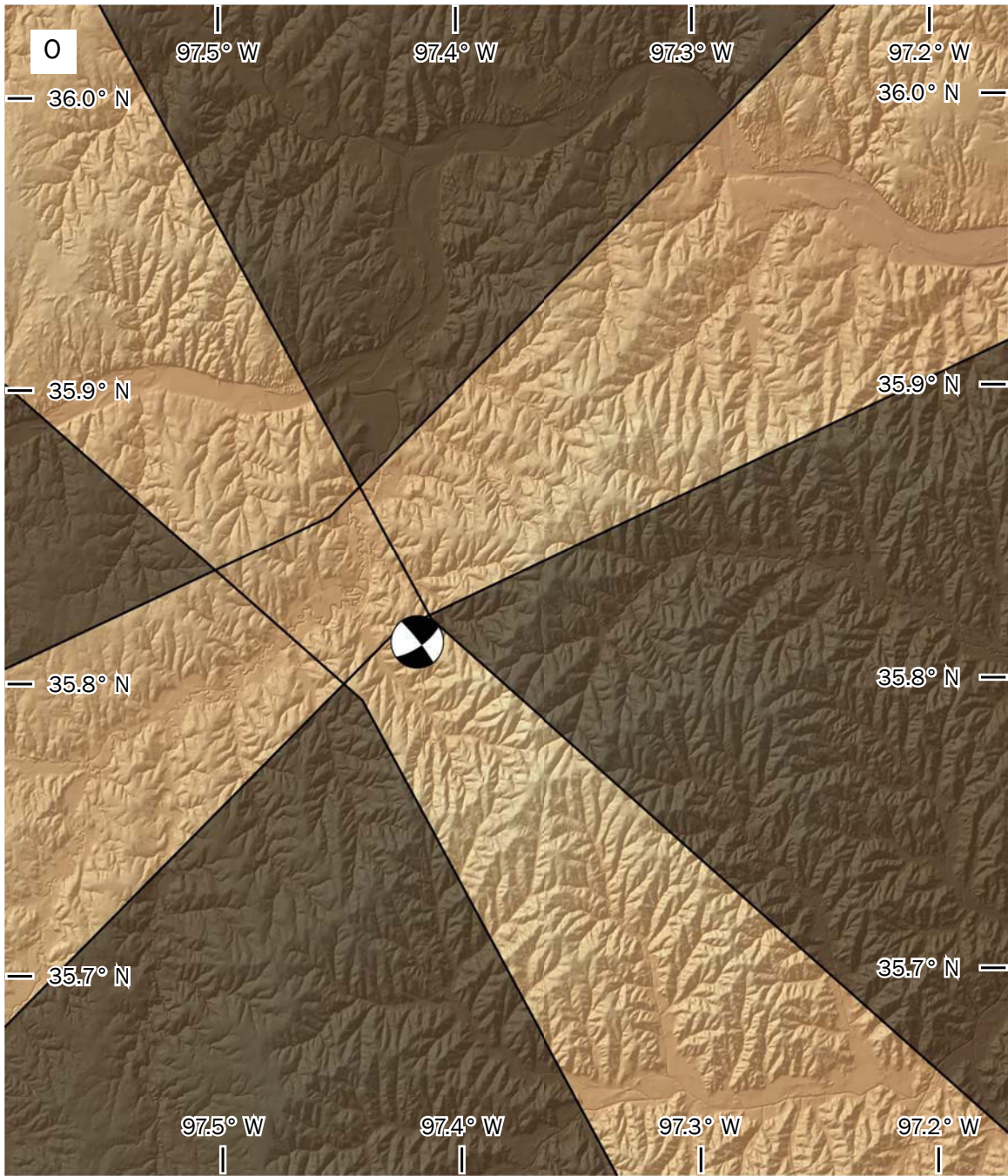




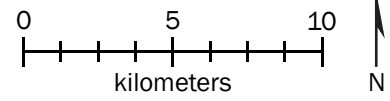




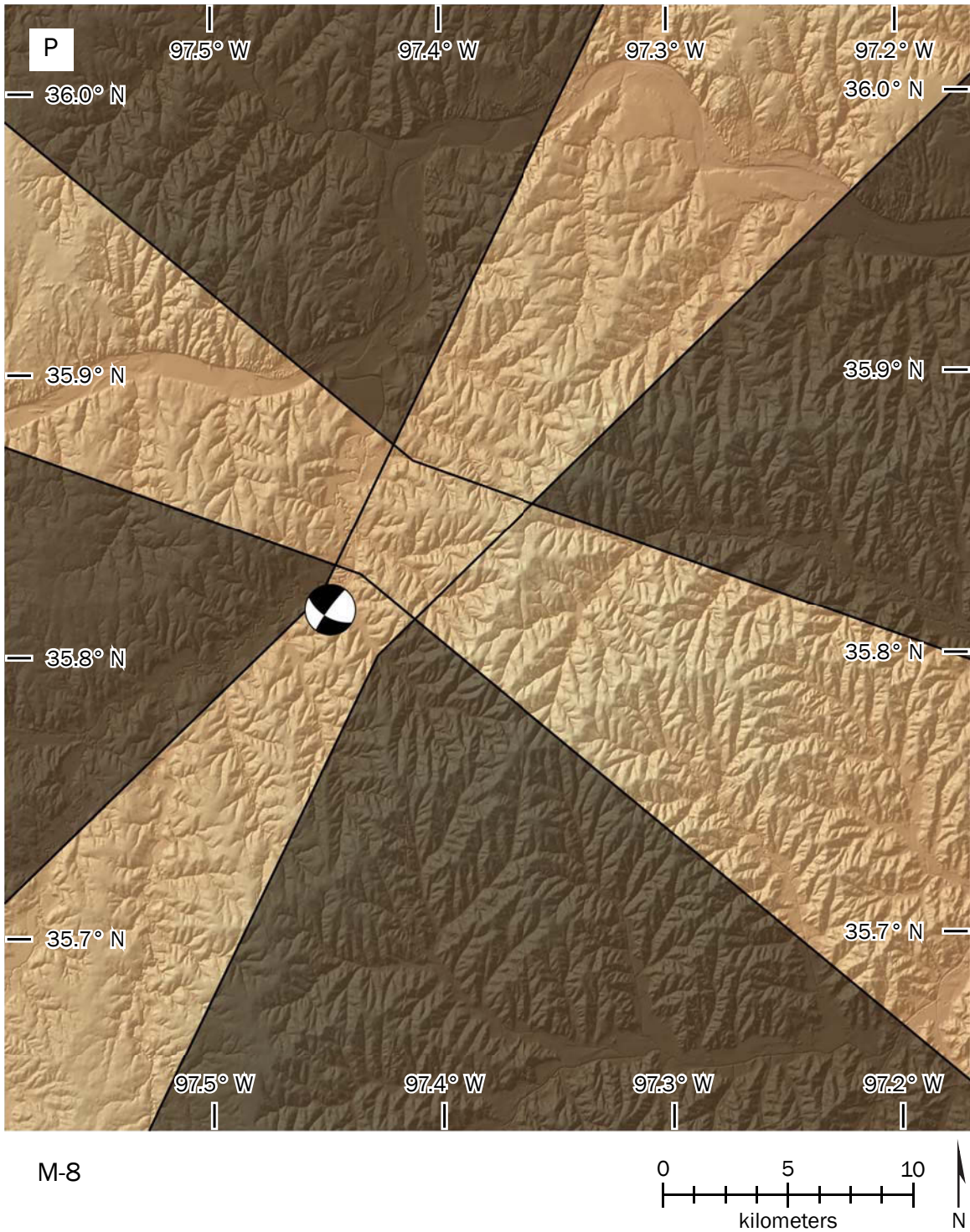


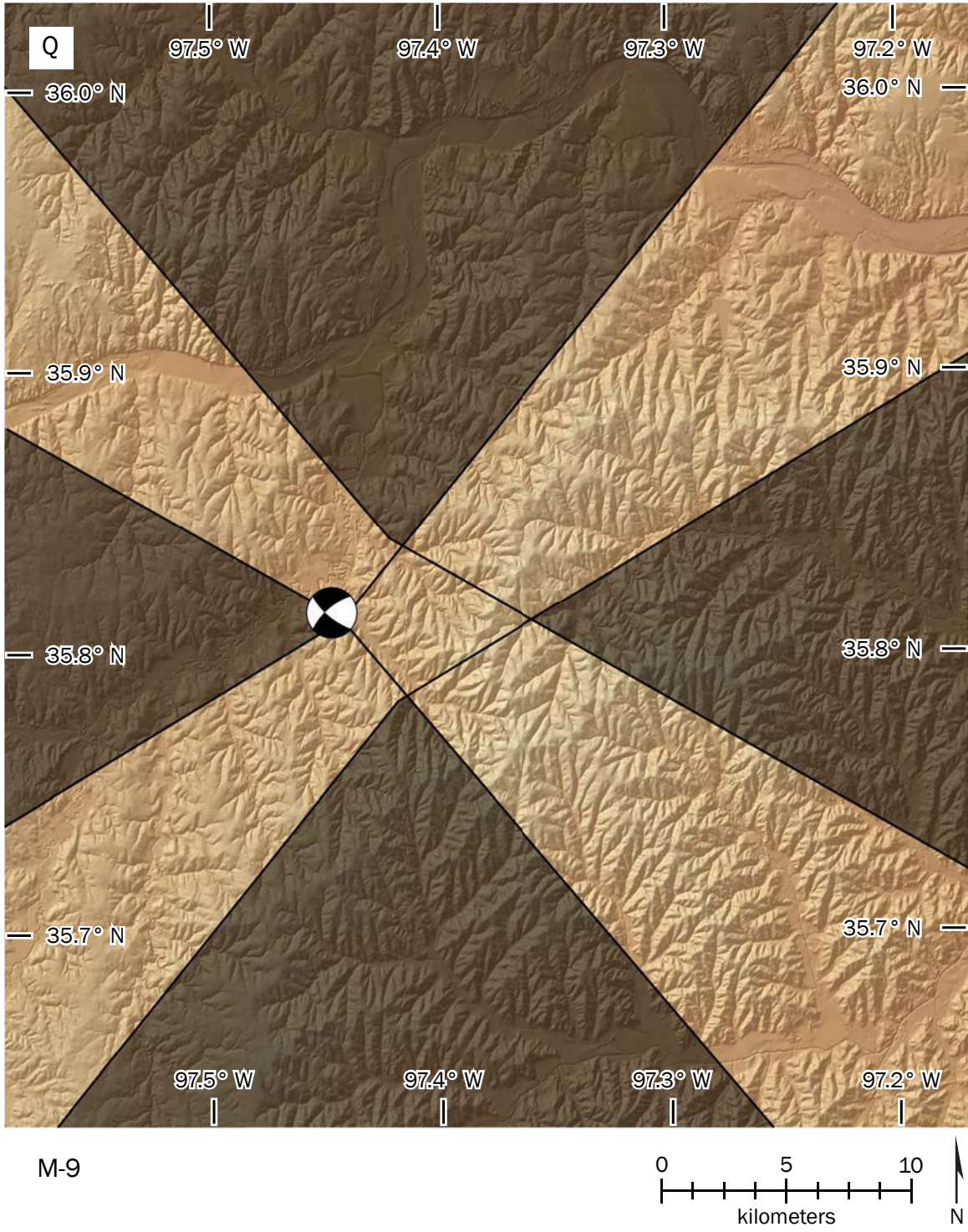


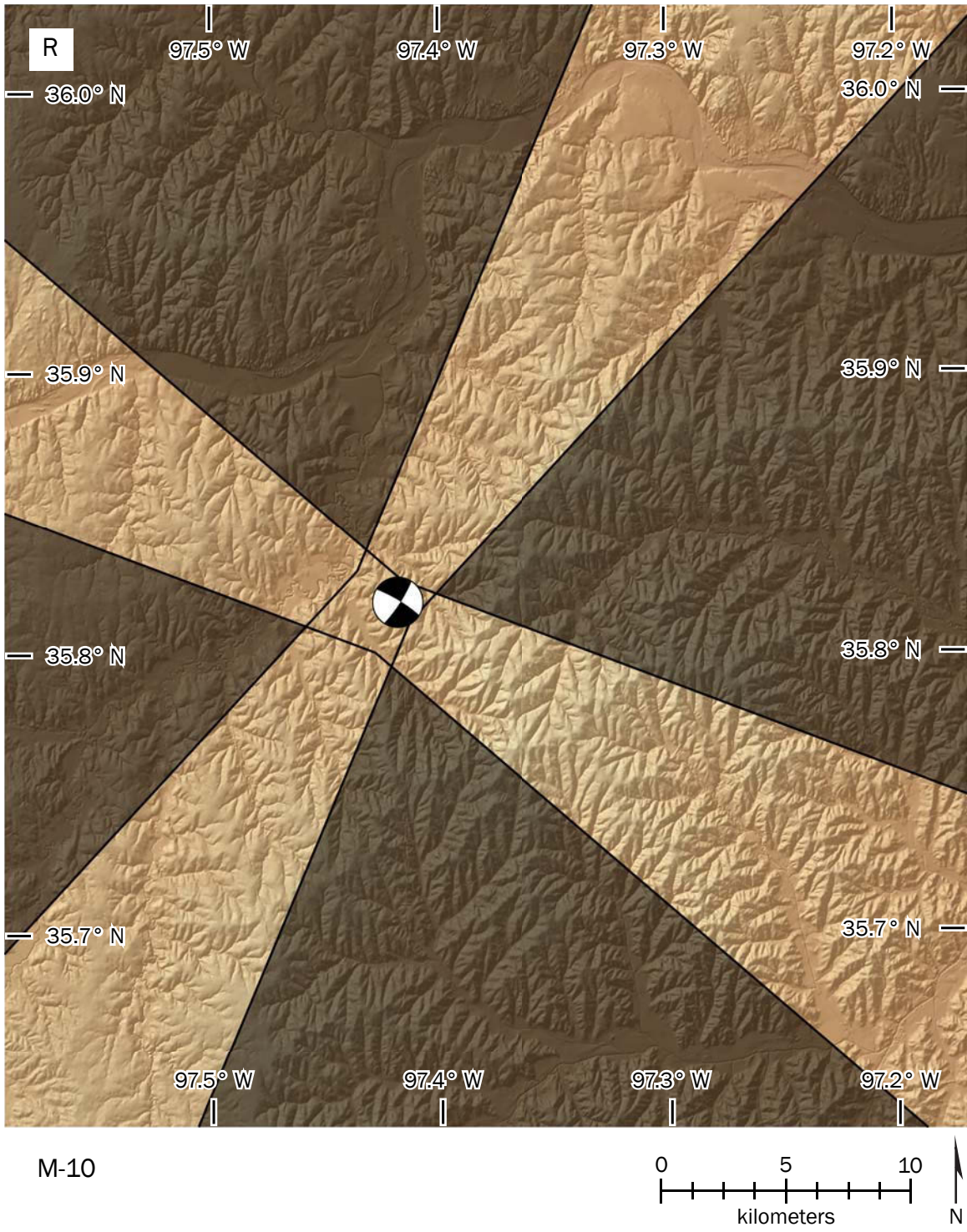
M-7

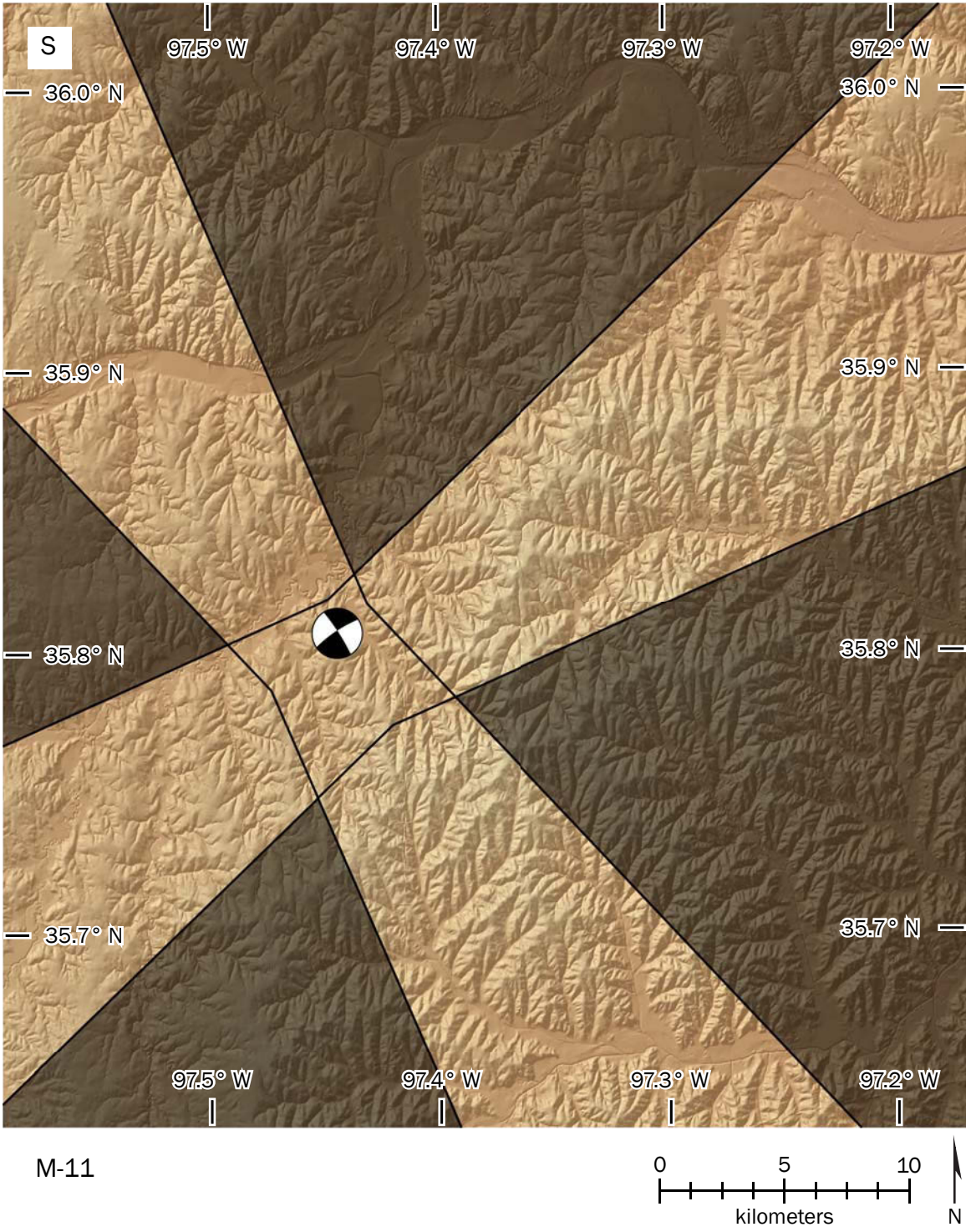


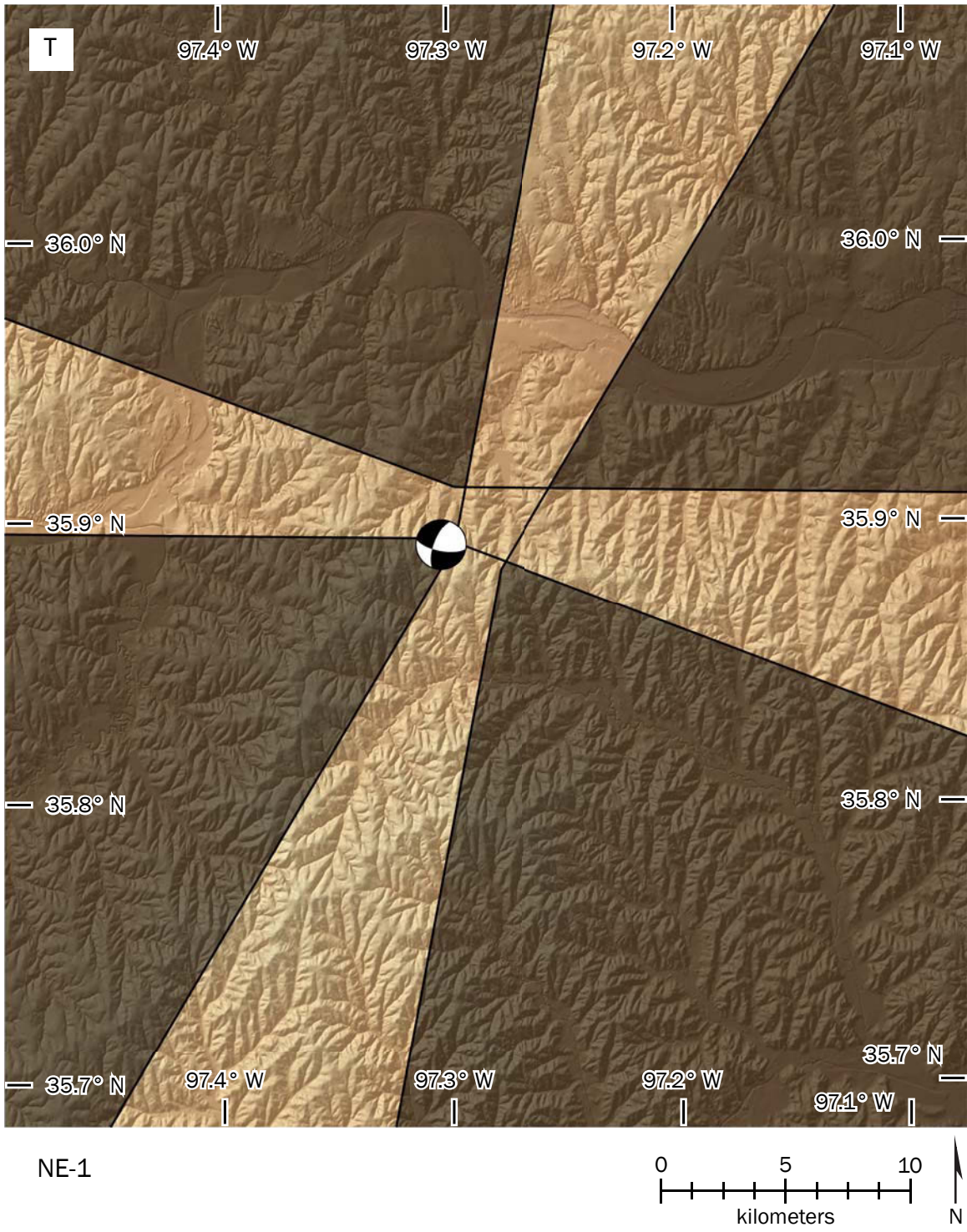




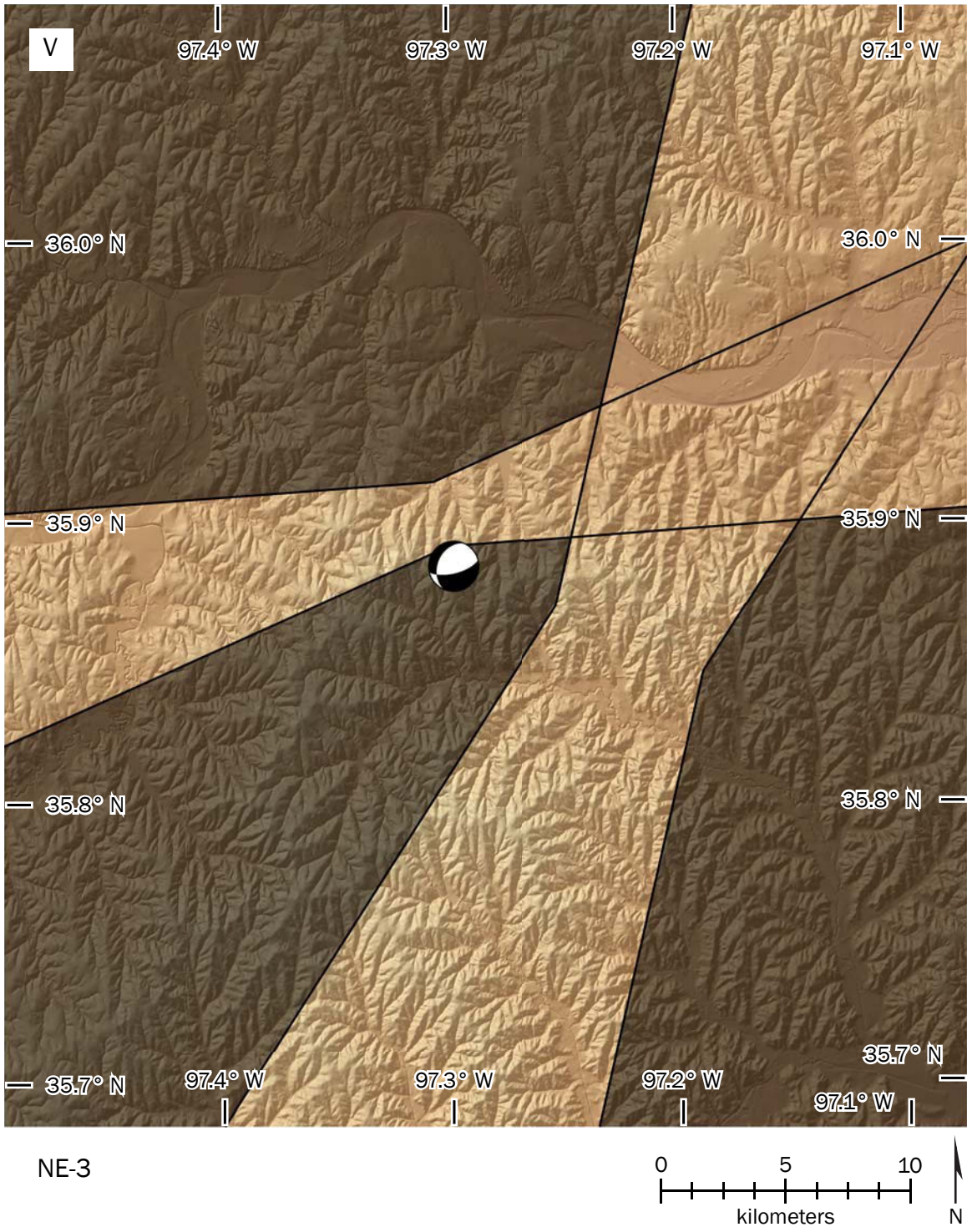


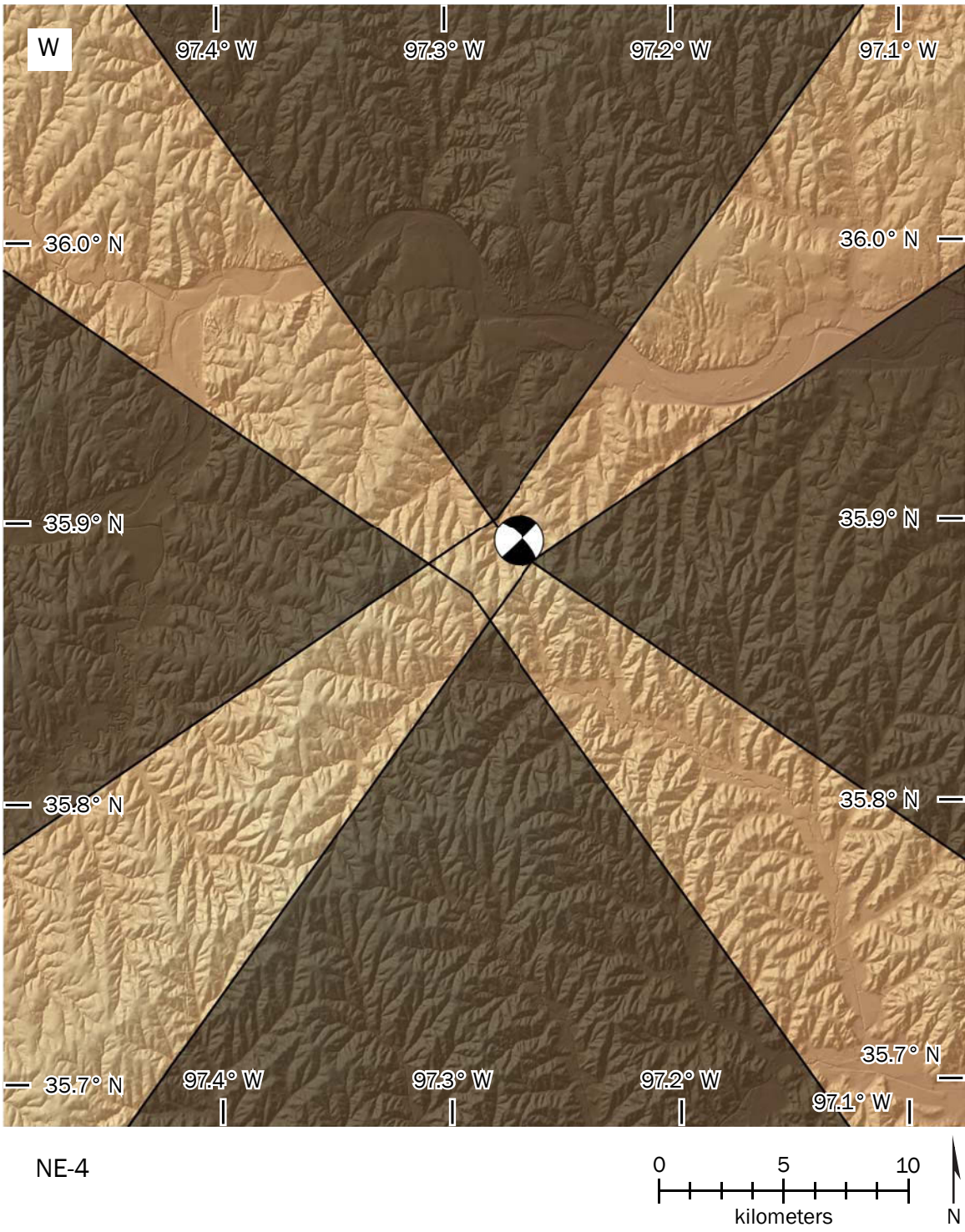






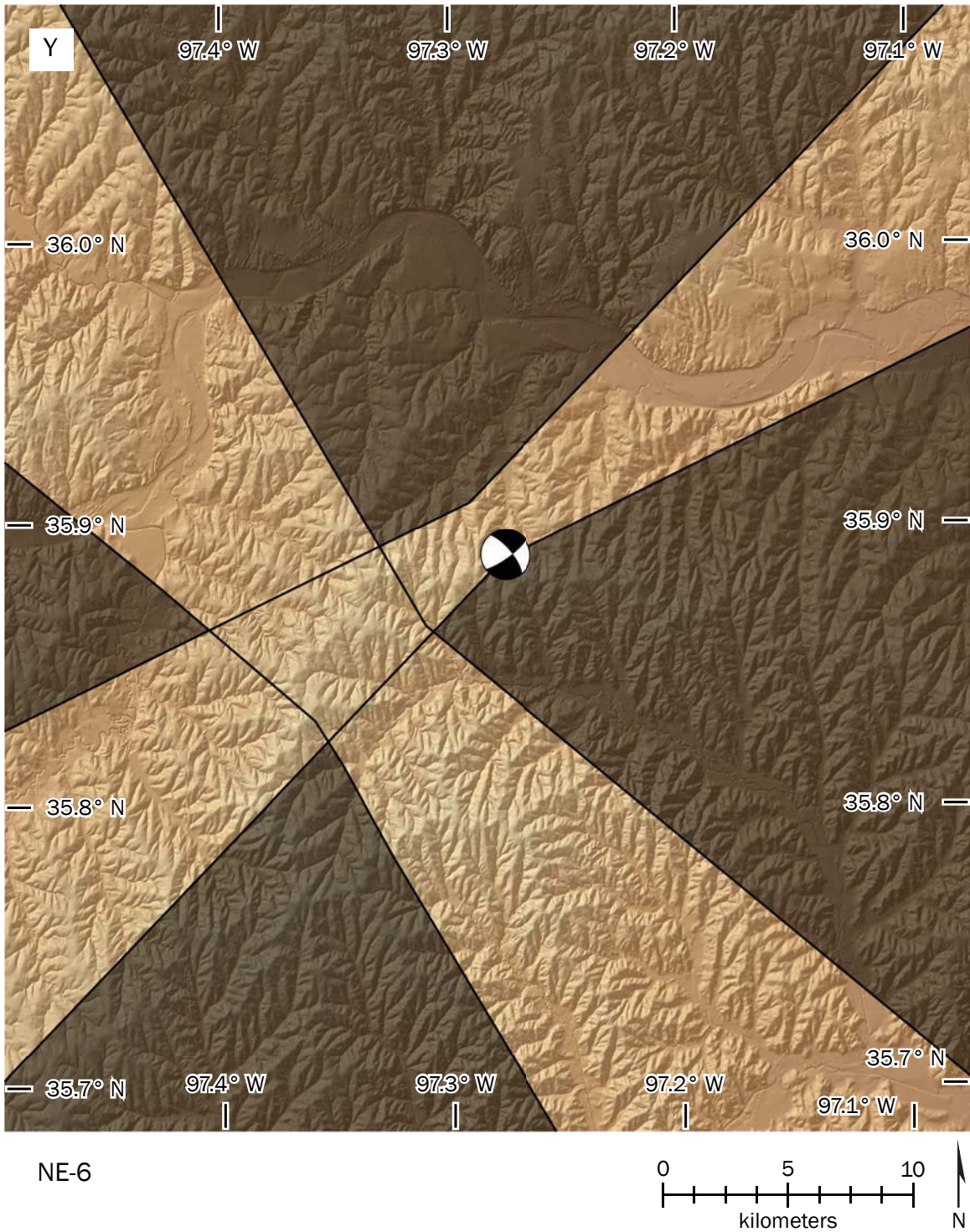




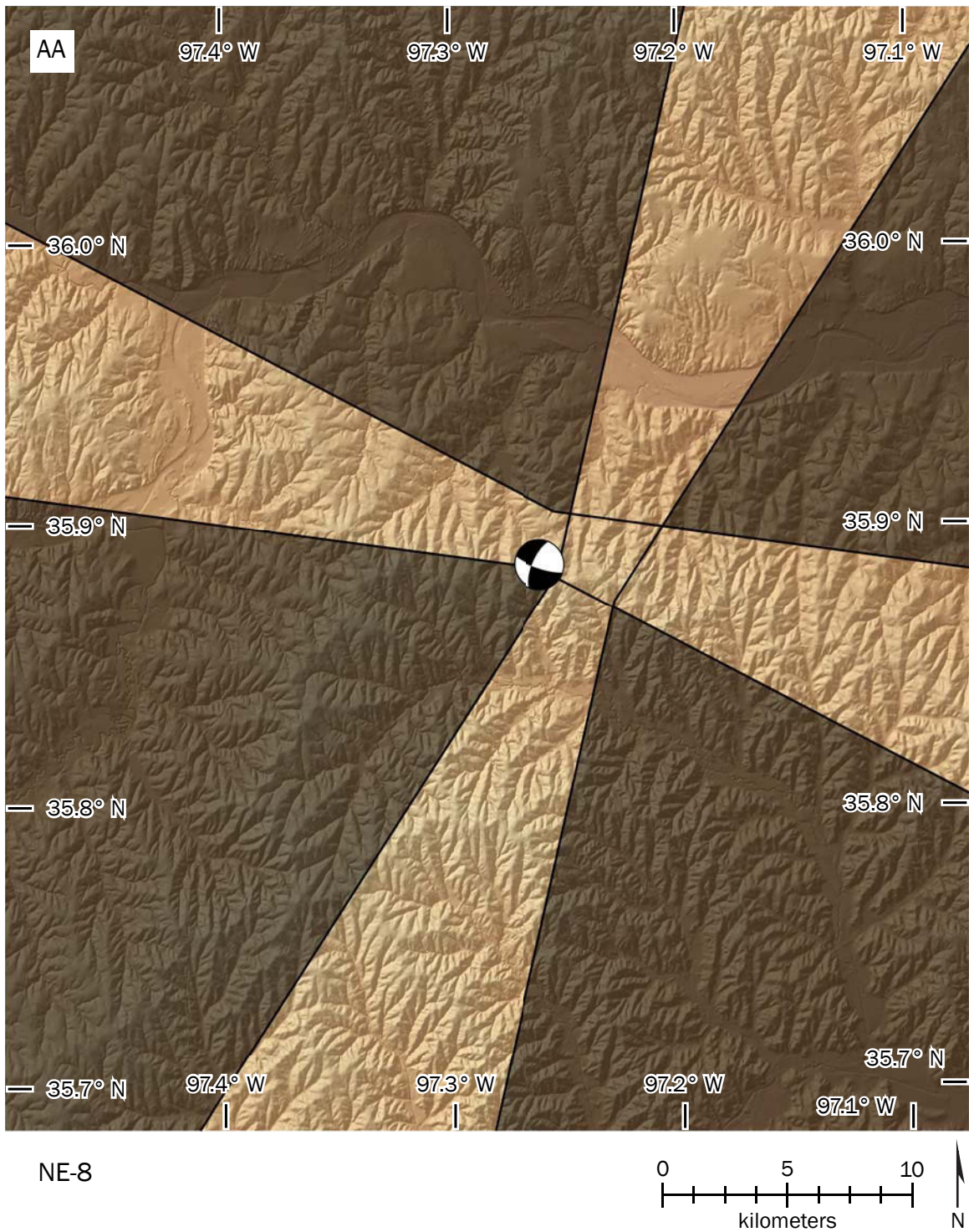


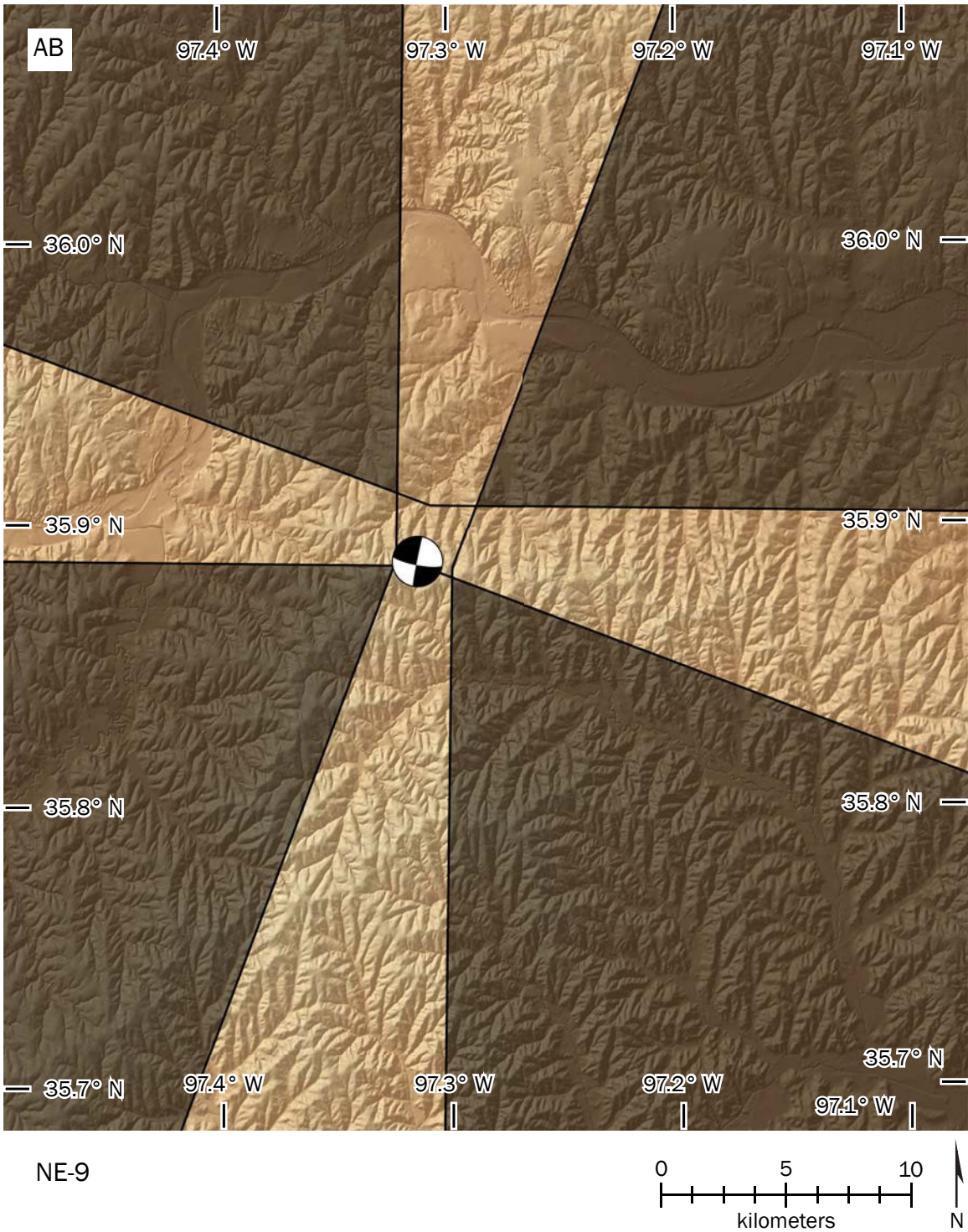


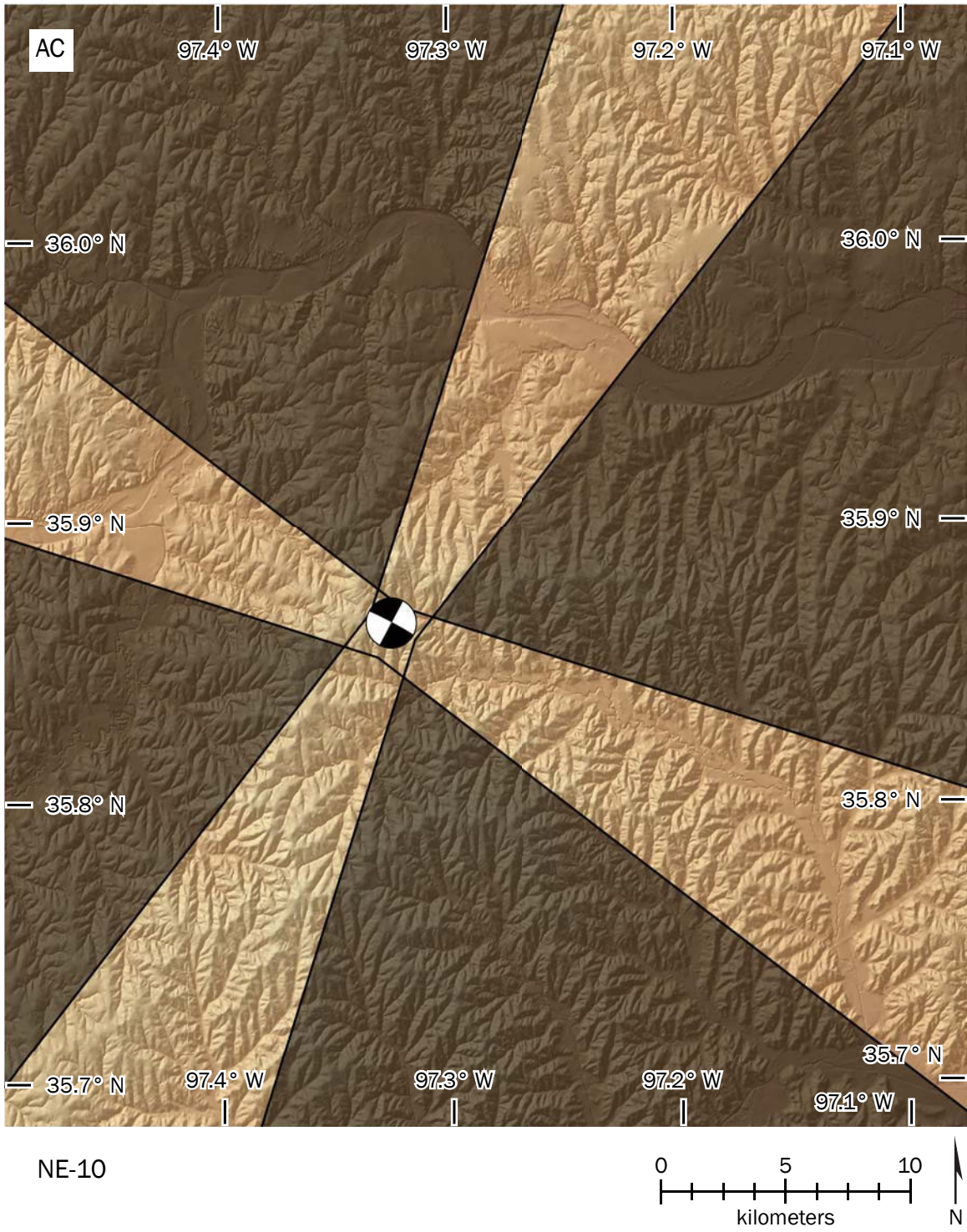












## REFERENCES CITED

- Andrews, R.D., and Holland, A.A., 2015, Statement on Oklahoma seismicity, [http://www.ogs.ou.edu/Documents/OGS\\_Statement-Earthquakes-21-April-2015.pdf](http://www.ogs.ou.edu/Documents/OGS_Statement-Earthquakes-21-April-2015.pdf) (accessed April 2015).
- Berendsen, P., and Blair, K.P., 1995, Structural development of the Nemaha tectonic zone in Kansas, *in* Johnson, K.S., (ed.), Structural styles in the southern Midcontinent, 1992 symposium: Oklahoma Geological Survey Circular 97, p. 208–214.
- Bonilla, M.G., 1982, Evaluation of potential surface faulting and other tectonic deformation, U.S. Geological Survey Open-File Report 82-732, 58 p.
- Burbank, D.W., and Anderson, R.S., 2011, Tectonic Geomorphology: Oxford, Blackwell Science, 274 p.
- Burchett, R.R., Wilson, F.W., Anderson, R.R., and Kisvarsanyi, E.B., 1983, Precambrian configuration map of Forest City basin and adjacent areas, of Iowa, Kansas, Missouri and Nebraska: Nebraska Geological Survey, Lincoln.
- Cronin, V.S., 2014a, Projecting the nodal planes from a focal mechanism solution onto a digital elevation model surface: Mathematica notebook file available at <http://croninprojects.org/Vince/SLAM/index.htm>.
- Cronin, V.S., 2014b, Seismo-lineament analysis method (SLAM), Using earthquake focal mechanisms to help recognize seismogenic faults, *in* Proceedings of the International INQUA Meeting on Paleoseismology, Active Tectonics and Archeoseismology, 21-27 September 2014, Busan, Korea: Seoul, Republic of Korea, The Geological Society of Korea, p. 28-31 (available via <http://croninprojects.org>)
- Cronin, V. S., and K. A. Sverdrup, 2003, Multiple-event relocation of historic earthquakes along Blanco Transform Fault Zone, NE Pacific, Geophysical Research Letters, v. 30, 2001, doi:10.1029/2003GL018086.
- Cronin, V.S., and Rasaka, B.M., 2015, Projecting the nodal planes from a focal mechanism solution onto a digital elevation model surface with output to USGS DEM format: Mathematica notebook file available via <http://croninprojects.org/Rasaka>
- Cronin, V.S., Schurter, G.J., and Sverdrup, K.A., 1993, Preliminary Landsat lineament analysis of the northern Nanga Parbat-Haramosh Massif, northwest Himalaya: Geological Society, London, Special Publication 74, p. 193–206, doi:10.1144/GSL.SP.1993.074.01.14.

- Cronin, V.S., Millard, M.A., Seidman, L.E., and Bayliss, B.G., 2008, The Seismo-Lineament Analysis Method (SLAM): A reconnaissance tool to help find seismogenic faults: *Environmental & Engineering Geoscience*, v. 14, p. 199–219, doi:10.2113/gseegeosci.14.3.199.
- Darold, A.P., Holland, A.A., Morris, J.K., and Gibson, A.R., 2015, Oklahoma earthquake summary report 2014: Oklahoma Geological Survey Open-File Report OF1-2015, [http://www.ogs.ou.edu/pubsscanned/openfile/OF1\\_2015.pdf](http://www.ogs.ou.edu/pubsscanned/openfile/OF1_2015.pdf) (accessed March 2015), <http://wichita.ogs.ou.edu/documents/2014/hypodd2014/> (accessed January 2016).
- Darold, A.P., and Holland, A.A., 2015, Preliminary Oklahoma optimal fault orientations: Oklahoma Geological Survey Open-File Report OF4-2015, <http://ogs.ou.edu/docs/openfile/OF4-2015.pdf> (accessed December 2015).
- Environmental Systems Research Institute (ESRI) ArcGIS Pro Desktop help, 2015, How Stream to Feature works, <http://pro.arcgis.com/en/pro-app/tool-reference/spatial-analyst/how-stream-to-feature-works.htm#GUID-899CB8B2-9A6C-4D5B-86F9-9142DAB5A619> (accessed December 2015).
- Filson, J.R., McCarthy, J., Ellsworth, W.L., and Zoback, M.L., 2003, The USGS Earthquake Hazards Program in NEHRP— Investing in a safer future: U.S. Geological Survey Fact Sheet 017-03, <http://pubs.usgs.gov/fs/2003/fs017-03/> (accessed January 2016).
- Gay, S.P., Jr., 1995, Basement control of selected oil and gas fields in Kansas as determined by detailed residual aeromagnetic data; in *Geophysical Atlas of Selected Oil and Gas Fields in Kansas*, Anderson, N.L., and Hedke, D.E., eds.: Kansas Geological Survey and Kansas Geological Society, Bulletin 237, p. 10–16.
- Gay, S. P., Jr., 1999, Strike-slip, compressional thrust-fold nature of the Nemaha system in eastern Kansas and Oklahoma; in, *Transactions of the American Association of Petroleum Geologists Midcontinent Section Meeting*, Merriam, D.F., ed.: Kansas Geological Society and Kansas Geological Survey, Open-file Report 99-28, p. 39-50.
- Gay Jr, S.P., 2003a, The Nemaha Trend—A system of compressional thrust-fold, strike-slip structural features in Kansas and Oklahoma, Part 1: *The Shale Shaker*, v. 54, No. 1, p. 9–17, <http://archives.datapages.com/data/ocgs/data/054/054001/0009.htm> (accessed April 2015).
- Gay Jr, S.P., 2003b, The Nemaha Trend—A system of compressional thrust-fold, strike-slip structural features in Kansas and Oklahoma, Part 2: *The Shale Shaker*, v. 54, No. 2, p. 39–49, <http://archives.datapages.com/data/ocgs/data/054/054002/0039.htm> (accessed April 2015).



- Gerhard, L.C., 2004, A new look at an old petroleum province: Current Research in Earth Sciences, Bulletin 250, Kansas Geological Survey, p. 1–27.
- Hartnady, C.J.H., 2015, Recent triggered (hydro)seismicity in Oklahoma: A cautionary tale?, *in* Proceedings of the Geological Society of America, South-Central Section 49th Annual Meeting, Stillwater, Oklahoma, 20 March 2015, <https://gsa.confex.com/gsa/2015SC/webprogram/Paper254249.html>.
- Holland, A.A., 2013a, Earthquakes triggered by hydraulic fracturing in south-central Oklahoma: Bulletin of the Seismological Society of America, v. 103, p. 1784–1792, doi:10.1785/0120120109.
- Holland, A.A., 2013b, Optimal fault orientations within Oklahoma: Seismological Research Letters, v. 84, p. 876–890, doi:10.1785/0220120153.
- Holland, A.A., 2014, Imaging time dependent crustal deformation using GPS geodesy and induced seismicity, stress and optimal fault orientations in the North American mid-continent Ph.D. Dissertation: University of Arizona.
- Holland, A.A., 2015a, Preliminary fault map of Oklahoma: Oklahoma Geological Survey, scale 1:750,000.
- Holland, A.A., 2015b, personal communication.
- Johnson, K.S., 2008, Geologic history of Oklahoma: Oklahoma Geological Survey, [http://www.ogs.ou.edu/pubsscanned/EP9\\_2-8geol.pdf](http://www.ogs.ou.edu/pubsscanned/EP9_2-8geol.pdf) (accessed November 2014).
- Keller, G.R., and Holland, A.A., 2013, Statement on 2011 Prague Earthquake Sequence: Oklahoma Geological Survey, [http://www.okgeosurvey1.gov/media/OGS\\_PragueStatement201303.pdf](http://www.okgeosurvey1.gov/media/OGS_PragueStatement201303.pdf) (accessed January 2016).
- Keranen, K.M., Savage, H.M., Abers, G.A., and Cochran, E.S., 2013, Potentially induced earthquakes in Oklahoma, USA: Links between wastewater injection and the 2011 Mw 5.7 earthquake sequence: *Geology*, v. 41, p. 699–702, doi:10.1130/G34045.1.
- Keranen, K. M., Weingarten, M., Abers, G. A., Bekins, B. A., & Ge, S., 2014, Sharp increase in central Oklahoma seismicity since 2008 induced by massive wastewater injection: *Science*, v. 345, p. 448-451, doi:10.1126/science.1255802.
- Lancaster, D.S., 2011, Correlation of earthquakes with seismogenic faults along the northern Arizona Seismic Belt, southwestern margin of the Colorado Plateau: M.S. Thesis: Waco, Texas, Baylor University, 98 p.
- Lindsay, R.D., 2012, Seismo-lineament analysis of selected earthquakes in the Tahoe-Truckee area, California and Nevada: M.S. Thesis: Waco, Texas, Baylor University, 147 p.

- McCalpin, J., ed., 1996, *Paleoseismology*: San Diego, California, Academic Press, 588 p.
- McNamara, D. E., Benz, H. M., Herrmann, R. B., Bergman, E. A., Earle, P., Holland, A., Baldwin, R., and Gassner, A., 2015, Earthquake hypocenters and focal mechanisms in central Oklahoma reveal a complex system of reactivated subsurface strike-slip faulting: *Geophysical Research Letters*, v. 42, p. 2742-2749, doi:10.1002/2014GL062730.
- Millard, M.A., 2007, Linking onshore and offshore data to find seismogenic faults along the eastern Malibu coastline: M.S. Thesis: Waco, Texas, Baylor University, 136 p.
- Miller, V.C., 1961, *Photogeology*: New York, McGraw-Hill, 248 p.
- Oklahoma Conservation Commission (OCC), 2015, OK Maps, <http://okmaps.org/ogi/Search.aspx> (accessed September 2015).
- Oklahoma Department of Emergency Management (OEM), 2014, Standard hazard mitigation plan update for the great state of Oklahoma: [https://www.ok.gov/OEM/Programs\\_&\\_Services/Mitigation/State\\_Mitigation\\_Plan.html](https://www.ok.gov/OEM/Programs_&_Services/Mitigation/State_Mitigation_Plan.html) (accessed January 2016).
- Oklahoma Geological Survey (OGS), 2015, Earthquake catalogs: <http://www.ou.edu/content/ogs/research/earthquakes/catalogs.html> (accessed January 2016).
- Ray, R.G., 1960, *Aerial Photographs in Geologic Interpretation and Mapping*: U.S. Geological Survey Professional Paper 373, 230 p.
- Reed, T.H., 2013, Spatial correlation of earthquakes with two known and two suspected seismogenic faults, north Tahoe-Truckee area, California: M.S. Thesis: Waco, Texas, Baylor University, 95 p.
- Seidman, L.E., 2007, Seismo-lineament analysis of the Malibu Beach quadrangle, southern California: M.S. Thesis: Waco, Texas, Baylor University, 95 p.
- Serpa, L., Setzer, T., Brown, L., 1989, COCORP seismic-reflection profiling in northeastern Kansas: *Geophysics in Kansas: Kansas Geological Survey Bulletin* 226, p. 165–176.
- Shreve, R.L., 1967, Infinite topologically random channel networks, *The Journal of Geology*, p. 178-186.
- Slemmons, D.B., and DePolo, C.M., 1986, Evaluation of active faulting and associated hazards, *in* *Studies in Geophysics—Active Tectonics*: National Research Council, National Academy Press, Washington, D.C., p. 45–62.
- Steeple, D.W., 1982, Structure of the Salina-Forest City interbasin boundary from seismic studies: *Kansas Geological Survey Bulletin* 226, p. 31–52.

- Stein, S., and Wysession, M., 2003, *An Introduction to Seismology, Earthquakes, and Earth Structure*: Malden, Massachusetts, Blackwell Publishing, 498 p.
- Stover, C.W., and Coffman, J.L., 1993, *Seismicity of the United States, 1568-1989* (revised): U.S. Government Printing Office, 428 p.
- Strahler, A.N., 1952, Hypsometric (area-altitude) analysis of erosional topography, *Geological Society of America Bulletin*, v. 63, p. 1117-1142, doi:10.1130/0016-7606(1952)63[1117:HAAOET]2.0.CO;2
- U.S. Geological Survey, 2011, Magnitude 5.6—Oklahoma earthquake: <http://earthquake.usgs.gov/earthquakes/eqinthenews/2011/usb0006klz/#summary> (accessed October 2015).
- U.S. Geological Survey, 2015a, Earthquake Hazards Program: Earthquake Archives: <http://earthquake.usgs.gov/earthquakes/search/> (accessed February 2015).
- U.S. Geological Survey, 2015b, The National Map Viewer: <http://viewer.nationalmap.gov/viewer/> (accessed September 2014).
- Waldhauser, F., and Ellsworth, W.L., 2000, A double-difference earthquake location algorithm: Method and application to the northern Hayward Fault, California: *Bulletin of the Seismological Society of America*, v. 90, p. 1353–1368, doi:10.1785/0120000006.
- Wells, D.L., and Coppersmith, K.J., 1994, New empirical relationships among magnitude, rupture length, rupture width, rupture area, and surface displacement: *Bulletin of the Seismological Society of America*, v. 84, p. 974–1002.
- Wesson, R. L., Helley, E. J., Lajoie, K. R., & Wentworth, C. M., 1975, Faults and future earthquakes, *in* Borchardt, R.D., ed., *Studies for seismic zonation of the San Francisco Bay region*: US Geological Survey Professional Paper, 941-A, p. 5–30.
- Zoback, M. D., Townend, J., & Grollimund, B., 2002, Steady-state failure equilibrium and deformation of intraplate lithosphere: *International Geology Review*, v. 44, p. 383-401.